



**Establishment and optimization of 3-dimensional mamma
carcinoma models for therapy simulation and drug testing**

**Etablierung und Optimierung 3-dimensionaler
Mammakarzinommodelle für die Therapiesimulation
und die Wirkstofftestung**

Doctoral thesis for a doctoral degree
at the Graduate School of Life Sciences,
Julius-Maximilians-Universität Würzburg,
Section Biomedicine

submitted by

Lena Nelke

born in Werneck

conducted at

Chair Tissue Engineering & Regenerative Medicine
of the
University Hospital Würzburg

Würzburg 2018

Submitted on:

Members of the committee

Chairperson: Prof. Dr. Thomas Dandekar

Primary Supervisor: Prof. Dr. Heike Walles

Supervisor (second): Prof. Dr. Torsten Blunk

Supervisor (third): Dr. Julia Schüler

Supervisor (fourth): Dr. Gudrun Dandekar

Date of public defence:

Date of receipt of certificates:

Table of contents

Abstract	V
Zusammenfassung	VII
List of abbreviations and units	X
List of figures	XIV
List of tables.....	XVI
1 Introduction.....	1
1.1 Mamma carcinoma	1
1.1.1 Epidemiology and biology of breast cancer	1
1.1.2 Hormone receptor status in breast cancer	1
1.1.3 Therapy of breast cancer.....	2
1.2 Cancer immunotherapies	3
1.3 Tissue engineering	5
1.3.1 <i>In vitro</i> tumour models for preclinical application.....	6
1.3.2 Modelling invasion and metastasis formation	7
1.4 Aim of the thesis	8
2 Materials	10
2.1 Equipment.....	10
2.2 Disposable materials.....	11
2.3 Laboratory materials.....	13
2.4 Chemicals and solutions	14
2.5 Media and solutions for cell culture	16
2.6 Chemicals and solutions for histology and immunohistochemistry	17
2.7 Commercially available kits	18
2.8 Antibodies	19
2.9 Biological material	20
2.9.1 Cell lines.....	20
2.9.2 Porcine material	20
2.9.3 Human material.....	21
2.9.4 Xenograft material.....	21

2.10 Software	21
3 Methods	22
3.1 General cell culture methods.....	22
3.1.1 Culturing of cell lines.....	22
3.1.2 Culturing of primary cells.....	23
3.2 2D cell culture.....	25
3.3 3D cell culture.....	25
3.3.1 Production of scaffold SISmuc	25
3.3.2 Generation of 3D tumour models.....	26
3.3.3 Static culture of cells on SISmuc	27
3.3.4 Culture of SKBR-3 cells on SISmuc on an orbital shaker	27
3.3.5 Dynamic culture of cells on SISmuc in a flow bioreactor	28
3.3.6 Treatment of 3D tumour models.....	28
3.4 Cell viability assays	30
3.4.1 CellTiter-Glo® luminescent cell viability assay.....	30
3.4.2 Quantitative MTT assay	31
3.5 Measurement of apoptosis	31
3.6 Determination of triglyceride and DNA content of hASCs.....	32
3.7 Histology.....	32
3.7.1 Fixation of cells grown on glass coverslips and on SISmuc.....	32
3.7.2 Paraffin embedding and microtome sectioning	33
3.7.3 Cryoembedding and cryosectioning	34
3.7.4 Haematoxylin-Eosin staining (H&E)	34
3.7.5 Lipid staining with Oil Red O	35
3.7.6 Lipid staining with BODIPY® 493/503	35
3.8 Immunohistochemistry	36
3.8.1 DAB staining	36
3.8.2 Immunofluorescence staining	37
3.9 Determination of proliferative index	38
3.10 Ultrastructural analysis	38
3.11 Quantification of invasive cells	40
3.12 <i>In situ</i> zymography combined with immunofluorescence staining	40

3.13 Statistical analysis	40
4 Results	41
4.1 Establishment and optimization of a 3D mamma carcinoma test system	41
4.1.1 Establishment of a 3D mamma carcinoma test system representing different molecular subsets of breast cancer	41
4.1.2 Optimization of the HER2-overexpressing tumour model	43
4.1.3 Determination of the optimum culture duration for compound testing	43
4.2 Characterization of the mamma carcinoma test system	44
4.2.1 Comparison of the proliferation index	44
4.2.2 Markers of tumour biology in 2D and 3D models and xenografts	48
4.2.3 Invasive behaviour of mamma carcinoma on the scaffold	52
4.3 Validation of the test system with a targeted therapy approach	58
4.4 Application of the established test system	62
4.4.1 Evaluation of an innovative drug formulation strategy	62
4.4.2 Testing of novel therapeutic strategies in the TNBC model	65
4.5 Establishment of coculture models	73
4.5.1 Coculture with dermal fibroblasts	73
4.5.2 Coculture with adipogenically differentiated hASCs	78
5 Discussion	82
5.1 Establishment and optimization of a 3D mamma carcinoma test system	82
5.2 Characterization of the mamma carcinoma test system	85
5.3 Validation of the test system with a targeted therapy approach	89
5.4 Application of the established test system	90
5.4.1 Evaluation of an innovative drug formulation strategy	90
5.4.2 Testing of novel therapeutic strategies in the TNBC model	91
5.5 Establishment of coculture models	94
5.5.1 Coculture with dermal fibroblasts	94
5.5.2 Coculture with adipogenically differentiated hASCs	96
5.6 Conclusion and outlook	97

References	98
Supplementary data	112
Affidavit/Eidesstattliche Erklärung	115
Acknowledgement.....	116
List of publications and conference contributions.....	118
Curriculum vitae	119

Abstract

Breast cancer is the most common cancer among women worldwide and the second most common cause of cancer death in the developed countries. As the current state of the art in first-line drug screenings is highly ineffective, there is an urgent need for novel test systems that allow for reliable predictions of drug sensitivity.

In this study, a tissue engineering approach was used to successfully establish and standardize a 3-dimensional (3D) mamma carcinoma test system that was optimized for the testing of anti-tumour therapies as well as for the investigation of tumour biological issues. This 3D test system is based on the decellularised scaffold of a porcine small intestinal segment and represents the three molecular subsets of oestrogen receptor-positive, HER2/Neu-overexpressing and triple negative breast cancer (TNBC). The characterization of the test system with respect to morphology as well as the expression of markers for epithelial-mesenchymal transition (EMT) and differentiation indicate that the 3D tumour models cultured under static and dynamic conditions reflect tumour relevant features and have a good correlation with *in vivo* tumour tissue from the corresponding xenograft models. In this respect, the dynamic culture in a flow bioreactor resulted in the generation of tumour models that exhibited best reflection of the morphology of the xenograft material. Furthermore, the proliferation indices of 3D models were significantly reduced compared to 2-dimensional (2D) cell culture and therefore better reflect the *in vivo* situation. As this more physiological proliferation index prevents an overestimation of the therapeutic effect of cytostatic compounds, this is a crucial advantage of the test system compared to 2D culture. Moreover, it could be shown that the 3D models can recapitulate different tumour stages with respect to tumour cell invasion. The scaffold SISmuc with the preserved basement membrane structure allowed the investigation of invasion over this barrier which tumour cells of epithelial origin have to cross in *in vivo* conditions during the process of metastasis formation. Additionally, the data obtained from ultrastructural analysis and *in situ* zymography indicate that the invasion observed is connected to a tumour cell-associated change in the basement membrane in which matrix metalloproteinases (MMPs) are also involved. This features of the model in combination with the mentioned methods of analysis could be used in the future to mechanistically investigate invasive processes and to test anti-metastatic therapy strategies.

The validation of the 3D models as a test system with respect to the predictability of therapeutic effects was achieved by the clinically relevant targeted therapy with the monoclonal antibody trastuzumab which induces therapeutic response only in patients with HER2/Neu-overexpressing mamma carcinomas due to its specificity for HER2. While neither in 2D nor in 3D models of all molecular subsets a clear reduction of cell viability or an increase in apoptosis could be observed, a distinct increase in antibody-dependent cell-mediated cytotoxicity (ADCC) was detected only in the HER2/NEU-overexpressing 3D model with the help of an ADCC reporter gene assay that had been adapted for the application in the 3D model in the here presented work. This correlates with the clinical observations and underlines the relevance of ADCC as a mechanism of action (MOA) of trastuzumab. In order to measure the effects of ADCC on the tumour cells in a direct way without the indirect measurement via a reporter gene, the introduction of an immunological component into the models was required. This was achieved by the integration of peripheral blood

mononuclear cells (PBMCs), thereby allowing the measurement of the induction of tumour cell apoptosis in the HER2/Neu-overexpressing model. Hence, in this study an immunocompetent model could be established that holds the potential for further testing of therapies from the emergent field of cancer immunotherapies.

Subsequently, the established test system was used for the investigation of scientific issues from different areas of application. By the comparison of the sensitivity of the 2D and 3D model of TNBC towards the water-insoluble compound curcumin that was applied in a novel nanoformulation or in a DMSO-based formulation, the 3D test system was successfully applied for the evaluation of an innovative formulation strategy for poorly soluble drugs in order to achieve cancer therapy-relevant concentrations. Moreover, due to the lack of targeted therapies for TNBC, the TNBC model was applied for testing novel treatment strategies. On the one hand, therapy with the WEE1 kinase inhibitor MK-1775 was evaluated as a single agent as well as in combination with the chemotherapeutic agent doxorubicin. This therapy approach did not reveal any distinct benefits in the 3D test system in contrast to testing in 2D culture. On the other hand, a novel therapy approach from the field of cellular immunotherapies was successfully applied in the TNBC 3D model. The treatment with T cells that express a chimeric antigen receptor (CAR) against ROR1 revealed in the static as well as in the dynamic model a migration of T cells into the tumour tissue, an enhanced proliferation of T cells as well as an efficient lysis of the tumour cells via apoptosis and therefore a specific anti-cancer effect of CAR-transduced T cells compared to control T cells. These results illustrate that the therapeutic application of CAR T cells is a promising strategy for the treatment of solid tumours like TNBC and that the here presented 3D models are suitable for the evaluation and optimization of cellular immunotherapies.

In the last part of this work, the 3D models were expanded by components of the tumour stroma for future applications. By coculture with fibroblasts, the natural structures of the intestinal scaffold comprising crypts and villi were remodelled and the tumour cells formed tumour-like structures together with the fibroblasts. This tissue model displayed a strong correlation with xenograft models with respect to morphology, marker expression as well as the activation of dermal fibroblasts towards a cancer-associated fibroblast (CAF) phenotype. For the integration of adipocytes which are an essential component of the breast stroma, a coculture with human adipose-derived stromal/stem cells (hASCs) which could be successfully differentiated along the adipose lineage in 3D static as well as dynamic models was established. These models are suitable especially for the mechanistic analysis of the reciprocal interaction between tumour cells and adipocytes due to the complex differentiation process.

Taken together, in this study a human 3D mamma carcinoma test system for application in the preclinical development and testing of anti-tumour therapies as well as in basic research in the field of tumour biology was successfully established. With the help of this modular test system, relevant data can be obtained concerning the efficacy of therapies in tumours of different molecular subsets and different tumour stages as well as for the optimization of novel therapy strategies like immunotherapies. In the future this can contribute to improve the preclinical screening and thereby to reduce the high attrition rates in pharmaceutical industry as well as the amount of animal experiments.

Zusammenfassung

Brustkrebs ist die häufigste Krebsart bei Frauen und die zweithäufigste Todesursache bei Krebserkrankungen in den Industrienationen. Aufgrund der Ineffizienz der derzeit verwendeten Modelle für die Identifizierung neuer Therapeutika herrscht ein hoher Bedarf an neuartigen Testsystemen, welche aussagekräftige Vorhersagen über die Wirksamkeit ermöglichen.

In dieser Arbeit wurde mit Hilfe des Tissue Engineerings erfolgreich ein 3-dimensionales (3D) Mammakarzinom-Testsystem etabliert, standardisiert und für die Testung von anti-tumoralen Therapien sowie weitere tumorbiologische Fragestellungen optimiert. Dieses 3D Testsystem basiert auf der dezellularisierten Gerüststruktur eines porcinen Dünndarmsegments und repräsentiert die drei molekularen Subtypen des Östrogen-Rezeptor-positiven, HER2/Neu-überexprimierenden sowie des tripel-negativen Brustkrebses (TNBC). Die Charakterisierung des Testsystems anhand der Morphologie sowie der Expression von Markern zur Bestimmung der epithelialen-mesenchymalen Transition (EMT) und der Differenzierung zeigte, dass die statisch und dynamisch kultivierten 3D Modelle Tumor-relevante Charakteristika widerspiegeln und eine deutliche Ähnlichkeit zu *in vivo* Tumormaterial aus entsprechenden Xenograft-Modellen aufweisen, wobei die dynamische Kultivierung in einem Flussreaktor zur Generierung von Tumormodellen führte, welche die Morphologie des Tumorgewebes aus Xenograft-Modellen am besten repräsentierten. Des Weiteren war die Proliferationsrate in den 3D Modellen im Vergleich zu 2-dimensionalen (2D) Zellkulturen signifikant reduziert und entspricht daher eher der Situation *in vivo*. Dies ist ein entscheidender Vorteil des Testsystems gegenüber der 2D Zellkultur, da durch die physiologischere Proliferationsrate eine Überschätzung des Therapieeffekts zytostatischer Medikamente vermieden wird. Zudem konnte gezeigt werden, dass mit Hilfe der 3D Modelle unterschiedliche Tumorstadien in Bezug auf die Tumorzellinvasion abgebildet werden können. Die Gerüststruktur SISmuc mit erhaltener Basalmembranstruktur ermöglichte eine Untersuchung der Invasion über diese Barriere, welche Tumorzellen epithelialen Ursprungs unter *in vivo*-Bedingungen beim Prozess der Metastasierung überwinden müssen. Zudem deuten die durch ultrastrukturelle Analysen und *in situ* Zymographie gewonnenen Daten darauf hin, dass die beobachtete Invasion mit einer Tumorzell-assoziierten Veränderung der Basalmembran, an der auch Matrix-Metalloproteinasen (MMPs) beteiligt sind, einhergeht. Diese Eigenschaften des Modells in Kombination mit den erwähnten Untersuchungsmethoden könnten in Zukunft dazu eingesetzt werden, Invasionsprozesse mechanistisch zu untersuchen sowie neue anti-metastatisch wirkende Therapiestrategien zu testen.

Die Validierung der 3D Modelle als Testsystem bezüglich der Vorhersagbarkeit von Therapieeffekten erfolgte mit Hilfe der klinisch relevanten, zielgerichteten Therapie mit dem monoklonalen Antikörper Trastuzumab, welcher aufgrund seiner Spezifität für HER2/Neu nur in Patienten mit HER2/Neu-überexprimierendem Mammakarzinom einen Therapieerfolg erzielt. Während weder in 2D noch in den 3D Modellen aller molekularer Subtypen eine eindeutige Reduktion der Zellviabilität oder ein Anstieg der Apoptose gemessen werden konnte, zeigte sich mit Hilfe eines ADCC-Reporterassays, der in dieser Arbeit für die Anwendung im 3D Modell angepasst wurde, ein deutlicher Anstieg der Antikörper-abhängigen zellvermittelten Zytotoxizität (ADCC) lediglich für das HER2/Neu-überexprimierende Modell. Dies entspricht den klinischen

Beobachtungen und unterstreicht die Relevanz der ADCC als Wirkmechanismus des Antikörpers. Um die direkten Effekte einer ADCC auf die Tumorzellen im 3D Testsystem direkt – ohne den Umweg über ein Reportergen – messbar zu machen, war die Einführung einer immunologischen Komponente notwendig. Dies gelang mit Hilfe der Integration von mononukleären Zellen des peripheren Blutes (PBMCs), wodurch die Induktion der Apoptose im HER2/Neu-überexprimierenden Modell messbar war. Somit konnte im Rahmen dieser Arbeit ein immunkompetentes Modell etabliert werden, welche das Potenzial für weitere Testungen aus dem aufstrebenden Bereich der Krebsimmuntherapien bietet.

Anschließend wurde das etablierte Testsystem zur Untersuchung von Fragestellungen aus unterschiedlichen Anwendungsbereichen eingesetzt. Durch den Vergleich der Sensitivität von Tumorzellen in 2D und im 3D Modell des TNBC gegenüber des wasserunlöslichen Wirkstoffs Curcumin, welcher in einer neuartigen Nanoformulierung bzw. in einer DMSO-basierten Formulierung appliziert wurde, konnte das 3D Testsystem für die Evaluation einer innovativen Formulierungsstrategie für unlösliche Wirkstoffe angewendet werden, um für die Krebstherapie relevante Dosierungen zu erreichen. Weiterhin wurden aufgrund des Mangels an zielgerichteten Therapien für das tripel-negative Mammakarzinom neuartige Therapiestrategien anhand des 3D Modells getestet. Zum einen wurde die Therapie mit dem WEE1-Kinase Inhibitor MK-1775 als Monotherapie sowie in Kombination mit dem Chemotherapeutikum Doxorubicin evaluiert. Diese zeigte im Gegensatz zu Testungen in 2D Kultur keinen eindeutigen Therapieeffekt im 3D Testsystem. Zum anderen wurde eine neuartige Behandlung aus dem Bereich der zellulären Immuntherapie erfolgreich im TNBC 3D Modell angewendet. Die Behandlung mit T-Zellen, welche einen chimären Antigen-Rezeptor (CAR) gegen ROR1 tragen, zeigte sowohl im statischen als auch im dynamischen Modell eine Migration der T-Zellen in das Tumorgewebe, eine erhöhte Proliferation der T-Zellen sowie eine effiziente Lyse der Tumorzellen mittels Apoptose und damit eine spezifische anti-tumorale Wirkung der CAR-transduzierten T-Zellen im Vergleich zu Kontroll-T-Zellen. Diese Ergebnisse verdeutlichen einerseits, dass die therapeutische Anwendung von CAR-T-Zellen eine vielversprechende Strategie für die Behandlung von soliden Tumoren wie des TNBC ist, zum anderen, dass die hier vorgestellten 3D Modelle als Testsystem für die Evaluierung und Optimierung von zellulären Immuntherapien geeignet sind.

Im letzten Teil der Arbeit wurde das 3D Modell für die zukünftige Anwendung um Komponenten des Tumorstromas erweitert. Durch die Kokultur mit Fibroblasten wurden die natürlichen Strukturen der Darmmatrix, bestehend aus Krypten und Villi, umgebaut und die Krebszellen bildeten zusammen mit den Fibroblasten tumorartige Strukturen aus. Das so erzeugte Gewebemodell zeigte sowohl in morphologischer Hinsicht als auch bezogen auf die Markerexpression und die Aktivierung der dermalen Fibroblasten hin zu Krebs-assoziierten Fibroblasten (CAFs) starke Ähnlichkeit mit Xenograft-Modellen. Für die Integration von Adipozyten, welche ein wichtiger Bestandteil des Stromas in der Brust sind, wurde eine Kokultur mit humanen, aus dem Fettgewebe stammenden Stroma-/Stammzellen (hASCs) etabliert, welche sowohl im statischen als auch im dynamischen 3D Modell erfolgreich adipogen differenziert werden konnten. Diese Modelle eignen sich aufgrund des komplexen Differenzierungsprozesses vor allem für die mechanistische Untersuchung der Interaktionen zwischen Tumorzellen und Adipozyten.

Zusammenfassend ist es in dieser Arbeit gelungen, ein humanes 3D Mammakarzinom-Testsystem zur Anwendung in der präklinischen Entwicklung und Testung anti-tumoraler Therapien sowie der Grundlagenforschung im Bereich der Tumorbilogie zu etablieren. Mit Hilfe dieses modularen Testsystems können relevante Daten zur Wirksamkeit von Therapien in Tumoren unterschiedlicher molekularer Subtypen sowie unterschiedlich fortgeschrittener Tumorstadien und zur Optimierung neuartiger Therapiestrategien wie Immuntherapien gewonnen werden. Dies kann in Zukunft dazu beitragen das präklinische Screening zu verbessern und somit die hohen klinischen Ausfallraten in der pharmazeutischen Industrie und die Zahl von Tierversuchen zu reduzieren.

List of abbreviations and units

Table 1: List of abbreviations and units

Abbreviation	Meaning
%	percent
µg	microgram
µM	micromolar
µm	micrometre
ADCC	antibody-dependent cell-mediated cytotoxicity
Akt	AKT serine/threonine kinase 1, protein kinase B
AT	Austria
ATR	ataxia-telangiectasia-related kinase
BC	breast cancer
BioVaSc [®]	Biological Vascularized Scaffold
<i>BRAF</i>	rapidly accelerated fibrosarcoma oncogene type B gene
CA	Canada
CAF	cancer-associated fibroblast
CAR	chimeric antigen receptor
ccK18	caspase-cleaved cytokeratin 18
CD	cluster of differentiation
CDC	complement-dependent cytotoxicity
CDK1	cyclin-dependent kinase 1
<i>CDKN2A</i>	cyclin-dependent kinase inhibitor 2A gene
CH	Switzerland
CHK1	checkpoint kinase 1
cm	centimetre
CO ₂	carbon dioxide
ctrl	control
d	day
DAPI	4',6-diamidino-2-phenylindole
DMEM	Dulbecco's Modified Eagle's Medium
DMSO	dimethyl sulfoxide
DNA	deoxyribonucleic acid
ECM	extracellular matrix
EDTA	ethylenediaminetetraacetic acid

Abbreviation	Meaning
EGFR	epidermal growth factor receptor
EGFRt	truncated epidermal growth factor receptor
ELISA	enzyme-linked immunosorbent assay
EMT	epithelial-mesenchymal transition
ER	oestrogen receptor
EtOH	Ethanol
FAP	fibroblast activation protein
FBS	fetal bovine serum
FcγRIIIa	Low affinity immunoglobulin gamma Fc region receptor III-A
FDA	US Food and Drug Administration
FOXC1	forkhead box protein C1
g	gram
GEMM	genetically engineered mouse model
GER	Germany
GSK3β	glycogen synthase 3' kinase β
h	hour(s)
H&E staining	Haematoxylin-Eosin staining
H ₂ O ₂	hydrogen peroxide
hASC	human adipose-derived stromal/stem cell
HCl	hydrochloric acid
HER2/Neu	human epidermal growth factor receptor 2
HRP	horseradish peroxidase
I	Italy
IBMX	3-isobutyl-1-methylxanthine
IC ₅₀	half maximal inhibitory concentration
IFNγ	interferon gamma
kg	kilogram
<i>KRAS</i>	Kirsten rat sarcoma viral oncogene homologue gene
l	litre
M	Molar
MAPK	mitogen-activated protein kinase
MEM	Minimum Essential Medium
MET	mesenchymal-epithelial transition

Abbreviation	Meaning
mg	milligram
MHC	major histocompatibility complex
min	minute(s)
ml	millilitre
mM	millimolar
mm	millimetre
MMP	matrix metalloproteinase
MMPI	MMP inhibitor
MOA	mechanism of action
ms	milliseconds
mTOR	mechanistic target of rapamycin
MTT	3-(4,5-dimethylthiazol-2-yl)-2,5-diphenyltetrazolium bromide
NADH	nicotinamide adenine dinucleotide
NADPH	nicotinamide adenine dinucleotide phosphate
NDL	Netherlands
NK	natural killer
nm	nanometre
NST	no special type
OS	orbital shaker
PBM	PGM-2 Basal Medium
PBMC	peripheral blood mononuclear cell
PBS ⁻	phosphate buffered saline without Mg ²⁺ /Ca ²⁺
PBS ⁺	phosphate buffered saline with Mg ²⁺ /Ca ²⁺
PCK	pan-cytokeratin
PD-L1	programmed cell death 1 ligand 1
PEEK	polyether ether ketone
Pen/Strep	penicillin/streptomycin
PFA	paraformaldehyde
PI3K	phosphatidylinositol-4,5-bisphosphate 3-kinase
<i>PIK3CA</i>	phosphatidylinositol-4,5-bisphosphate 3-kinase gene
PR	progesterone receptor
RLU	relative light unit
ROR1	receptor tyrosine kinase like orphan receptor 1

Abbreviation	Meaning
rpm	revolutions per minute
RT	room temperature
SEM	scanning electron microscopy
SISmuc	small intestinal submucosa and mucosa
SOP	standard operating procedure
SVF	stromal vascular fraction
SWE	Sweden
TEM	transmission electron microscopy
TGF β	transforming growth factor β
TIMP	tissue inhibitor of metalloproteinase
TNBC	triple negative breast cancer
TP53	Tumor protein p53
U	unit
U/l	units per litre
UK	United Kingdom
USA	United States of America
v/v	volume per volume
w/v	weight per volume
WHO	World Health Organization
α -SMA	α -smooth muscle actin
RPMI-1640 medium	Roswell Park Memorial Institute 1640 medium
CTLA-4	cytotoxic T-lymphocyte-associated protein 4
IL-2	interleukin-2
PD-1	programmed cell death protein 1
ZO-1	zonula occludens-1
2D	2-dimensional
3D	3-dimensional

List of figures

Figure 1: Insertion of SISmuc into cell crowns	27
Figure 2: Dynamic cell culture in a flow bioreactor	28
Figure 3: FBS batch testing	42
Figure 4: Optimization of SKBR-3 tumour models	43
Figure 5: Determination of the optimum culture duration	45
Figure 6: Proliferation and apoptosis over culture duration	46
Figure 7: Comparison of proliferation index in different culture conditions	47
Figure 8: Expression of tumour biology markers in MCF-7 cells in 2D, 3D static, 3D dynamic or in a xenograft model	49
Figure 9: Expression of tumour biology markers in MDA-MB-231 cells in 2D, 3D static, 3D dynamic or in a xenograft model	50
Figure 10: Expression of tumour biology markers in SKBR-3 cells in 2D and 3D OS culture conditions	51
Figure 11: Preservation of basement membrane and invasive behaviour of tumour cells	52
Figure 12: Differences in invasive behaviour of MCF-7 and MDA-MB-231 cells on SISmuc	54
Figure 13: Structural analysis of scaffold SISmuc after tumour cell culture	56
Figure 14: Gelatinolytic activity in 3D models of MCF-7 and MDA-MB-231 cells	57
Figure 15: Cell viability after treatment with trastuzumab	59
Figure 16: Apoptosis after treatment with trastuzumab	60
Figure 17: Antibody-dependent cell-mediated cytotoxicity after treatment with trastuzumab	61
Figure 18: ADCC in 3D models with integrated immunological component	61
Figure 19: Apoptosis in 3D models with integrated immunological component	62
Figure 20: Treatment with curcumin in DMSO-formulation or with curcumin-loaded A-pPrOzi-A micelles under 2D and 3D conditions	63
Figure 21: Cell viability after treatment with curcumin in DMSO-formulation or with curcumin-loaded A-pPrOzi-A micelles under 2D and 3D conditions	64
Figure 22: Cell viability of MDA-MB-231 cells treated with different doses of doxorubicin +/- MK-1775 in 2D conditions	66
Figure 23: Treatment with doxorubicin +/- MK-1775 under 2D and 3D conditions	66
Figure 24: Cell viability after treatment with doxorubicin +/- MK-1775 under 2D and 3D conditions	67
Figure 25: Apoptosis after treatment with doxorubicin +/- MK-1775 under 2D and 3D conditions	68
Figure 26: Treatment with ROR1-CAR T cells under 2D conditions	70

Figure 27: Treatment with ROR1-CAR T cells under 3D static conditions	71
Figure 28: Treatment with ROR1-CAR T cells under 3D dynamic conditions	72
Figure 29: Monoculture of dermal fibroblasts cultured on SISmuc.....	74
Figure 30: Static mono- and coculture models of MCF-7 and MDA-MB-231 cells with dermal fibroblasts	74
Figure 31: Dynamic mono- and coculture models of MCF-7 and MDA-MB-231 cells with dermal fibroblasts	75
Figure 32: Static and dynamic mono- and coculture models of MCF-7 cells with dermal fibroblasts – PCK-Vim staining.....	76
Figure 33: Static and dynamic mono- and coculture models of MDA-MB-231 cells with dermal fibroblasts – PCK-Vim staining	77
Figure 34: Static and dynamic coculture models of MCF-7 and MDA-MB-231 cells with dermal fibroblasts – PCK-FAP staining	78
Figure 35: Media testing for hASC differentiation	80
Figure 36: hASC adipogenic differentiation on SISmuc.....	81
Figure 37: Coculture of MDA-MB-231 cells with hASCs on SISmuc	81
Figure S 1: Structure of the scaffold SISmuc.....	112
Figure S 2: FBS batch testing - cell morphology in 2D	113
Figure S 3: Expression of mamma carcinoma-relevant markers in different FBS batches	114

List of tables

Table 1: List of abbreviations and units	X
Table 2: List of equipment	10
Table 3: List of disposable materials	11
Table 4: List of laboratory material	13
Table 5: List of chemicals and solutions	14
Table 6: List of media and solutions for cell culture	16
Table 7: List of chemicals and solutions for histology and immunohistochemistry	17
Table 8: List of commercially available kits	18
Table 9: List of antibodies	19
Table 10: List of cell lines	20
Table 11: List of software	21
Table 12: Cell seeding conditions for different assays	25
Table 13: Paraffin infiltration program of the embedding station	33
Table 14: Deparaffination and rehydration of tissue sections	34
Table 15: H&E staining procedure	35
Table 16: DAB staining procedure	36
Table 17: Immunofluorescence staining procedure	37
Table 18: Buffers and solutions for SEM and TEM	38
Table 19: Sample preparation for SEM	39
Table 20: Sample preparation for TEM	39

1 Introduction

1.1 Mamma carcinoma

1.1.1 Epidemiology and biology of breast cancer

Breast cancer is the most frequent cancer among women with estimated 1.67 million new cases worldwide in 2012 and is the second cause of cancer death in developed countries (Ferlay *et al.*, 2015). Tumour cells are derived from epithelial cells lining the ducts or lobules of the breast. Histologically, breast cancer is divided into *in situ* and invasive disease. The latter is histologically categorized according to the fourth edition of the “WHO Classification of Tumours of the Breast” into more than 21 invasive subtypes (Lakhani *et al.*, 2012; Vuong *et al.*, 2014). The invasive carcinoma of no special type (NST), which is also known as invasive ductal carcinoma NST, is the most frequent subtype with 40-75 % of all cases. This subtype is diagnosed by the exclusion of the remaining special subtypes. Among these are invasive lobular, mucinous, tubular, metaplastic, and medullary carcinomas as well as many other subtypes with distinct histological features. Some of these special types of breast cancers do not solely have a characteristic morphology but are also associated with a specific genetic signature and clinical behaviour, making the correct histological classification crucial for prognostic and predictive information (Weigelt *et al.*, 2008). Irrespective of the histological type, all breast tumours are histologically graded according to the scoring system of Bloom and Richardson (Bloom & Richardson, 1957) as modified by Elston and Ellis (Elston & Ellis, 1991). This scoring system evaluates the proportion of tubule formation, the degree of nuclear pleomorphism and the mitotic count. According to the scores of these three categories breast tumours are classified into grades between 1 and 3, with 1 being most differentiated and 3 least differentiated. Together with the lymph node status, the tumour grade is a powerful prognostic factor and is therefore also used for the determination of therapy options. Furthermore, information about tumour size (T), the status of regional lymph nodes (N) and the spread into distant metastatic sites (M) is used for the staging of the breast cancer according to the TNM system (Lakhani *et al.*, 2012).

1.1.2 Hormone receptor status in breast cancer

Apart from the histological classification, breast cancers can be subdivided into molecular subsets according to their receptor status. The expression of oestrogen receptor (ER), progesterone receptor (PR) and the amplification of human epidermal receptor 2 (HER2/Neu) are routinely assessed in breast cancer patients (Rakha *et al.*, 2010). According to these three molecular markers, the breast cancer tumours are classified as hormone receptor positive tumours (ER+ and/or PR+; approx. 80%), HER2/Neu-amplified tumours (approx. 13-20 %) or TNBC (ER-, PR- and HER2/Neu-; approx. 10-15 %). Patients with TNBC have a very poor prognosis as this subset is very aggressive and there are no targeted therapies available so far (Dent *et al.*, 2007; Mudvari *et al.*, 2013).

The analysis of gene expression arrays allows to divide these molecular subsets into intrinsic subtypes (Goldhirsch *et al.*, 2011). However, as not in all cases the possibility of gene expression profiling is given, surrogate definitions have been identified that allow for intrinsic subtyping of breast cancers. According to this, the subset of hormone receptor positive breast cancers can be subdivided into luminal A (ER+ and/or PR+, HER2/Neu-, Ki67 low) and luminal B breast cancer subtype (ER+ and/or PR+, HER2/Neu- and Ki67 high or ER+ and/or PR+, HER2/Neu+). Patients with luminal A tumours have a better survival rate compared to patients with luminal B tumours. Approximately 80 % of the subset of TNBCs belong to the intrinsic subtype of basal-like breast cancers. This is a highly diverse subtype characterized by the expression of basal cytokeratins together with epidermal growth factor receptor (EGFR), c-Kit and forkhead box protein C1 (FOXC1) as well as a high proliferation index. Also, mutations in *TP53* are very frequent in this subtype (Vuong *et al.*, 2014).

1.1.3 Therapy of breast cancer

After diagnosis and classification, the tumour is, if possible, removed by mastectomy or by breast-conserving surgery also called lumpectomy. In some cases, neoadjuvant therapies are applied before resection in order to reduce the tumour size. Surgery is usually followed by radiation and adjuvant therapies. The type of therapy administered is determined according to molecular subset and grade of the tumour.

For the treatment of hormone receptor-positive tumours there is the option of targeted therapies. As these tumours depend on hormones for their growth (Vuong *et al.*, 2014), the ER can be blocked by tamoxifen or fulvestrant or the production of endogenous oestrogen can be reduced by aromatase inhibitors. In high grade hormone receptor-positive tumours, targeted therapy is combined with chemotherapy.

In the case of HER2/Neu-amplified tumours, survival rates and prognosis could significantly be improved by the targeted therapy approach with the humanized monoclonal antibody trastuzumab (Herceptin®) which binds to HER2/Neu (Carter *et al.*, 1992; Slamon *et al.*, 2001). Another HER2-targeting antibody is pertuzumab (Perjeta®) that blocks dimerization of HER2 with other receptors of the HER family. As it has a binding site different from trastuzumab, the combination of trastuzumab, pertuzumab and a chemotherapeutic agent from the class of taxanes is the standard first line therapy of metastasised HER2-positive mamma carcinoma (Degenhardt *et al.*, 2015). HER2 is a receptor tyrosine kinase anchored in the cell membrane of epithelial cells of different tissues and binds growth factors resulting in the activation of different signalling pathways (Yarden & Sliwkowski, 2001). Upon ligand binding, it forms heterodimers with HER1, HER3 or HER4 (Johannessen *et al.*, 2001). This leads to the activation and phosphorylation of the receptors, thereby inducing different downstream pathways like the MAPK, PI3K/Akt and mTOR, which regulate apoptosis, migration, growth, adhesion and differentiation (Yarden & Sliwkowski, 2001). Trastuzumab, which is in clinical application already since 1998 in the US and 2000 in the EU, has several discussed MOAs that directly or indirectly suppress the tumour cells' growth, proliferation and survival like the prevention of HER2 shedding, triggering internalisation and degradation of HER2, blocking of downstream signalling pathways, thereby

suppressing cell growth and proliferation and flagging the tumour cell for elimination by the immune system known as ADCC (Morris & Carey, 2006; Vu & Claret, 2012). During ADCC an effector cell of the immune system binds the Fc region of the target cell-bound antibody via CD16 and releases different mediators like granzymes and perforins resulting in the lysis of the target cell (Seidel *et al.*, 2013; W. Wang *et al.*, 2015). Effector cells that induce ADCC are mostly natural killer (NK) cells but also eosinophilic and neutrophilic granulocytes as well as macrophages (Stockmeyer *et al.*, 2003; Mellor *et al.*, 2013).

TNBC is the only subtype of breast cancer for which there is no targeted therapy available so far. Therefore, this very aggressive tumour type can only be treated with chemotherapy. Over the past decade, there have been numerous attempts to identify targets in TNBC that are suitable for treatment. An alteration that frequently occurs is the mutation or loss of *p53* which can be found in approximately 70 % of TNBC (Cerami *et al.*, 2012; Gao *et al.*, 2013). This led to the exploration of approaches to target mutated *p53* in TNBC. *p53* is primarily responsible for mediating the G1 checkpoint of the cell cycle leading to an arrest of the cell cycle at this checkpoint when DNA-damages occur, thereby allowing the cell the time for DNA-repair. As cells without *p53* function lack this cell cycle checkpoint, they rely on the G2-M checkpoint when DNA-damages occur. This suggests that abrogation of this checkpoint leads to the premature entry of the cells into mitosis and in case of DNA-damage to mitotic catastrophe and apoptosis preferentially in *p53*-defective tumour cells (Leijen *et al.*, 2010). One approach to achieve this is the inhibition of WEE1 kinase. When DNA-damage is detected by ataxia-telangiectasia-related kinase (ATR), checkpoint kinase 1 (CHK1) and subsequently WEE1 kinase are activated. Activated WEE1 kinase in turn phosphorylates CDK1-cyclinB complex, thereby maintaining this complex in its inactive state and preventing entry into mitosis until DNA-damage is repaired. This led to the investigation of the efficacy of WEE1 inhibitors in combination with DNA-damaging chemotherapy (Do *et al.*, 2013). MK-1775 (AZD1775) is a potent small molecule inhibitor of WEE1 kinase that demonstrated enhanced efficacy in *p53*-mutant or -deficient cell lines of different entities in combination with DNA-damaging agents (Hirai *et al.*, 2009; Hirai *et al.*, 2010). Newer studies also suggest a single agent activity of this compound that is independent of *p53* mutation (Kreahling *et al.*, 2012; Guertin *et al.*, 2013). This can be explained by the critical role of WEE1 kinase in the regulation of appropriate initiation and progression of DNA replication forks. Therefore, the inhibition of WEE1 can cause an increase in DNA double strand breaks, thereby inducing apoptosis (Beck *et al.*, 2010; Dominguez-Kelly *et al.*, 2011; Beck *et al.*, 2012). Next to MK-1775, other inhibitors of WEE1 kinase have been developed, but MK-1775 has so far shown best potency and selectivity and is therefore tested in several clinical trials for different types of tumours at the moment (Matheson *et al.*, 2016).

1.2 Cancer immunotherapies

One of the characteristics of cancer postulated by Hanahan and Weinberg is its ability to avoid the destruction by the immune system (Hanahan & Weinberg, 2011). This immunoevasion is achieved by a plethora of strategies like the secretion of immunosuppressive factors such as transforming growth factor β (TGF β) (L. Yang *et al.*, 2010) or the downregulation of the major histocompatibility complex 1 (MHC1) on the tumour cells, thereby evading antigen recognition

by T cells (Algarra *et al.*, 1997; Schreiber *et al.*, 2011). Furthermore, tumour cells are capable of recruiting immunosuppressive cells like myeloid-derived suppressor cells or regulatory T cells (Ostrand-Rosenberg & Sinha, 2009; Mougiakakos *et al.*, 2010) or they express immunoregulatory proteins that activate immune checkpoints which downregulate the activation of T cells and their effector functions (Krummel & Allison, 1995; Okazaki & Honjo, 2007). This mechanism is part of the natural regulation of the immune response but can be exploited by tumour cells.

This weakness of the immune system against cancer cells is the target of cancer immunotherapy which is successfully applied for several years for the treatment of cancer and pursues diverse strategies. In monoclonal antibody therapies, the antibody recognizes a target molecule on the cancer cell, thereby marking it for destruction by the immune system. This is achieved either by the activation of the complement system leading to complement-dependent cytotoxicity (CDC) or by the aforementioned process of ADCC. With trastuzumab, this type of therapy is approved and established for the treatment of cancer already since 1998 (Rueckert *et al.*, 2005). Another and more recent approach is the treatment of cancer with checkpoint inhibitors. By blocking the immune checkpoints, the inactivation of T cells by tumour cells via the expression of the respective ligands is abrogated, thereby stimulating the immune response of T cells against cancer. Among these checkpoint inhibitors is the monoclonal antibody ipilimumab, that inhibits the cytotoxic T-lymphocyte-associated protein 4 (CTLA-4) checkpoint and is approved for the therapy of metastasised melanoma since 2011 (Lipson & Drake, 2011), as well as the antibodies nivolumab and pembrolizumab, that target the PD-1 – PD-L1 axis (Pardoll, 2012). The great success of these checkpoint inhibitors led to the development of several other checkpoint inhibitors that are under investigation at the moment. A promising new approach are cellular therapy strategies in which autologous T cells are expanded and modified *in vitro* in order to express tumour-specific T cell receptors or chimeric antigen receptors (CAR). After being reintroduced into the patient, these modified cells recognise and eliminate the tumour. Such cellular immunotherapy strategies demonstrated great success with excellent remission rates in haematological cancers like acute and chronic lymphatic leukaemia upon treatment with CD19-CAR T cells (Kochenderfer *et al.*, 2012; Brentjens *et al.*, 2013), leading to US Food and Drug Administration (FDA) approval in 2017 (P. P. Zheng *et al.*, 2018). Such CARs are composed of an extracellular variable antigen binding domain which is derived from a monoclonal antibody and is connected to a transmembrane domain and an intracellular signalling module (Beatty & O'Hara, 2016). A major advantage of these CARs is their major histocompatibility complex (MHC)-independence, whereby the immunoevasion strategy of MHC-1 downregulation on tumour cells is abrogated. A major objective in the field is now to test and optimize this therapy strategy also for solid tumours. However, there are several challenges that have to be overcome to achieve the transfer of this technology to solid tumours (Newick *et al.*, 2016; H. Zhang *et al.*, 2016) like the evaluation of an appropriate target antigen on the tumour cells and optimization of the expansion and persistence of CAR T cells *in vivo*. Furthermore, efficacy is limited due to inefficient tumour homing of T cells in the body and diverse mechanisms of immunosuppression in the tumour microenvironment (Beatty & O'Hara, 2016).

Taken together, cancer immunotherapy is a promising concept for the future and the testing of novel strategies from this field in suitable *in vitro* and *in vivo* models is a prerequisite for their efficient development and approval.

1.3 Tissue engineering

The term “tissue engineering” stands for the artificial production of functional biological tissues *in vitro*. These tissues can be transplanted into the human body and thus replace damaged tissues. Other applications of these artificial tissues are the investigation of molecular principles in healthy as well as in pathologically altered tissues or the testing of the specificity and efficacy of pharmacological substances (Griffith & Swartz, 2006). The usage of such disease models can help to reduce animal experiments in basic research as well as in commercial drug development in the future.

In principle, the generation of human tissues *in vitro* is based on the co-culturing of different human cell types, which can be isolated from biopsy material. Cells have to be expanded before they can be cultured on an appropriate 3D scaffold. Scaffolds form a matrix where cells can attach to, grow on and replace the natural extracellular matrix (ECM) in the process of ECM remodelling. The scaffolds can be synthetically produced, e.g. like polymer-based electrospun scaffolds or they can be produced from biological materials like alginate-based substrates or collagens (F. J. O'Brien, 2011). Furthermore, the use of natural scaffolds is possible after the decellularisation of tissues or organs. A complex natural xenogenic scaffold applied at the chair of Tissue Engineering and Regenerative Medicine is the so called BioVaSc® (**B**iological **V**ascularized **S**caffold). This vascularized biological matrix is obtained by decellularisation of porcine small intestine (Mertsching *et al.*, 2005; Schanz, 2007; Pusch, 2009). A simplified version of this scaffold without preserved vessel structures is the SISmuc (small intestinal submucosa and mucosa). It consists of the mucosal and submucosal part of segments of porcine jejunum that had been completely decellularised. The basement membrane on top of the mucosa is preserved in large parts. As the SISmuc lacks the serosa and former vessel structures, it is not possible to create reseeded vessels in the matrix. Hence, it allows for the production of smaller 3D models compared to the whole BioVaSc® construct with shorter culturing periods under standardized conditions in a cell incubator. This goes in line with lower costs. This scaffold has been successfully used for the generation of a lung cancer model and a standardized model of colorectal cancer (Stratmann *et al.*, 2014; Nietzer *et al.*, 2016)

Instead of freshly isolated primary cells, established and often commercially available cell lines can also be used for the synthesis of *in vitro* tissues. Cell lines have some disadvantages compared to primary cells. In order to grant survival in cell culture and for long culture periods, they are genetically altered. This might also lead to differences in the transcriptome or on the protein level. It can - on the other hand - not be excluded, that primary cells cultured in 2D cultures lose some of their characteristics as well because the microenvironment always has an impact on the cell phenotype. Furthermore, the media for cell culture have to be adjusted to the special needs of the cultured cells and should contain adequate amounts of nutrients and growth factors. Moreover, the dynamic cell culture in so called bioreactors allows the simulation of extern parameters such

as mechanic shear stress, fluid pressure, medium flow and temperature variations and thus the creation of conditions as physiological as possible. These parameters influence cell properties and allow the generation of artificial tissues that are similar to native tissues.

1.3.1 *In vitro* tumour models for preclinical application

The current situation in cancer drug development with attrition rates of up to 95 % causes enormous costs and is a key challenge for pharmaceutical industry (Moreno & Pearson, 2013). Only 1 in 10,000 positively tested preclinical compounds reaches a marketing authorization and approximately 60 % of the compounds fail in the clinical phases I to III due to the lack of efficacy (Arrowsmith & Miller, 2013; Moreno & Pearson, 2013; Schuhmacher *et al.*, 2016). A reason for this is the usage of poorly predictive preclinical models for drug development and testing. Especially 2D cell line-based tumour test systems in the form of high-throughput screens as well as murine xenograft tumour models are used for the identification of new drug targets and pharmacologically effective substances today (Kamb, 2005; Stratmann *et al.*, 2013). However, 2D cell line-based high-throughput screens do not sufficiently meet the demand of predicting the clinical response of potential anti-cancer drugs. Reasons for this are that cells grown in 2D culture on a plastic surface lack the complex and dynamic cell-cell and cell-matrix interactions as well as the mechanical properties and biochemical networks found in *in vivo* tumours (Xu *et al.*, 2014). Furthermore, other cell types like stromal cells, ECM and immunomodulators, which influence processes like proliferation, growth, migration and therefore also the response to anti-cancer compounds, are missing in this simplistic approach (Caponigro & Sellers, 2011; Xu *et al.*, 2014; Santo *et al.*, 2017). On the other hand, xenograft tumour models that are established by injecting tumour cell lines or primary tumour cells into the body of immunodeficient mice comprise a natural tumour microenvironment with vascularisation. This, however, is of murine origin and due to the incompatibility of different factors between human and mouse not all cell-matrix interactions can form properly. Also immune system evading strategies of tumours cannot be analysed in these models due to immunodeficiency of the mice (Caponigro & Sellers, 2011). Therefore, xenograft tumour models do not always sufficiently represent *in vivo* tumours. In order to resolve the aforementioned shortcomings, there are several more advanced tumour models like genetically engineered mouse models (GEMMs) where the introduction of one or more driver mutations in mice with an intact immune system leads to the formation of murine tumours (Sharpless & Depinho, 2006) or humanized mice that are engrafted with human tumour cells and human immune cells. However, such mouse models are technically demanding, time consuming, expensive and associated with ethical concerns.

An attempt to combine the positive aspects of cell line-based 2D models and animal models are 3D cell line-based tumour models. One strategy is the culturing of cell line aggregates called spheroids. In these spheroids, cells form cell-cell-interactions in a 3D setting, deposit their own ECM, show a more physiologic proliferation behaviour and form multilayered structures (Burdett *et al.*, 2010). Spheroid cultures can be extended with other cell types like fibroblasts or endothelial cells. Even though spheroid cultures are an all-human model with a biology closer to the *in vivo* tumour, there are severe limitations like the variation in size, the formation of artificial cell-cell

contacts that are different from those *in vivo* and diffusion limits of nutrients as well as drug compounds (Stratmann *et al.*, 2013).

All in all, there is a great need for novel tissue-engineered tumour models with a human background and a high complexity that better mimic the clinical situation and therefore show improved predictability of sensitivity to new drug candidates. Even though such models might not fully replace animal models, they could at least contribute to a drastic reduction, help to make anti-cancer drug development more efficient and facilitate the investigation of complex tumour biology.

1.3.2 Modelling invasion and metastasis formation

Tumour models can not only be applied for drug screening assays but also for studying the mechanisms underlying tumour initiation, progression and metastasis formation.

Metastasizing of primary tumours into distinct sites and the formation of secondary tumour tissues is usually linked with poor prognosis and the formation of such metastases occurs in multiple steps: At first, tumour cells invade the surrounding tissue, intravasate into blood or lymph vessels and are transported to other organs. Before the tumour can form micrometastases, the circulating tumour cells have to extravasate and migrate into the tissue of the pre-metastatic site, where the cells start to proliferate and form a secondary tumour (Tsai & Yang, 2013). The process of EMT has long been thought to be a prerequisite for invasive outgrowth of cancer cells. This process is naturally occurring in embryogenic development or wound healing but can be hijacked by tumour cells (Wendt *et al.*, 2012). In this process, epithelial cancer cells lose their polarized epithelial phenotype and achieve mesenchymal properties. This results in the loss of cell-cell-contacts like adherens junctions, desmosomes and tight junctions. Additionally, by the reorganization of the cytoskeletal architecture, the phenotype of tumour cells switches to a more migratory one (Lamouille *et al.*, 2014). This event is characterized by the loss of epithelial markers like E-Cadherin, specific keratins and the tight junction protein zonula occludens-1 (ZO-1), whereas mesenchymal markers like fibronectin, α -smooth muscle actin (α -SMA), vimentin and matrix remodelling proteins like MMPs are upregulated (Moustakas & Heldin, 2007; Wendt *et al.*, 2012). The loss of E-Cadherin, which is regarded as the gatekeeper of the epithelial phenotype, is a critical event in EMT. B-Catenin is a factor that is closely linked to E-Cadherin and also plays a role in EMT. It is usually located in the cytoplasm of the cell and is bound to axin or glycogen synthase 3' kinase β (GSK3 β) or at the plasma membrane in a complex with E-Cadherin forming the adherens junctions of the cell. Upon the loss of E-Cadherin, β -Catenin is released from this complex and translocates to the nucleus where it can act as a transcription factor for its target genes (Moustakas & Heldin, 2007). EMT is also suggested to provide transformed cells with stem-like properties like the ability to self-renew, tumour initiating capability, resistance to apoptosis and chemoresistance (Wendt *et al.*, 2012).

Although the mechanisms of EMT are well defined and its occurrence in *in vivo* tumours is accepted, the consequences and role of EMT in cancer remain to be elucidated. While the role of EMT in cancer dissemination has long been regarded as a paradigm, newer reports suggest that

EMT is not necessary for metastasis formation but rather leads to enhanced chemoresistance in tumours (Fischer *et al.*, 2015; Maheswaran & Haber, 2015; X. Zheng *et al.*, 2015).

Another key player in the invasion process are MMPs. These zinc-dependent endopeptidases are of high interest in cancer research as they are involved in the proteolysis of the ECM and therefore play a crucial role in matrix remodelling (Egeblad & Werb, 2002; Kessenbrock *et al.*, 2010). Apart from their role in cancer progression, they are involved in physiological processes like wound healing, mammary involution and angiogenesis (Page-McCaw *et al.*, 2007).

The family of MMPs comprises at least 28 members of which 14 are implicated in breast cancer development and progression (Kohrmann *et al.*, 2009). They have different substrate specificity, can be secreted or membrane-bound and are synthesised both by cancer and stromal cells in tumours (Lebeau *et al.*, 1999; Kohrmann *et al.*, 2009). Their protease activity can be inhibited by tissue inhibitors of metalloproteinases (TIMPs), of which four have been described and which are abundant in breast tissue as their well-orchestrated interplay with MMPs is required for the structural and functional changes during pregnancy and menstrual cycle (Lebeau *et al.*, 1999; Fata *et al.*, 2000).

The ability of MMPs to remodel the microenvironment, thereby enhancing tumour progression, makes them a potential target for cancer therapy and led to the development of a large number of MMP inhibitors (MMPIs). However, the hopes based on the promising preclinical results could not translate into clinical success for various reasons: Due to the structural similarities in the catalytic domain across the family of MMPs, MMPIs did not achieve sufficient selectivity leading to serious adverse effects. Furthermore, patients enrolled in the clinical trials were not stratified according to the stage of their disease, whereas preclinical testing focused on models of early stage cancer (Cathcart *et al.*, 2015). The role of MMPs in driving tumour progression suggests that they might be more efficient in early stage disease or as a preventive measure compared to advanced cancers that have already formed metastases (Overall & Lopez-Otin, 2002; Pavlaki & Zucker, 2003). Therefore, the study design of clinical trials might not have been optimal. With this knowledge, development of next-generation MMPIs is under way, which will have to prove their efficacy in clinical trials in the next years (Levin *et al.*, 2017).

For the evaluation of such novel compounds targeting cancer progression and invasion as well as for the mechanistic investigation of the processes occurring during cancer dissemination, suitable models are necessary that can recapitulate cancer cell invasion, which is not the case in conventional 2D culture approaches.

1.4 Aim of the thesis

The current situation in cancer drug development with attrition rates of up to 95 % urgently demands for the development of novel models that better mimic the clinical situation and therefore show better predictability of sensitivity to new drug candidates. Therefore, these models have to be more complex than 2D cultures of cell lines that are currently used for the first-line drug screening but still easy to handle, highly reproducible and inexpensive. With the help of such

models, predictions in screening would be more reliable, animal models could be reduced and investigation of complex tumour biology would be possible.

In this study it was aimed to create breast cancer models with the help of a tissue engineering approach on the basis of the scaffold SISmuc that represent the different molecular subsets of mamma carcinoma: ER-positive, HER2/Neu-overexpressing and TNBC.

In the first part, these mamma carcinoma models should be established and optimized for the application of compound testing as well as for the mechanistic investigation of tumour biology-relevant processes and a standard operating procedure (SOP) for tumour model generation had to be defined. Subsequently, these models should be characterized with respect to tumour cell proliferation, expression of relevant markers of tumour biology in comparison to xenograft material and the suitability of the models for studying invasion should be assessed.

Secondly, the 3D models should be validated as a test system with the help of a targeted therapy approach with known clinical efficacy. In order to achieve this, the introduction of an immunological component into the models was necessary.

The validated test system should then be applied for the investigation of scientific issues from different areas of application. By the comparison of the sensitivity of the 2D and 3D model of TNBC towards the water-insoluble compound curcumin applied in different formulations, an innovative formulation strategy with the copolymer A-pPrOzi-A for the administration of poorly soluble compounds should be evaluated in order to achieve cancer therapy-relevant concentrations. Furthermore, the validated test system for TNBC should then be used to assess the efficacy of different novel therapeutic strategies for the treatment of TNBC. On the one hand, sensitivity and response of the 3D model to the small molecule inhibitor of WEE1 kinase MK-1775 alone and in combination with the chemotherapeutic agent doxorubicin should be evaluated. On the other hand, an innovative treatment approach with CAR T cells should be investigated in the 3D model in order to determine if the test system is suitable for the evaluation and optimization of such alternative anti-cancer strategies from the field of cancer immunotherapies. In the light of the FDA approval of a CD19-CAR therapy for haematological cancer and ongoing efforts to transfer such therapies to solid tumours, the evaluation of the suitability of the here presented test system for such therapies is of high relevance, as tumour models that allow such investigations are urgently needed.

In the last part, the model should be expanded by the introduction of a stromal component in order to provide a more realistic model for future compound testing as well as for the mechanistic investigation of the interplay between tumour and stroma. Therefore, fibroblasts and adipocytes were integrated into the models.

2 Materials

2.1 Equipment

Table 2: List of equipment

Equipment/Device	Producer
Accu-jet pipettor	Brand, Wertheim (GER)
Analytical Balance	Kern & Sohn, Balingen-Frommern (GER)
Aspiration Device: VacuBoy	Integra Biosciences, Fernwald (GER)
Autoclaves:	
DX-45 Bench-top Autoclave	Systec GmbH, Wettengel (GER)
Steam sterilizer (Varioklav)	HP Medizintechnik, Oberschleißheim (GER)
Technoclav	Integra Biosciences AG, Zizers (CH)
Biological safety cabinet NU-425-600 E	Nuaire, Plymouth (USA)
Bioreactor board	Chair of Tissue Engineering & Regenerative Medicine, Würzburg (GER)
Blocking Station	Leica, Wetzlar (GER)
Cell incubator: 37 °C, 5 % CO ₂	Heraeus, Hanau (GER)
Centrifuges:	
Centrifuge 5417R	Eppendorf, Hamburg (GER)
Multifuge X12	Thermo Fisher Scientific, Dreieich (GER)
Multifuge X1R	Thermo Fisher Scientific, Dreieich (GER)
Pico 17	Thermo Fisher Scientific, Dreieich (GER)
Rotilabo	Carl Roth, Karlsruhe (GER)
Cold storage room, 4 °C	Genheimer, Höchberg (GER)
Cooling plate	Leica, Wetzlar (GER)
Cryostat (Leica CM3050 S)	Leica, Wetzlar (GER)
Digital camera	Canon, Krefeld (GER)
Drying oven	Memmert, Schwabach (GER)
Embedding cassette printer VCP-5001	Vogel Medizintechnik, Gießen (GER)
Embedding center	Thermo Fisher Scientific, Dreieich (GER)
Freezer -20°C: Comfort	Liebherr, Biberach a.d. Riss (GER)
Freezer -80°C: HFU586 Basic	Heraeus Med, Hanau (GER)
Freezing container: Mr. Frosty™	VWR, Darmstadt (GER)
Fume hood	Prüschner Laboratory Systems, Neudorf (AT)
Ice machine AF-80	Scotsman, Mailand (I)
Immersion thermostat for water bath	Lauda, Lauda-Königshofen (GER)

Equipment/Device	Producer
Laboratory dish washer	Miele, Gütersloh (GER)
Liquid nitrogen storage tank MVE 815 P190	German-cryo, Jüchen (GER)
Magnetic stirrer and heater 720-HPS	VWR, Darmstadt (GER)
Microplate reader Tecan Infinite [®] M200	Tecan, Crailsheim (GER)
Microscopes:	
Bright field (Axio Lab.A1)	Carl Zeiss Microscopy GmbH, Göttingen (GER)
Confocal (SP8)	Leica, Wetzlar (GER)
Fluorescence (BZ-9000)	Keyence, Neu-Isenburg (GER)
Multichannel pipette plus	Eppendorf, Hamburg (GER)
Multistep pipette	Brand, Wertheim (GER)
Neubauer cell counting chamber (hemocytometer)	Marienfeld GmbH & Co. KG, Lauda- Königshofen (GER)
Orbital shaker (KM-2 Akku)	Edmund Bühler GmbH, Hechingen (GER)
Peristaltic pump	Ismatec, Wertheim-Mondfeld (GER)
pH meter	Mettler Toledo, Giessen (GER)
Pipette plugger	Bellco Glass, Asbach (GER)
Pump tubing cassette	Ismatec, Wertheim-Mondfeld (GER)
Refrigerator (MedLine)	Liebherr, Biberach a.d. Riss (GER)
Rocking platform shaker	VWR, Darmstadt (GER)
Slide printer VSP-5001	Vogel Medizintechnik, Gießen (GER)
Sliding microtome (Leica SM2010 R)	Leica, Wetzlar (GER)
Spectrophotometer (MRX microplate reader)	Dynatech Laboratories, Chantilly, Virginia (USA)
Steamer (MultiGourmet)	Braun, Kronberg (GER)
Thermostat	Eppendorf, Hamburg (GER)
Tissue floatation bath (GFL1052)	GFL, Burgwedel (GER)
Ultrasonic homogenizer	Bandelin electronic, Berlin (GER)
Vortexer (Genie 2)	Carl Roth, Karlsruhe (GER)
Water purification system (MilliQ [®])	Merck-Millipore, Darmstadt (GER)

2.2 Disposable materials

Table 3: List of disposable materials

Disposable material	Producer
Aluminium Foil	Carl Roth GmbH, Karlsruhe (GER)
Air filter, sterile (16596-HYK)	Sartorius AG, Göttingen (GER)

Disposable material	Producer
Cell culture flasks (25 cm ² , 75 cm ² , 150 cm ²)	TPP Techno Plastik Products AG, Trasadingen (CH)
Cell culture multiwall plates (6 well, 12 well, 24 well, 96 well)	TPP Techno Plastik Products AG, Trasadingen (CH)
Cell scrapers	Sarstedt, Nümbrecht (GER)
Centrifuge tubes (15ml; 50 ml)	Greiner Bio-One, Frickenhausen (GER)
Combitips Plus (0.5 ml, 1 ml, 2.5 ml, 5 ml)	Eppendorf, Hamburg (GER)
Cover slips for object slides (24x60 mm)	Menzel-Gläser, Braunschweig (GER)
Cover slips (round, Ø 12 mm)	Marienfeld GmbH & Co KG, Lauda-Königshofen (GER)
Cryo tubes (1.8 ml)	Nunc, Wiesbaden (GER)
Disposable microtome blades (type S35)	pfm medical, Köln (GER)
Disposable pipettes (5 ml, 10 ml, 25 ml, 50 ml)	Greiner Bio-One, Frickenhausen (GER)
Disposal bags	Hartenstein, Würzburg (GER)
Embedding cassettes	Klinipath, Duiven (NDL)
Embedding filter paper	Labonord, Mönchengladbach (GER)
Medical gloves, nitrile	Medline, Kleve (GER)
Microscope slides: Uncoated	Menzel, Braunschweig (GER)
Polylysine TM	Langenbrinck, Emmendingen (GER)
O-rings (sealing rings)	Dichtelemente areus GmbH, Seevetal (GER)
Paper towel	IGEFA, Ahrensfelde (GER)
Parafilm® M	Carl Roth, Karlsruhe (GER)
Petri Dishes: 145 x 20 mm	Greiner Bio-One, Frickenhausen (GER)
Pipette tips (0.5-10 µl, 10-100 µl, 100-1000 µl)	Eppendorf, Hamburg (GER)
PTFE thread seal tape (BS7786:1995 Grade L)	Hydrasun Ltd., Aberdeen (UK)
Pump tubing	Ismatec, Wertheim-Mondfeld (GER)
Reaction tubes (1.5 ml, 2 ml)	Sarstedt, Nümbrecht (GER)
Scalpel blades, rounded	Bayha, Tuttlingen (GER)
Silicone tube (9531.1)	Carl Roth GmbH, Karlsruhe (GER)
Sterile filter (pore size:0.2 µm)	Sartorius Stedium Biotech, Göttingen (GER)
Syringes (20 ml, 50 ml)	BD Biosciences, Heidelberg (GER)
Weighing dish	Hartenstein, Würzburg (GER)
Whatman filter paper	Hartenstein, Würzburg (GER)

Disposable material	Producer
Wrapping film	Cofresco Frischhalteprodukte, Minden (GER)

2.3 Laboratory materials

Table 4: List of laboratory material

Laboratory material	Producer
Beakers	Schott, Mainz (GER)
Cell crowns for static three-dimensional culture (stainless steel, smaller: PEEK)	Chair of Tissue Engineering & Regenerative Medicine, Würzburg (GER)
Centrifuge tube racks	neoLab, Heidelberg (GER)
Cold protection gloves	VWR, Darmstadt (GER)
Eppendorf pipettes (0.5-10 µl, 10-100 µl, 100-1000 µl)	Eppendorf, Hamburg (GER)
Funnel	Hartenstein, Würzburg (GER)
Glass cuvettes	Mercateo, München (GER)
Glass pasteur pipettes	Brand, Wertheim (GER)
Glass pipettes (5 ml, 10 ml, 25 ml)	Brand, Wertheim (GER)
Grease pencil	Dako, Hamburg (GER)
Handy tally counter	neoLab, Heidelberg (GER)
Humidity chamber	Chair of Tissue Engineering & Regenerative Medicine, Würzburg (GER)
Laboratory glass bottle (50 ml, 100 ml, 250 ml, 1000 ml, 2000 ml)	Schott, Mainz (GER)
Magnetic stirring bar	Hartenstein, Würzburg (GER)
Magnetic stirring bar retriever	Hartenstein, Würzburg (GER)
Object slide rack (glass or stainless steel)	Mercateo, München (GER)
Protective goggles	neoLab, Heidelberg (GER)
Racks for reaction vessels	neoLab, Heidelberg (GER)
Scalpel blade handles	Bayha, Tuttlingen (GER)
Small components for bioreactor (Luer lock adapters etc.)	Nordson Medical, Loveland (USA)
Spatula	Hartenstein, Würzburg (GER)
Spoon spatula	Hartenstein, Würzburg (GER)
Spray flasks (Ethanol 70 %)	Hartenstein, Würzburg (GER)
Stainless steel casting moulds for embedding tissue	Labonord, Mönchengladbach (GER)
Tweezers	Assistent, Sondheim (GER)

2.4 Chemicals and solutions

Table 5: List of chemicals and solutions

Chemical/Solution	Producer	Catalog No
3-(4,5-Dimethylthiazol-2-yl)-2,5-diphenyltetrazolium bromide (MTT)	Serva, Heidelberg (GER)	20395.01
Albumin fraction V (BSA)	Carl Roth, Karlsruhe (GER)	90604-29-8
Antibody Diluent	DCS Innovative Diagnostik-Systeme, Hamburg (GER)	AL120R500
BODIPY [®] 493/503	Invitrogen, Darmstadt (GER)	D3922
Calcium chloride	VWR, Darmstadt (GER)	1.02391.1000
Citric acid	VWR, Darmstadt (GER)	1.00244.1000
Curcumin in A-pPrOzi-A- and DMSO-formulation	provided by the laboratory of Prof. Dr. Luxenhofer, Würzburg (GER)	-
Deoxycholic acid sodium salt ($\geq 98\%$)	Carl Roth, Karlsruhe (GER)	3484.2
Descosept [®] AF	Dr. Schumacher GmbH, Karlsruhe (GER)	00-311-050
Dexamethasone	Sigma-Aldrich, München (GER)	D4902
Dimethyl sulfoxide (DMSO)	Sigma-Aldrich, München (GER)	D2438-50ML
DNase	Roche, Penzberg (GER)	10104159001
Donkey Serum	BIOZOL Diagnostika Vertrieb GmbH, Eching (GER)	ECL-ECS0217D
Doxorubicin (Adriamycin, 10 mM)	Selleckchem, München (GER)	S1208
DQ [™] Gelatin From Pig Skin, Fluorescein Conjugate	Thermo Fisher Scientific, Dreieich (GER)	D12054
Dulbecco's Modified Eagle Medium, high glucose, GlutaMAX [™] (DMEM)	Gibco [®] Life Technologies [™] , Darmstadt (GER)	10564011
DMEM/F-12	Gibco [®] Life Technologies [™] , Darmstadt (GER)	31331028
Entellan [®]	Merck, Darmstadt (GER)	1079600500
Eosin 1 % aqueous solution	Morphisto GmbH, Frankfurt a. M. (GER)	10177.01000
Ethanol 96%, denatured	Carl Roth, Karlsruhe (GER)	T171.4
Ethanol, absolute	Carl Roth, Karlsruhe (GER)	9065.4
Ethylenediaminetetraacetic acid (EDTA)	Sigma-Aldrich, München (GER)	E5134-1KG
Fetal Calf Serum	PAN Biotech, Aidenbach (GER)	P30-3306 Lot. P150508

Chemical/Solution	Producer	Catalog No
Ficoll-Paque Plus	GE Healthcare, Freiburg (GER)	17-1440-02
Fluoromount-G™ DAPI	SouthernBiotech, Birmingham (USA)	SBA-0100-20
Formaldehyde, phosphate buffered (4 %, pH7)	Carl Roth, Karlsruhe (GER)	P087.3
Glycerol Standard Solution, 2.5 mg/ml equivalent	Sigma-Aldrich, München (GER)	G7793
Glycine	Carl Roth, Karlsruhe (GER)	3908.3
Haematoxylin Solution acidic	Morphisto GmbH, Frankfurt a. M. (GER)	10231.01000
Hydrochloric acid (1M)	Carl Roth, Karlsruhe (GER)	K025.1
Hydrogen peroxide (30 %)	Sigma-Aldrich, München (GER)	216763-500ml
human IgG1 isotype control (InVivoMAB)	BioXcell, New Hampshire (USA)	BE0297
human insulin	Promocell, Heidelberg (GER)	C-52310
IBMX (3-Isobutyl-1-methylxanthine)	Serva, Heidelberg (GER)	26445
Incidin® plus	Ecolab, Monheim am Rhein (GER)	3011520
Indomethacin	Sigma-Aldrich, München (GER)	I7378
Isopropyl	Carl Roth, Karlsruhe (GER)	2316.5
McCoy's 5A (modified) medium	Gibco® Life Technologies™, Darmstadt (GER)	26600023
Methanol	Sigma-Aldrich, München (GER)	32213-2,5L
MK-1775	Selleckchem, München (GER)	S1525
Mowiol® 4-88	Sigma-Aldrich, München (GER)	81381-250G
Non-essential amino acids (NEAA)	Invitrogen, Darmstadt (GER)	11140-035
Oil Red O	Sigma-Aldrich, München (GER)	O0625
Paraffin	Carl Roth, Karlsruhe (GER)	6642.6
PGM-2 Basal Medium (PBM)	Lonza, Basel (CH)	PT-8202
Phosphate Buffered Saline (PBS with Mg and Ca)	Sigma-Aldrich, München (GER)	D8662
Phosphate Buffered Saline (PBS without Mg and Ca)	Sigma-Aldrich, München (GER)	D8537
RPMI-1640 medium with GUTAMAX™	Gibco® Life Technologies™, Darmstadt (GER)	61870010
Sodium chloride	Carl Roth, Karlsruhe (GER)	HN00.3
Sodium dodecyl sulfate	Carl Roth, Karlsruhe (GER)	CN30.3

Chemical/Solution	Producer	Catalog No
Sodium pyruvate (100 mM)	Invitrogen, Darmstadt (GER)	11360-039
TissueTek [®] O.C.T. [™] compound	Sakura, Staufen (GER)	4586
Total bile acids assay control	Diazyme Europe GmbH, Dresden (GER)	DZ042A-Con
Trastuzumab (Herceptin [®])	Apotheke Uniklinikum Würzburg Zytostatika-Abteilung, Würzburg (GER)	-
Tris base	Sigma-Aldrich, München (GER)	T6066-5kg
Triton [™] X-100	Sigma-Aldrich, München (GER)	X100-1L
Trypan blue, 0.4 %	Sigma-Aldrich, München (GER)	T8154-100ml
Trypsin 0,5% 10x	Invitrogen, Darmstadt (GER)	15400-054
Tween [®] -20	Sigma-Aldrich, München (GER)	P7949-500ml
Xylene (>98 %)	Carl Roth, Karlsruhe (GER)	9713.3

2.5 Media and solutions for cell culture

Table 6: List of media and solutions for cell culture

Medium/Solution		Composition
0.05 % Trypsin/EDTA working solution	10 ml	Trypsin/EDTA stock solution (10 x)
	90 ml	PBS ⁻ Stored at 4 °C.
Fibroblast culture medium	10 %	FBS in DMEM GlutaMAX [™]
hASC culture medium	10 %	FBS
	1 %	Pen/Strep in PBM
Induction medium for adipogenic differentiation	1 µM	Dexamethasone
	1.7 µM	human insulin
	500 µM	IBMX
	200 µM	Indomethacin in hASC culture medium or mixed medium
MCF-7 cell culture medium	10 %	FBS
	10 µg/ml	human insulin
	1 %	MEM non-essential amino acids
	1 mM	Sodium pyruvate in RPMI-1640 GlutaMAX [™]

Medium/Solution		Composition
MDA-MB-231 cell culture medium	10 %	FBS in RPMI-1640 GlutaMAX™
MTT reagent	3 mg/ml	MTT in ultrapure water pH=7.2 Sterile-filtered before use. Stored at -20 °C.
MTT solution	33,3 % (v/v)	MTT reagent in cell specific medium Prepared immediately before use.
PBS-/EDTA	500 µl 500 ml	0.5 M Na ₂ -EDTA 2H ₂ O PBS-
SKBR-3 cell culture medium	20 %	FBS, heat inactivated in McCoy's 5A (Modified) medium
Switched to:	20 % 1 mM	FBS, heat inactivated Sodium pyruvate in DMEM GlutaMAX™ medium

2.6 Chemicals and solutions for histology and immunohistochemistry

Table 7: List of chemicals and solutions for histology and immunohistochemistry

Chemical/Solution		Composition
Antibody diluent	5 % (w/v)	BSA in PBS-Solution Stored at 4 °C.
Blocking solution	5 % (v/v)	Donkey Serum in Antibody Diluent
Citrate buffer (10x stock solution)	42 g/l 17.6 g/l	Citric acid monohydrate Sodium hydroxide pellets in deionized water pH 6.0 Stored at RT.
Citrate buffer working solution	10 %	Citrate Buffer Stock Solution in deionized water
Embedding solution	0,1 %	DAPI in Mowiol® 4-88 Stored at -20°C.

Chemical/Solution		Composition
H ₂ O ₂ , 3 %	10 %	H ₂ O ₂ solution (30 %) in demineralized water
HCl /EtOH (H&E Staining)	6.85 % (v/v)	HCl, 1M in ethanol (50%) Stored at RT.
Oil Red O working solution	0.5 g 100 ml 66.6 ml	Oil Red O Isopropyl alcohol demineralized water filtered through a 0.2 µm filter before use
Permeabilisation solution	0.2 % (v/v)	Triton TM -X100 in PBS ⁻ Stored at 4°C
Washing buffer (PBS-T)	10 % (v/v) 0,5 % (v/v)	PBS Stock Tween [®] -20 In demineralized water Stored at RT.

2.7 Commercially available kits

Table 8: List of commercially available kits

Kit	Description	Producer
ADCC Reporter Bioassay	MOA-based bioassay to measure ADCC via FcγRIIIa function	Promega, Mannheim (GER) Cat. No. G7010
CellTiter-Glo® Luminescent Cell Viability Assay	Kit for the determination of cell viability based on metabolic activity (ATP quantification)	Promega, Mannheim (GER) Cat. No. G7570
M30 CytoDeath TM ELISA	Immunoassay for the quantitative determination of apoptosis in epithelial cells	Peviva, Bromma (SWE) Prod. No. 10900
Serum Triglyceride Determination Kit	Kit for the determination of triglyceride content in biological samples	Sigma-Aldrich, München (GER)
Super Vision 2 HRP Polymer-Kit	Kit containing secondary mouse- and rabbit-antibody, a polymer conjugated with horse radish peroxidase (HRP) against secondary antibody, DAB	DCS Innovative Diagnostik-Systeme, Hamburg (GER) Cat. No. PD000KIT

2.8 Antibodies

Table 9: List of antibodies

Antibodies for immunofluorescence stainings (IF) and DAB-based immunohistochemistry (DAB) are listed. * N/A: conc. is not provided by the producer.

Antibody	Clone	Host	Conc.	Applied Dilution	Producer
Alexa Fluor® 555 Donkey Anti-Mouse IgG	polyclonal	Donkey	2 mg/ml	1:400 (IF)	Life Technologies, Darmstadt (GER) Cat. No. A-31570
Alexa Fluor® 647 Donkey Anti-Rabbit IgG	polyclonal	Donkey	2 mg/ml	1:400 (IF)	Life Technologies, Darmstadt (GER) Cat. No. A-31573
Beta-Catenin	E247	Rabbit	N/A*	1:100 (IF)	abcam, Cambridge (UK) Cat No. ab32572
CD45	2B11 + PD7/26	Mouse	385 µg/ml	1:100 (IF)	Agilent DAKO (GER) Cat. No. M0701
Collagen IV	polyclonal	Rabbit	1 mg/ml	1:100 (IF)	abcam, Cambridge (UK) Cat No. ab6586
E-Cadherin	36/E-Cadherin	Mouse	250 µg/ml	1:100 (IF)	BD Transduction Laboratories, Heidelberg (GER) Cat No. 610181
ER	6F11	Mouse	N/A*	1:20 (DAB)	abcam, Cambridge (UK) Cat. No. ab93021
FAP	EPR20021	Rabbit	683 µg/ml	1:100 (IF)	abcam, Cambridge (UK) Cat. No. ab207178
HER2	polyclonal	Rabbit	N/A*	1:75 (DAB)	Cell Signaling (USA) Cat. No 2242S
Ki67	SP6	Rabbit	N/A*	1:100 (IF)	abcam, Cambridge (UK) Cat No. ab16667
Muc-1	polyclonal	Rabbit	200 µg/ml	1:100 (IF)	Novus Biologicals (USA) Car. No NB120-15481
Pan cytokeratin	C-11+PCK-26+CY-90+KS-1A3+M20+A53-B/A2	Mouse	N/A*	1:50 (IF)	Sigma-Aldrich, München (GER) Cat. No. C 2562-2ML
Vimentin	EPR3776	Rabbit	153 µg/ml	1:100 (IF)	abcam, Cambridge (UK) Cat. No. ab92547
Vimentin	V9	Mouse	300 µg/ml	1:100 (IF)	abcam, Cambridge (UK) Cat. No. ab8069

2.9 Biological material

2.9.1 Cell lines

Table 10: List of cell lines

Cell line	Description	DSMZ No	Source
MCF-7	Breast adenocarcinoma cell line established in 1970 from the pleural effusion of a 69-year-old Caucasian woman with metastatic mammary carcinoma after radio- and hormone-therapy	ACC 115	DSMZ, Braunschweig (GER)
MDA-MB-231	Breast carcinoma cell line established in 1973 from the pleural effusion of a 51-year-old Caucasian woman with breast carcinoma	ACC 732	ATCC, Manassas (USA)
SKBR-3	Breast carcinoma cell line established in 1970 from the pleural effusion of a 43-year-old woman with breast carcinoma	ACC 736	DSMZ, Braunschweig (GER)

MCF-7 is a breast adenocarcinoma cell line that grows adherently in a monolayer and shows epithelial characteristics. The doubling time of this cell line is between 30 and 72 hours (h). MCF-7 cells are ER-positive and carry mutations in the *PIK3CA* gene (c.1633G>A, heterozygous) and the *CDKN2A* gene (c.1_471del471 homozygous) (Bamford *et al.*, 2004).

MDA-MB-231 is a breast carcinoma cell line with a doubling time of 25-30 h. The epithelial cells grow adherently in monolayers and carry mutations in the *BRAF* gene (c.1391G>T, heterozygous), the *CDKN2A* gene (c.1_471del471, homozygous), the *KRAS* gene (c.38G>A, heterozygous) and the *p53* gene (c.839G>A, homozygous) (Bamford *et al.*, 2004).

SKBR-3 is a breast carcinoma cell line with a doubling time of 48-72 h that grows adherently in a monolayer and changes from a rounded shape after seeding to an epithelial-like phenotype during culture. The cell line overexpresses the HER2/c-erb-2 gene product.

2.9.2 Porcine material

For 3D cell culture, the biological matrix SISmuc was used as a scaffold. The SISmuc is a decellularised segment of the jejunum of the German landrace pig (Deutsche Landrasse) that comprises the small intestinal submucosa (SIS) and the mucosa (muc) and is derived from the biological vascularized scaffold BioVaSc®. It is composed of a dense layer of cross-linked collagen and elastin fibers. Protocols for the preparation of the BioVaSc® have been published previously (Schultheiss *et al.*, 2005; Linke *et al.*, 2007; Mertsching *et al.*, 2009). For the preparation of SISmuc, the mesentery with the vascular tree is removed after complete

decellularisation, thereby preserving the mucosal part with its villi, crypts and structures of the basement membrane (Stratmann *et al.*, 2014).

2.9.3 Human material

Fibroblasts were isolated from prepuces of donors with different ages according to the approval by the Institutional Ethics Committee of the University Hospital Würzburg (approval number 182/10).

Peripheral blood samples for the isolation of PBMCs were obtained under informed consent according to ethical approval granted by the Institutional Ethics Committee of the University Hospital Würzburg (approval number 182/10) from Bavarian Red Cross blood donation service (Blutspendedienst des Bayerischen Roten Kreuzes, München, GER).

hASCs were kindly provided by the group of Prof. Dr. Blunk (Klinik und Poliklinik für Unfall-, Hand-, Plastische und Wiederherstellungschirurgie, University Hospital Würzburg).

2.9.4 Xenograft material

Xenograft material was kindly provided by Oncotest GmbH (Charles River).

2.10 Software

Table 11: List of software

Software	Purpose	Manufacturer
BZ Analyzer	Software for microscopy	Keyence Corporation (GER)
Corel Draw X7	Image processing and figure composition	Corel™ (CA)
GraphPad Prism 5	Graph composition	GraphPad Software Inc. (USA)
ImageJ (Fiji)	Image processing	Wayne Rasband, NIH (USA)
Microsoft Excel 2013	Spreadsheet analysis	Microsoft® (USA)
Microsoft Word 2013	Text processing	Microsoft® (USA)
Microsoft Power Point 2013	Figure composition	Microsoft® (USA)
Origin Pro	Evaluation of M30 CytoDeath™ ELISA data	OriginLab® (USA)
Pressure control	Control of the pumping speed in bioreactor boards	Chair of Tissue Engineering and Regenerative Medicine University of Würzburg (GER)
R 3.3.0	Statistical analysis	R Foundation (AT)

3 Methods

3.1 General cell culture methods

All cell culture methods were performed under sterile conditions in a safety cabinet. All disposable materials were sterile and the laboratory materials as well as all solutions were sterilized by autoclaving or by sterile-filtering, respectively. The cells were cultured in an incubator at 37 °C, a CO₂ concentration of 5 % and under steam saturated conditions unless otherwise mentioned. Cells were cultured without the use of antibiotics and daily checked by microscopy for their morphology, growth and possible microbiological contamination. Cell cultures were regularly checked for mycoplasma contamination.

3.1.1 Culturing of cell lines

MCF-7 cells were cultured in RPMI-1640 GlutaMAXTM medium containing 10 % (v/v) FBS, 10 µg/ml human insulin, 1 mM sodium pyruvate and 1 % MEM non-essential amino acids in T75 culture flasks. They were seeded at a density of $1\text{--}2 \times 10^6/75\text{ cm}^2$ and reached a cell number of $7\text{--}10 \times 10^6$ cells/75 cm² at a confluence of 70–90 %.

MDA-MB-231 cells were cultured in RPMI-1640 GlutaMAXTM medium containing 10 % (v/v) FBS. Cells were seeded at a density of $1\text{--}2 \times 10^6$ cells/75 cm² and reached cell numbers of $4\text{--}6 \times 10^6$ cells/75 cm² at a confluence of 70–90 %.

SKBR-3 cells were initially cultured in McCoy's 5A medium containing 20 % (v/v) heat-inactivated FBS. After media testing for the optimization of 3D cell culture models with SKBR-3 cells medium was changed to DMEM GlutaMAXTM medium containing 20 % (v/v) heat-inactivated FBS and 1 mM sodium pyruvate. Cells were seeded at a density of $2\text{--}3 \times 10^6$ cells/75 cm² and reached cell numbers of $3\text{--}7 \times 10^6$ cells/75 cm² at a confluence of 70–90 %.

3.1.1.1 Freezing and thawing of cells

Cells were delivered in a cryo tube on dry ice by the producer. The cells were thawed by gently swaying the cryo tube in the water bath at 37 °C until only a small piece of ice remained in the tube. The cell suspension was then immediately transferred to a 50 ml centrifuge tube containing 10 ml of pre-warmed cell-specific medium and centrifuged for 5 minutes (min) at 1200 rpm. Afterwards, the supernatant was aspirated and the cell pellet was resuspended in 10 ml fresh pre-warmed medium and added to a cell culture flask. On the following day, the medium was changed. Thawed cells were passaged at least once before they were used for experiments.

For the preservation of a cell stock in a low passage number, cells were frozen at 1×10^6 /ml in cryo tubes. After expansion, cells were detached from the culture flask by trypsinization (see section 3.1.1.2). Cells were counted and adjusted to 1×10^6 cells/ml cell culture freezing medium which was composed of the cell culture-specific medium and additional 10 % FBS as well as 10 % DMSO. This cell suspension was distributed to cryo tubes at 1 ml per tube and inserted into the freezing container “Mr. Frosty” which ensures a gentle freezing process of the cells by a

temperature fall of 1 °C per min. This container was immediately put into the -80 °C freezer and the cryo tubes containing the frozen cells were transferred to -180 °C in the liquid nitrogen tank the next day.

3.1.1.2 Passaging cells

All cell lines were passaged twice a week at a confluence of 70–90 %. At first, the medium was aspirated and cells were washed with PBS⁻/EDTA to remove remnants of the serum. Cells were then incubated with 0.05 % Trypsin/EDTA solution at 37 °C for 3–5 min. The detachment of the cells was confirmed by microscopy and the trypsin reaction was stopped by adding FBS. Via pipetting the suspension up and down for several times, remaining cell clusters were disrupted and the resulting single cell suspension was then transferred to a 50 ml centrifuge tube. The suspension was centrifuged at 1200 rpm for 5 min and the supernatant was removed by aspiration. After resuspending the cells in fresh medium and counting the cells, they were reseeded at their respective densities (see section 3.1.1). All cell lines were used until passage 20.

3.1.1.3 Determination of cell number and viability

Cell number and viability was determined with the help of trypan blue staining. For this, an aliquot of the cell suspension was mixed 1:2 with 0.4 % trypan blue solution. 10 µl of this mixture were pipetted into a Neubauer counting chamber and cells were counted in all four quadrants under the microscope. Living cells appeared colourless whereas dead cells were coloured in blue and could therefore be discriminated by the staining.

Cell number was calculated as follows:

$$\text{Mean}_{LC} \times \text{factor of the chamber} \times \text{dilution factor} = \text{living cells/ml}$$

Mean_{LC}: mean of living cells per quadrant

Factor of the chamber: 10⁴

Dilution factor: 2

Cell viability was determined as the quotient of living cell number to total cell number.

3.1.2 Culturing of primary cells

3.1.2.1 PBMCs

PBMCs were isolated from peripheral blood samples by ficoll gradient centrifugation (GE Healthcare, Freiburg, Germany). Briefly, whole blood was diluted 1:2 with PBS⁻ and slowly and carefully pipetted on top of the density gradient medium. After centrifugation at 400 x g for 35 min with brakes off, the buffy coat was harvested into a fresh centrifuge tube and washed twice with PBS⁻ (centrifugation at 200 x g for 10 min with brakes on). Cell pellets from the same donor were combined and resuspended in a defined volume of PBS depending on the pellet size. The total number of PBMCs and viability was determined by counting in a Neubauer chamber. After a last centrifugation step, the cell pellet was resuspended in the desired volume of prechilled

cryopreservation medium (10 % DMSO, 90% FBS heat-inactivated) and cells were cryopreserved until use.

3.1.2.2 Fibroblasts

Human primary fibroblasts were isolated from prepuces that have been stored in PBS⁻ 1% (v/v) Pen/Strep for transport. Before removing fat and connective tissue, the prepuces were washed three times with PBS⁺. After cutting the tissue into pieces of 2–3mm with a scalpel and washing again three times with PBS⁺ they were incubated overnight with dispase II solution (2 U/ml, 5–10 ml for 6 cm²) at 4°C in a Petri dish. A sterile control of the transport medium was taken and incubated at 37°C and 5% CO₂ in a T25 cell culture flask. The next day, the epidermal part was removed using sterile tweezers, the dermis was washed with PBS⁻ and cut into pieces of 1–2mm width with a scalpel prior to incubation for 45 min at 37°C with collagenase solution (500 U/ml, 10 ml). After centrifugation at 1200 rpm for 5 min, the remaining pellet was resuspended in 10 ml fibroblast culture medium followed by an additional centrifugation step. After resuspending the pellet in 2 ml fibroblast culture medium with 1% (v/v) Pen/Strep, the tissue fragments were transferred into a T75 cell culture flask allowing the dermis pieces to adhere. The following day, 3–7 ml of prewarmed fibroblast culture medium with 1% Pen/Strep were slowly added to prevent detachment of dermis pieces from the bottom of the culture flask. A medium change was performed every 2–3 days and after 7 days of culture, the antibiotics in the culture medium were omitted. The fibroblasts growing out of the dermis tissue were allowed to reach a confluency about 80–90% before passaging and used no longer than passage 5.

3.1.2.3 hASCs

hASCs were kindly provided by the group of Prof. Dr. Blunk (Klinik und Poliklinik für Unfall-, Hand-, Plastische und Wiederherstellungschirurgie, University Hospital Würzburg). Briefly, for isolation of hASCs from human adipose tissue, abdominal lipoaspirates or fat flaps from healthy female donors were digested enzymatically with collagenase NB4. After removal of the mature adipocytes, the remaining stromal vascular fraction (SVF) was directly cryopreserved or seeded in tissue culture flasks in DMEM/F-12 supplemented with 10 % FBS and 1 % Pen/Strep for cell expansion.

For adipogenic differentiation of the hASCs, cells in 2D culture were seeded at a density of 25,000 cells/cm² and cultured in basal medium without inducers for two days before the adipogenic differentiation was induced. The day of induction was referred to as day 0 and adipogenic differentiation was induced by replacing the basal medium with induction medium (basal medium containing 1.7 µM insulin, 1 µM dexamethasone, 500 µM IBMX and 200 µM indomethacin). Cells were treated with induction medium for 9 days until harvest. Non-induced control groups were cultured in basal medium during the whole experiment. The respective media in all groups were exchanged every second day.

3.2 2D cell culture

In order to compare 3D tumour models with conventional models, drug testing experiments were performed in 2D in parallel. Cells were seeded as described in Table 12 at day 0. For immunohistochemical characterization of the cell lines, the cells were directly grown on glass cover slips. For this, autoclaved round glass cover slips were transferred to a 24 well plate and seeded with cells. Cells were cultured to a confluence of approx. 70 % and then fixed with 4 % PFA for immunohistochemical staining (see section 3.7.1). For all 2D experiments with compound testing, cells were cultured for a period of 4 days and treated according to the respective 3D experiments.

Table 12: Cell seeding conditions for different assays

Read out parameter	Type of tissue culture plate	Seeding density (cells/well)	Volume of medium (ml)
Immunofluorescence staining	24 well plate with glass cover slips	SKBR-3: $5 \cdot 10^4$ MCF-7: $1 \cdot 10^5$ MDA-MB-231: $5 \cdot 10^4$	1.0
M30 CytoDeath TM	12 well plate	SKBR-3: $8 \cdot 10^4$ MCF-7: $9 \cdot 10^4$ MDA-MB-231: $3.5 \cdot 10^4$	0.8
Proliferation	12 well plate with glass cover slips	SKBR-3: $8 \cdot 10^4$ MCF-7: $9 \cdot 10^4$ MDA-MB-231: $3.5 \cdot 10^4$	0.8
MTT assay	12 well plate	SKBR-3: $8 \cdot 10^4$ MCF-7: $9 \cdot 10^4$ MDA-MB-231: $3.5 \cdot 10^4$	0.8

3.3 3D cell culture

3.3.1 Production of scaffold SISmuc

The 3D human mamma carcinoma test system was generated on the basis of SISmuc. For the production of this biological scaffold, the small intestinal segment was explanted from 8–11 weeks old pigs weighing 15–25 kg. All animals received humane care according to the Guide for Care and Use of Laboratory Animals published by the National Institutes of Health (NIH publication no. 85–23, revised 1996) after approval from the institutional animal protection board. Explantation was performed at the Center for Experimental Molecular Medicine (ZEMM, Würzburg). Before explanting the small intestinal segment with its supplying artery and vein, the pigs were anaesthetized, heparinized and sacrificed with an anaesthesia overdose. After explantation, the jejunum segments were stored in PBS containing 1 % (v/v) gentamycin at 4 °C for a maximum of one day until the tissue was decellularised (Schanz, 2007; Pusch, 2009). The decellularisation of the intestinal section was performed at the Chair of Tissue Engineering according to previously published protocols that had been adapted (Schultheiss *et al.*, 2005; Linke

et al., 2007). Briefly, the lumen as well as the vascular system were thoroughly rinsed with PBS⁻ until free of faeces and blood. After overnight incubation of the intestinal segment filled with PBS⁻ (with 1 % Pen/Strep) at 4 °C on a rocking platform shaker, the lumen as well as the vascular system were rinsed with 500 ml of PBS⁻ to remove the antibiotics. Subsequently, the lumen was filled with a solution of sodium deoxycholate (22.5 g/l) and 2 l of the same solution were pumped through the cannulated vascular system with a pressure of maximum 80 mmHg. The pumping speed was regulated via a pressure sensor. The pump was stopped and the sodium deoxycholate solution inside the lumen was replaced after 500 ml of solution having been pumped through the vascular system. Afterwards, lumen and vascular system were rinsed accordingly with PBS⁻ (2 l through the vascular system) with a maximum pressure of 100 mmHg and afterwards filled with sodium deoxycholate solution and incubated overnight on a rocking platform shaker at 4 °C. The next day, lumen and vascular system were rinsed with PBS⁻ (3 l through the vascular system) with a maximum pressure of 100 mmHg, before the serosa together with the vascular system was removed from the submucosa and mucosa. In a last step, the decellularised scaffold was cut into pieces of 8–10 cm, rinsed three times with PBS⁻ (with 1 % Pen/Strep) and incubated overnight in DNase I solution (300 mg/ml in PBS⁺ with Pen/Strep) at 4 °C. Before gamma-sterilization (25 kGy, BBF Sterilisationsservice GmbH, Rommelshausen) on the next day, the scaffold pieces were rinsed three times with PBS⁻. After sterilization, a sample of the buffer solution was withdrawn for determination of residual bile acid, PBS⁻ solution was changed and the SIS muc was stored at 4 °C until use.

As a quality control, successful decellularisation of SIS muc was controlled by H&E staining as well as DNA staining according to Feulgen. Proper removal of sodium deoxycholate was checked with the help of a total bile acids assay kit (Diazyme Europe GmbH, Dresden) allowing the quantitative determination of residual bile acid deriving from deoxycholic acid.

3.3.2 Generation of 3D tumour models

For 3D culture, cells were seeded on the luminal side of the SIS muc and cultured for 14 days. At first, SIS muc had to be fixed into cell crowns. Each cell crown was composed of two metal rings—one smaller inner ring and a larger outer ring with little stands on it to prevent the matrix from touching the cell culture plate. The fixation of SIS muc into the cell crown is visualized in Figure 1. A piece of SIS muc was spread onto a petri dish and a small stripe was cut off along one side (Figure 1 A, B). Then the SIS muc was opened and cut into square pieces (Figure 1 C, D). These squares were then pulled over the inner ring of the cell crown with the luminal side facing downwards to the inside of the inner ring (Figure 1 E, F). The outer ring of the cell crown was then placed over the inner ring in order to fix the piece of matrix (Figure 1 G, H). After turning the cell crown upside down, it was transferred to a well of a 12 well plate (Figure 1 I) and covered with cell-specific medium. After incubating the cell crowns overnight at 37 °C in the incubator so that the matrix could absorb medium, they were ready to be seeded with cells. 1×10^5 cells were seeded into the inner ring onto the luminal side of the SIS muc in a volume of 500 μ l of medium per cell crown. After incubating the seeded cell crowns in the incubator for 2 h in order to allow cells to attach to the matrix, each well was filled up with additional 2 ml medium.

If smaller PEEK cell crowns were used, 4×10^4 cells in 250 μ l of medium were seeded and cell crowns were filled up with 1.45 ml of medium after incubation for 2 h (37 °C, 5 % CO₂).

For coculture experiments with fibroblasts, 1×10^5 cells from each cell type were simultaneously seeded and mixed medium (1:2) was used for the coculture models.

For coculture experiments with hASCs, tumour cells and hASCs were simultaneously seeded in mixed medium (1:2) containing inducers for adipogenic differentiation.

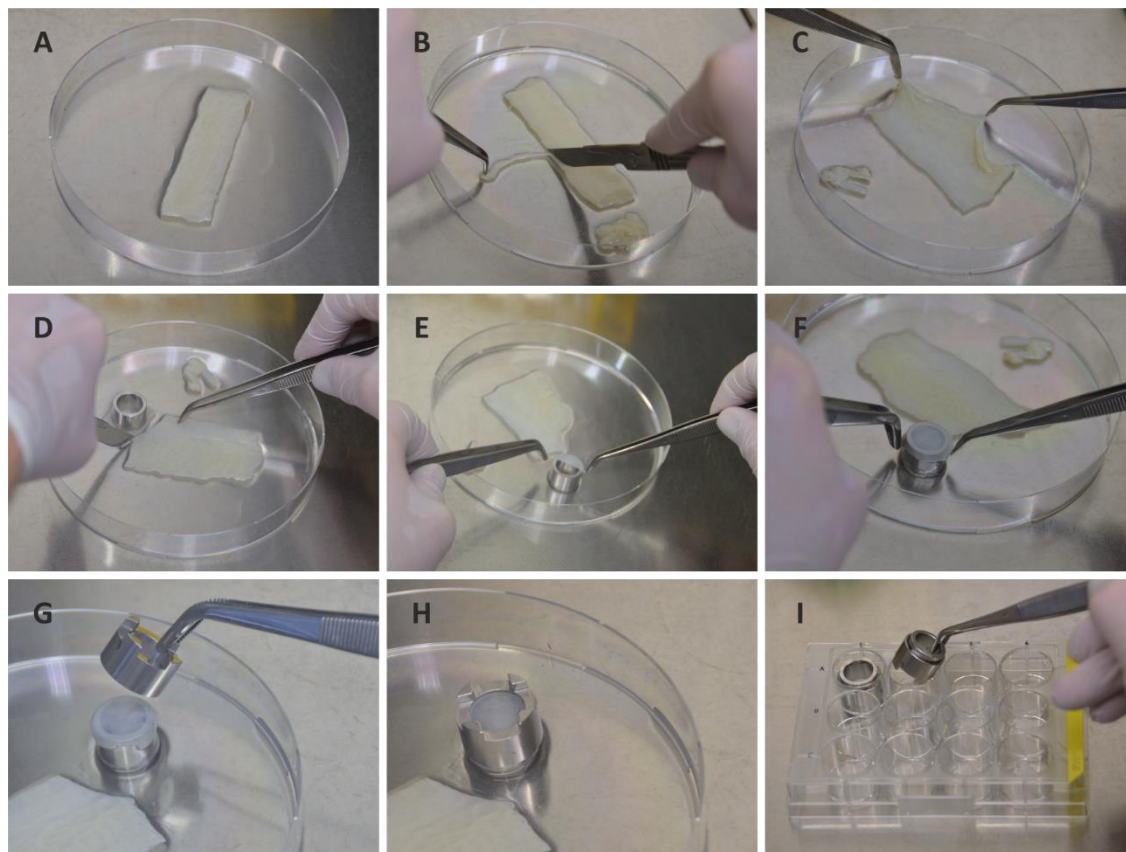


Figure 1: Insertion of SISmuc into cell crowns

A: SISmuc spread on a petri dish B: Cutting off a small strip at the side C: Opened SISmuc with its luminal side facing upwards D: Cutting the SISmuc into squares E + F: Placing the SISmuc onto the inner ring of the cell crown with the luminal side facing downwards G + H: Fixing the SISmuc by placing the outer ring of the cell crown over the inner ring I: Transfer of cell crowns into a 12 well plate.

3.3.3 Static culture of cells on SISmuc

The medium was changed every 2–3 days. If static 3D models were treated with different therapeutics and/or other cells, this treatment was applied in the last 48-72 h of culture depending on the therapy (see section 3.3.6). Inhibitors were exchanged with a complete medium change after the first 48 h of treatment.

3.3.4 Culture of SKBR-3 cells on SISmuc on an orbital shaker

Seeding of the SISmuc fixed into cell crowns with SKBR-3 was performed as described for static culture conditions. After 3 h of incubation, wells were filled up only with an additional 1.2 ml of

medium to prevent leaking of the medium and the plate was immediately placed on an orbital shaker inside the incubator (100 rpm). Medium was changed every 2–3 days.

3.3.5 Dynamic culture of cells on SISmuc in a flow bioreactor

For the dynamic 3D culture, the pre-seeded SISmuc had to be inserted into a flow bioreactor system. This system is composed of the reactor body with a small window where the matrix is inserted and a medium reservoir bottle which is connected to the reactor body via silicone tubes.

All parts of the bioreactor were autoclaved before the matrix was inserted and the piece of SISmuc was seeded with cells (as described in section 3.3.2) 2 days before the dynamic culture was started. After the matrix was unfixed from the cell crown it was spread with its seeded part over the small window in one half of the bioreactor body and was covered with the other half of the bioreactor body (Figure 2). Then, the two halves were screwed together tightly, thereby creating two chambers with a volumetric capacity of approx. 2 ml each, separated by the seeded matrix. After the silicone tubes were attached to the reactor body and an air filter was added to the medium reservoir bottle for gas exchange, the bottle was filled with 40 ml of cell-specific medium containing 1 % Pen/Strep. Subsequently, the pump tubing cassette was attached to the pumping tube, the reactor system was placed into the incubator and the pump tubing cassette was attached to the peristaltic pump (Figure 2 B). Medium was pumped through the tubes with constant flow and pumping speed was set to 3 rpm which corresponds to a medium flow of 2.5 ml/min. Cells were dynamically cultured for 14 days and medium was exchanged after 7 days of dynamic culture.

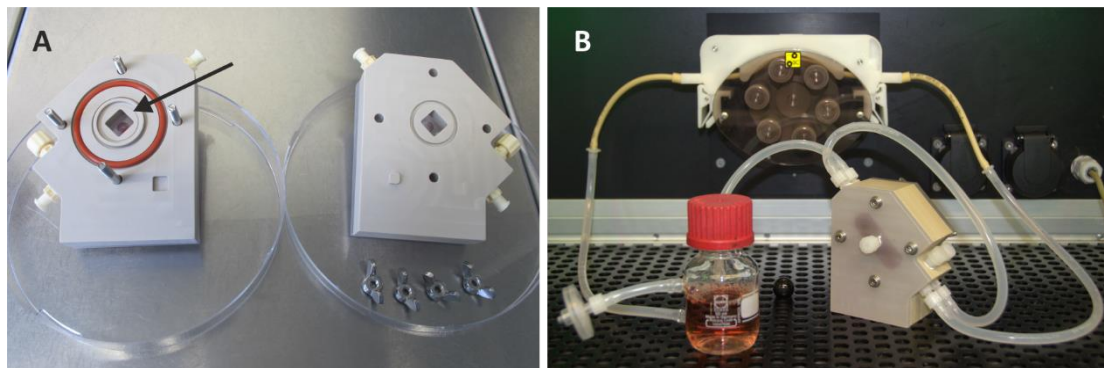


Figure 2: Dynamic cell culture in a flow bioreactor

A: Bioreactor body halves. Arrow indicates the window where seeded part of the SISmuc is placed. B: Bioreactor system with reactor body, reservoir bottle, connecting tubes and peristaltic pump.

3.3.6 Treatment of 3D tumour models

3.3.6.1 Treatment with trastuzumab

Static 3D tumour models of all 3 cell lines as well as conventional 2D cultures were treated with trastuzumab in different concentrations for the last 48 h of culture. Before and during treatment, supernatant samples for the determination of apoptosis were collected and on the last day of

culture, 3D models or 2D cultures were either fixed for histological and immunohistological analysis or an MTT test was performed to determine cell viability.

In order to investigate if ADCC is a MOA that can be measured in the 3D tumour models, an ADCC Reporter Bioassay (Promega, Mannheim) was adapted for 3D cell culture. Briefly, at day 13 of culture tumour models in small cell crowns were treated with different concentrations of trastuzumab and freshly thawed ADCC effector cells in assay buffer were added to the inner compartment of the cell crown at a concentration of 1.5×10^6 cells per cell crown. After 24 h of incubation (37 °C, 5 % CO₂), tumour models were allowed to reach RT for 15 min, 250 µl of the BioGlo reagent were added to the inner compartment of each cell crown and luminescence signal with an integration time of 0.5 sec/well was measured at the microplate reader. Tumour models without effector cells as well as models with effector cells but without trastuzumab were included as controls. Fold of induction of ADCC was calculated as follows:

$$\text{Fold of induction of ADCC} = \frac{RLU \text{ (induced-background)}}{RLU \text{ (no antibody ctrl-background)}}$$

Furthermore an ADCC assay based on the addition of PBMCs was established. For the last 48 h of culture, static tumour models were treated with different concentrations of trastuzumab and 3×10^6 PBMCs that had been thawed the day before and allowed to rest overnight (37 °C, 5 % CO₂ in RPMI GlutaMAXTM medium + 10 % heat-inactivated FBS). Samples for the determination of apoptosis were collected before and during treatment and at the last day of culture the tissue models were fixed and paraffin embedded for histological and immunohistological analysis. Tumour models without PBMCs as well as models with PBMCs but without trastuzumab and an isotype control for trastuzumab were included as controls.

3.3.6.2 Treatment with curcumin in nanoformulation with A-pPrOzi-A

Static tumour models as well as conventional 2D cultures of MDA-MB-231 were treated for 72 h with different concentrations of curcumin formulated with the copolymer A-pPrOzi-A or in DMSO as a control. After 48 h of treatment, a medium change with the addition of fresh curcumin was performed. Cells and tissues were either fixed for histological analysis or an MTT assay for determination of viability was performed. Nanoformulations of curcumin in the copolymer A-pPrOzi-A were kindly provided by Michael Lübtow from the laboratory of Prof. Dr. Luxenhofer (Functional Polymer Materials, Chair for Advanced Materials Synthesis, Department of Chemistry and Pharmacy and Bavarian Polymer Institute, Julius-Maximilians-Universität Würzburg).

3.3.6.3 Combination therapy with doxorubicin and MK-1775

Static tumour models as well as conventional 2D cultures of MDA-MB-231 were treated for 72 h with 0.1 µM or 0.5 µM doxorubicin alone or in combination with 0.5 µM MK-1775 or with 0.5 µM MK-1775 alone. After 48 h of treatment, a medium change with the addition of fresh inhibitors was performed. Supernatant samples for the determination of apoptosis were collected before and during treatment and on the last day of culture cells and tissues were either fixed for

histological and immunohistological analysis or an MTT assay for determination of viability was performed.

3.3.6.4 Treatment with ROR1-CAR-T cells

Static and dynamic tumour models of MDA-MB-231 cells were treated with receptor tyrosine kinase-like orphan receptor 1 (ROR1)-specific CAR CD8⁺ cells or a combination of CD4⁺ and CD8⁺ T cells. These ROR1-CAR T cells as well as untransduced control T cells were generated and kindly provided by the group of Dr. Michael Hudecek (Department of Medicine II - Hematology and Medical Oncology, University Hospital Würzburg). Briefly, purified CD8⁺, CD45RO⁺, CD62⁺ memory and CD4⁺ cells, which were isolated from PBMCs of healthy donors, were activated with anti-CD3/CD28 beads. The next day, they were lentivirally transduced with a CAR construct based on the monoclonal antibody R12 with a T2A element and truncated EGFR (EGFRt) (Hudecek *et al.*, 2010; Hudecek *et al.*, 2013). Ten to 14 days after transduction, the EGFRt-positive cells could be selected and propagated for usage (Riddell & Greenberg, 1990).

In the 3D static tumour model, CD8⁺ ROR1-CAR T cell therapy was applied in different dosages from day 11 of tumour model culture for 72 h. Supernatant samples for determination of apoptosis were taken before as well as 6, 24, 48 and 72 h after T cell addition.

In the 3D dynamic tumour model, a mixture of CD4⁺ and CD8⁺ ROR1-CAR T cells (5×10^5 each) was added directly to the medium reservoir of the bioreactor after 14 d of dynamic culture for 5 days. A small magnetic stirring bar prevented the T cells from sedimentation, thereby ensuring that the T cells could enter the tubing system and reach the tumour model. Supernatant samples for the determination of apoptosis as well as cytokine secretion were taken via the sampling device before and during treatment every 24 h.

At the last day of treatment in static as well as dynamic experiments, the T cells in the remaining supernatant were analysed for activation markers via flow cytometry by the Hudecek group. The tumour tissue was fixed and paraffin embedded for histological and immunohistochemical analysis.

As a control, CD4⁺ and/or CD8⁺ untransduced control T cells were included in each experiment.

3.4 Cell viability assays

3.4.1 CellTiter-Glo® luminescent cell viability assay

For the investigation of cell viability in 2D cultures, the CellTiter-Glo® Luminescent Cell Viability assay (Promega, Mannheim) was performed. This assay is based on viability measurement by quantifying the amount of ATP per well. For this, cells were seeded in a 96 well plate at 1.5×10^4 (MCF-7), 6×10^3 cells/well (MDA-MB-231) or 1.5×10^4 cells/well (SKBR-3) in 200 µl medium. A medium control without any cells was added to obtain a value for background luminescence. After one day of culture, cells were treated with the test substance for 3 days in triplicates. On day 4, CellTiter-Glo® buffer was mixed with CellTiter-Glo® substrate and

equilibrated at RT. Medium was aspirated and cells were washed with PBS⁻. Afterwards, 100 µl/well of cell-specific medium and 100 µl/well of the CellTiter-Glo® reagent were added. After shaking the plate for 2 min and incubating for 10 min, the luminescent signal was measured in the microplate reader with an integration time of 1000 ms. The average of the measured background values was subtracted from the mean of the triplicates.

3.4.2 Quantitative MTT assay

MTT (3-(4,5-dimethylthiazol-2-yl)-2,5-diphenyltetrazolium bromide) is a yellow tetrazolium salt that changes to a purple solid formazan when it is metabolically reduced. Its reduction is dependent on enzymes of the endoplasmic reticulum and the pyridine nucleotides NADH (nicotinamide adenine dinucleotide) and NADPH (nicotinamide adenine dinucleotide phosphate); and to a far lesser extent on succinate. All viable cells reduce MTT and the formed formazan is captured inside the cell.

To determine cell viability of the cells cultured under 2D or 3D conditions after treatment, quantitative MTT was performed. For this purpose, the medium was aspirated and replaced with MTT solution. After incubation in the incubator for 3 h, the formazan was repeatedly extracted with isopropanol/0.04 N HCl. Extracts from one sample were pooled and absorption was measured at a wavelength of 570 nm and a reference wavelength of 630 nm. Cell viability was calculated with the following equation:

$$\text{Cell viability} = \frac{\text{Absorption (treated sample)}}{\text{Absorption (untreated sample)}} \times 100 \%$$

3.5 Measurement of apoptosis

For the evaluation of the effectiveness of treatments, apoptosis was determined using the M30 CytoDeath™ ELISA (Peviva). This ELISA is based on the antibody M30 which binds to K18Asp396 neo-epitope, a caspase cleavage site in cytokeratin18 which is found in early apoptosis of epithelial cells. Caspase-cleaved cytokeratin18 (ccK18) is released from apoptotic bodies during secondary necrosis and can therefore also be measured in cell culture supernatants.

ELISAs were performed according to the manufacturer's instruction using supernatants that had been collected before and during treatment of cells in 2D or 3D culture. The supernatants were stored at -80 °C until use.

The microtiter plate provided in the kit is coated with cytokeratin18 antibody. After the addition of 25 µl/ well of the diluted supernatants and the standards provided in the kit in duplicates, 75 µl of M30 antibody conjugated to HRP were added and the plate was sealed and shaken for 4 h at RT. Afterwards, the plate was washed with 200 µl/well washing buffer five times and 200 µl/well of the HRP substrate were added. The plate was then incubated in the dark for 20 min and 50 µl/well of the stop solution were added. After shaking the plate for 30 sec in the microplate reader, the absorbance was measured at 450 nm.

For interpretation, the standards were used to define a sigmoidal standard curve with OriginPro 8.6 and the concentration of ccK18 in each well was determined in units/l (U/l). The arithmetic mean of duplicates was calculated. For final evaluation of 3D experiments, the measured ccK18 concentration of each treated sample was normalized to its corresponding baseline ccK18 concentration directly before start of the treatment. Subsequently, the fold increase of apoptosis was calculated as a quotient of these values to the untreated control. For 2D culture, this quotient was calculated directly from ccK18 concentrations.

3.6 Determination of triglyceride and DNA content of hASCs

Quantitative analysis of intracellular lipid accumulation during differentiation was performed by using the Serum Triglyceride Determination Kit (Sigma-Aldrich, München). For the determination of triglyceride content, cells of 2D monolayers were washed twice with PBS, harvested in 0.5 % aqueous thesit solution and sonicated. Intracellular triglyceride content was determined in three biological replicates. The assay was carried out according to manufacturer's instructions. It is based on the enzymatic hydrolysis of the intracellular triglycerides to glycerol and free fatty acids by lipase. Measurement of the produced glycerol is performed by coupled enzyme reactions followed by formation of a quinoneimine dye that shows an absorbance maximum at 540 nm. The absorbance of the samples was measured with a spectrophotometric MRX microplate reader (Dynatech Laboratories, Chantilly, Virginia, USA) at 540 nm. Triglyceride concentrations of the samples were determined by correlating measured absorbances to glycerol contents using standard dilutions of a glycerol standard. Calculated triglyceride contents were normalized to the DNA content of the samples, which was determined as described in the following: DNA quantification was also performed with three biological replicates. Cells of 2D culture were washed twice with PBS, harvested in phosphate-saline-buffer (50 mM phosphate buffer, 2 mM Na₂-EDTA*2 H₂O, 2 M NaCl, pH 7.4) and subsequently sonicated with an ultrasonic homogenizer (Sonopuls, Bandelin electronic, Berlin). DNA content was determined by using the intercalating fluorescence dye Hoechst 33258. The fluorescence intensities were measured with a fluorescence spectrometer at an excitation wavelength of 365 nm and an emission wavelength of 458 nm. DNA content was calculated by correlating measured fluorescence intensities to the intensities of known DNA contents using standard dilutions of double-stranded DNA from calf thymus.

3.7 Histology

3.7.1 Fixation of cells grown on glass coverslips and on SISmuc

For histological as well as for immunohistochemical staining, cells on glass cover slips and SISmuc had to be fixed with 4 % paraformaldehyde (PFA). Cells on glass cover slips were directly fixed in the 24 well plate and cells on SISmuc were fixed in the cell crown within the 12 well plate.

At first, samples were washed with PBS⁻ to remove medium and serum remnants. Then, 4 % PFA was added to the well plates and cells on glass cover slips were fixed for 10 min whereas cells on SIS muc were fixed for 3 h at RT. After that, PFA was removed, the wells with the glass cover slips were immersed with PBS⁻ and the plate was stored at 4 °C until staining. SIS muc samples were prepared for paraffin embedding (see next section).

3.7.2 Paraffin embedding and microtome sectioning

The fixed SIS muc was removed from the cell crown and excess matrix that had not been seeded with cells was cut off with a scalpel. The piece of seeded matrix was then spread onto a filter paper and inserted into an embedding cassette. In order to remove PFA, the embedding cassettes were stored in a beaker with demineralized water until the embedding station was started. This embedding station performed automatized paraffin infiltration overnight according to the program described in Table 13.

After paraffin embedding, the cassettes were pre-incubated in the paraffin bath of a blocking station for at least 30 min. After that, the matrix was removed from the cassette and cut into 2 or 3 stripes dependent on the size of the matrix. These pieces were blocked inside a stainless steel casting mould with the cutting edges facing downwards.

Table 13: Paraffin infiltration program of the embedding station

Step	Solution	Time (h)
Washing out fixative	Demineralized water	1
	Ethanol 50 %	1
Ascending ethanol series for dehydration	Ethanol 70 %	1
	Ethanol 80 %	1
	Ethanol 96 %	1
	Isopropyl I	1
	Isopropyl II	1
	Isopropyl / Xylene (1:2)	1
Removing alcohol from tissue	Xylene I	1
	Xylene II	1
Infiltrating tissue with paraffin	Paraffin I	1.5
	Paraffin II	1.5

Tissue sections were produced at a sliding microtome with a thickness of 3 µm, mounted onto microscopic glass slides and dried at 40 °C overnight. Polylysine-coated microscopic glass slides were used for immunohistochemical staining and uncoated microscopic glass slides for H&E staining.

3.7.3 Cryoembedding and cryosectioning

For the preparation of cryosections, tumour models were washed with PBS and fixed with 3.7 % buffered formalin for 2 h in the case of coculture models with hASCs. Models for *in situ* zymography were not fixed before cryoembedding. Cell free edges of fixed or unfixed models were removed with a scalpel and cut into quarters. Two quarters each were transferred to a cryomold with TissueTek® and vertically positioned at the bottom of the cryomold with the help of a cannula. After directly snap freezing them in liquid nitrogen, the samples were stored at -20 °C until cryosectioning. Coculture models with hASCs were cut into 6 µm sections using a Leica CM3050 S cryostat. Models for *in situ* zymography were cut into 14 µm sections and fixed on the glass slides for 10 min in acetone at 4°C. Fixed glass slides were dried at RT and stored at -20 °C until *in situ* zymography was performed.

3.7.4 Haematoxylin-Eosin staining (H&E)

Before performing H&E or immunohistochemical staining, the microtome sections had to be deparaffinised and rehydrated. Therefore, the microscopic slides with the tissue sections were incubated at 60 °C for 1 h in order to let the paraffin melt. Subsequently, they were immediately transferred to the first cuvette of the deparaffinising and descending ethanol series with Xylene. The deparaffination was performed according to Table 14.

Table 14: Deparaffination and rehydration of tissue sections

Step	Solution	Time (min)
Deparaffination	Xylene I	10
	Xylene II	10
Rehydration	Ethanol 96 % I	Dipped 3 times
	Ethanol 96 % II	Dipped 3 times
	Ethanol 70 %	Dipped 3 times
	Ethanol 50 %	Dipped 3 times
	Demineralized water	Swayed until disturbances cleared

H&E staining was used as an overview staining to analyse the morphology of the tissue. It was performed on the deparaffinized sections according to the following procedure:

Table 15: H&E staining procedure

Step	Solution	Time (min)
Staining basophilic structures	Hematoxylin solution	6
Rinsing of hematoxylin	Demineralized water	Until solution is clear
Blueing	Tap water	5
Staining acidophilic structures	Eosin 1 % aqueous solution	6
Rinsing of eosin	Demineralized water	Until solution is clear
Dehydration	Ethanol 70 %	Dipped 3 times
	Ethanol 96 %	2
	Isopropyl I	5
	Isopropyl II	5
	Xylene I	5
	Xylene II	5

Cover slides were then mounted in entellan for preservation.

3.7.5 Lipid staining with Oil Red O

Oil red O is a fat-soluble dye and was used as an indicator for intracellular lipid accumulation in differentiating cells. To visualize accumulated lipid droplets in the cells of the conventional 2D culture, Oil Red O staining was performed directly within the wells. For this purpose, the cells were incubated for 3 min in 60 % isopropanol and directly stained for 6 min with an Oil Red O working solution (0.5 g Oil Red O, 100 ml isopropanol and 66.6 ml H₂O), which had been filtered before with a 0.2 µm filter to remove solid particles. The Oil Red O solution was removed from the wells and the cells were washed several times with cold tap water. Subsequently, a counterstaining with Mayer's Hematoxylin for visualization of nuclei was performed for 1 min and rinsing three times with cold tap water, afterwards. Wells were covered with PBS and stored at 4 °C until microscopy was performed.

For Oil Red O staining cryosections of the 3D models were first washed in distilled water for 30 s to remove residual TissueTek®. Afterwards, sections were stained for 6 min with the filtered Oil Red O working solution. The stained sections were rinsed shortly with constant cold tap water. After counterstaining with Mayer's Hematoxylin as described above and rinsing for 10 min with cold tap water again, the microscopic slides were mounted in Mowiol®.

3.7.6 Lipid staining with BODIPY® 493/503

The fluorescence dye BODIPY® 493/503 was used to stain accumulated lipid droplets for fluorescence imaging. The cryosections were first washed in distilled water for 30 s to remove residual TissueTek®. The BODIPY® 493/503 stock solution (1 mg/ml in DMSO) was diluted 1:100 with PBS, added to the sections and subsequently incubated for 15 min in the dark.

Afterwards, the sections were washed five times with PBS for 2 min on an orbital shaker, before they were mounted in Fluoromount-G™ with DAPI.

3.8 Immunohistochemistry

In immunohistochemistry, the desired antigen is recognized by a specific primary antibody and this antibody is then in turn detected by mediators binding to the Fc region of the primary antibody. In this work, tissues were analysed by the use of DAB-based immunohistochemistry (section 3.8.1) or immunofluorescence staining (section 3.8.2).

3.8.1 DAB staining

DAB-based immunohistochemical staining was performed with DCS Super Vision 2 Kit. In this protocol, the primary antibody is detected by a secondary antibody binding to the Fc region of antibodies from mouse as well as rabbit. This secondary antibody is linked to a polymer which is in turn conjugated to horseradish peroxidase (HRP). This enzyme processes the substrate DAB resulting in a brown colour at sites of the desired antigen. The stained tissue sections can then be analysed by brightfield microscopy.

DAB-based immunohistochemical staining was performed on tissue sections as well as on cell-seeded glass cover slips. Cells on glass cover slips had to be pre-treated with a triton-X permeabilising solution for 5 min and washed with washing buffer for 5 min and the staining was performed within the well plate containing the glass cover slips. Tissue sections had to be deparaffinized, rehydrated as described in Table 14 and heat-induced antigen retrieval was performed subsequently by heating the sections in citrate buffer (pH 6.0) or EDTA buffer (pH 9.0) for 20 min at 100 °C. After that, the sections on the microscopic slides were encircled with a grease pen in order to create a barrier for the administration of small volumes of all solutions applied to the sections in the following steps. If not otherwise indicated, all incubation steps were carried out at RT and for glass cover slips on a rocking platform shaker. Incubation steps for the tissue sections were performed in a humidity chamber whereas washing steps were performed in a cuvette on a rocking platform shaker. As a negative control, all stainings included samples stained with isotype controls. Isotypes were chosen in clonality and species according to the respective primary antibody and were used in the same concentration.

The primary antibodies were diluted as listed in Table 9. The performance of the DAB staining is described in Table 16.

Table 16: DAB staining procedure

Step	Solution	Time (min)
Blocking of endogenous peroxidases	3 % H ₂ O ₂	10
Washing	PBS-T	5

Step	Solution	Time (min)
Staining with primary antibody	Primary antibodies or their isotypes	60
Washing (3 times)	PBS-T	5 each
Amplifying I	DCS Enhancer Solution	10
Washing (3 times)	PBS-T	5 each
Amplifying II	DCS Polymer Solution	20
Washing (3 times)	PBS-T	5 each
Detection step	DAB Solution	5
Washing	PBS-T	slewed
Nucleus staining	Hemalm	0.5 – 0.75
Blueing	Tap water	1 – 1.5
Preparation for embedding	Demineralized water	Infinite

Hemalm staining was performed as a counter staining to stain nuclei blue. After transferring the samples to demineralized water, the sections were dehydrated by the ascending ethanol series and embedded in entellan (see Table 15) while glass cover slips were directly mounted in Mowiol®.

3.8.2 Immunofluorescence staining

In immunofluorescent staining, the secondary antibody binds to the Fc region of an antibody from a specific host. The secondary antibody is directly coupled to a fluorochrome that can be visualized by fluorescent microscopy.

Primary and secondary antibodies were diluted as listed in Table 9. For double staining with two primary antibodies from different species the primary antibodies and the two secondary antibodies were combined in one solution, respectively. As a negative control, all stainings included samples incubated with antibody diluent without the primary antibodies to ensure that binding of the secondary antibodies is specific and for determining the background staining of the fluorochromes. Tissue sections on glass slides were prepared as described in Table 14. Subsequently, the following procedure was performed:

Table 17: Immunofluorescence staining procedure

Step	Solution	Time (min)
Blocking	5 % donkey serum	20
Staining with primary antibody	Primary antibody or antibody diluent	Overnight at 4 °C
Washing (3 times)	PBS-T	5 each
Incubation with secondary antibody	Secondary antibodies	60

Step	Solution	Time (min)
Washing (3 times)	PBS-T	5 each

Samples were kept in the dark during and after incubation with secondary antibody, as it was conjugated to a light-sensitive fluorochrome. Sections and seeded glass cover slips were mounted in Fluoromount-GTM with DAPI and were stored in the dark until fluorescence microscopy.

3.9 Determination of proliferative index

In order to evaluate the efficacy of a compound, the proliferative index of tumour cells was determined. For this, an immunofluorescence staining against Ki67 was performed and subsequently five images per 3D dynamic sample or 10 images per 2D and 3D static sample of non-overlapping parts of the sample were taken. The images of the samples were then used to count the total number of cells (DAPI-positive) and the number of Ki67-positive cells and the proliferative index was calculated according to the following formula:

$$\text{Proliferative index} = \frac{\text{number of Ki67-positive cells}}{\text{total cell number}} \times 100 \%$$

3.10 Ultrastructural analysis

For ultrastructural analysis of the unseeded scaffold as well as the 3D tumour models, scanning (SEM) and transmission (TEM) electron microscopy images were taken under the direction of Prof. Dr. Georg Krohne at the Department of electron microscopy (Biocenter, University Würzburg). The samples were prepared by washing them with prewarmed PBS⁺ and removing the cell-free edges with a scalpel. Afterwards, samples were fixed in a 6.25 % or 2.5 % solution of glutaraldehyde overnight at 4 °C for SEM and TEM, respectively. Further sample preparation was performed at the Department of electron microscopy and is summarized in Table 19 and Table 20. For the experiments, where changes in scaffold structure after tumour cell culture were investigated, the tumour models were decellularised again after 14 days of culture. This was achieved by incubating the samples twice in sodium deoxycholate for 1 h at RT, washing them twice in PBS⁻ for 10 min, incubating them in DNase I solution for 2 h at 37 °C and rinsing them with PBS⁻ again before fixation.

Table 18: Buffers and solutions for SEM and TEM

Buffer	Composition
2 % buffered osmium (VIII)-oxide	2 % OsO ₄ in 50 mM cacodylic acid pH 7.2
2.5 % glutaraldehyde solution	2.5 % glutaraldehyde in 50 mM cacodylic acid pH 7.2 50 mM KCl 2.5 mM MgCl ₂

Buffer	Composition
6.25 % glutaraldehyde solution	6.25 % glutaraldehyde in 100 mM Sörensen
Epon 821	Component A (soft): 97.1 g Epon 812 130.8 g Dodecenylsuccinicanhydride Component B (hard): 90 g Epon 812 81.37 g Methyladicanhydride Mixed in appropriate ratio according to sample
Sörensen buffer 100 mM	Solution A: 100 mM KH_2PO_4 , 12.2 ml Solution B: 100 mM Na_2HPO_4 , 81.8 ml

Table 19: Sample preparation for SEM

Step	Solution	Time (min)
Washing	Sörensen buffer	5
Dehydration	30 % acetone	15
	50 % acetone	20
	70 % acetone	30
	90 % acetone	45
	100 % acetone	5-times 0.5
	100 % acetone	Until further processing

Table 20: Sample preparation for TEM

Step	Solution	Time/Condition
Washing	50 mM cacodylic acid, pH 7.2	5-times 3 min, 4 °C
Staining	2 % buffered Osmium(VIII)-oxide	2 h, 4 °C
Washing	Ultrapure H_2O	5-times 3 min, 4 °C
Staining	0.5 % uranyl acetate	Overnight, 4 °C
Washing	Ultrapure H_2O	5-times 3 min, 4 °C
Dehydration	50 % Ethanol	30 min, 4 °C
	70 % Ethanol	30 min, 4 °C
	90 % Ethanol	30 min, 4 °C
	96 % Ethanol	30 min, 4 °C
	100 % Ethanol	30 min, 4 °C
	100 % Ethanol	60 min, RT
	propylenoxide	3-times 30 min, RT

Step	Solution	Time/Condition
Embedding	Epon 812 in propylenoxide (1:2)	Overnight
	Epon	2 h
	Epon	2 h
	Epon in embedding mould	1 h
Polymerisation		At least 48 h, 60 °C

3.11 Quantification of invasive cells

Tumour cells that migrated into the scaffold were quantified with the help of an immunofluorescence staining against collagen IV, as it stains basement membrane structures and therefore allows the discrimination between cells that have overcome the basement membrane and cells that are located inside the former crypt structures. The images of the samples were used to count the total number of cells (DAPI-positive) and the number of cells that had migrated into the scaffold and the ratio of migrated cells was calculated according to the following formula:

$$\text{Ratio of migrated cells} = \frac{\text{number of migrated cells}}{\text{total cell number}} \times 100 \%$$

3.12 *In situ* zymography combined with immunofluorescence staining

For *in situ* zymography, DQTM gelatin fluorescein conjugate was used as a substrate for the detection of MMP activity. This is a highly quenched, fluorescein-labelled gelatine that reveals its green fluorescence upon proteolytic digestion and can therefore be used to measure enzymatic activity. The DQ-gelatin powder was dissolved in 1 ml ultrapure water and incubated in an ultrasound bath at 50 °C for 5 min to facilitate the solving process. The 1 mg/ml stock solution was stored at 4 °C in the dark. After thawing the cryosections, they were washed for 5 min with PBS⁻ and permeabilised with 0.1 % Triton-X-100 and 1 % BSA in PBS⁻ for 20 min at RT. Subsequently, sections were blocked with 5 % donkey serum for 20 min, washed twice for 5 min with PBS-T and incubated with a dilution of the desired primary antibody. Afterwards, sections were washed with PBS⁻ for 5 min and incubated with a dilution of the secondary antibody in PBS⁺ containing 10 µg/ml DQ-gelatin for 6 h at 37 °C in the dark. Before the sections on the glass slides were mounted in Fluoromount-GTM with DAPI, they were washed 5 times for 1 min with PBS⁻. *In situ* zymography images were taken at a confocal microscope with excitation at 460–500 nm and emission at 512–542 nm.

3.13 Statistical analysis

Statistical analysis of all data was performed with the OpenSource software R 3.3.0. For the comparison of all experiments, the non-parametric Kruskal-Wallis-test was performed followed by Wilcoxon rank sum test as a posthoc-analysis.

4 Results

4.1 Establishment and optimization of a 3D mamma carcinoma test system

4.1.1 Establishment of a 3D mamma carcinoma test system representing different molecular subsets of breast cancer

For the generation of the 3D mamma carcinoma models, the biological matrix SISmuc was used as a scaffold in order to provide more physiologic tissue conditions. This scaffold is composed of the small intestinal submucosa (SIS) and the mucosal layer (muc) on top of it with its preserved villi and crypt structures. An overview of the structure of this scaffold is provided in Figure S 1. This cell-free scaffold was reseeded with different types of breast cancer cell lines representing different molecular subsets of mamma carcinoma.

As FBS has a major influence on cell growth, four different batches of FBS were tested for all cell lines under 2D and 3D culture conditions (Figure 3). In 2D culture, no pronounced difference in cell growth (Figure 3 B) or cell morphology (Figure S 2) could be determined between the different batches of FBS. However, in 3D culture, there were distinct FBS-dependent differences in cell growth and morphology especially for the MCF-7 cells. Whereas only few MCF-7 cell aggregates could be found on top of the scaffold for Bio&Sell and two different batches of Invitrogen FBS, the cells formed a closed monolayer on top of the scaffold and resettled former crypt structures with PAN Biotech FBS. SKBR-3 cells only showed single cell growth on the scaffold for all FBS batches but best adherence to the scaffold with PAN Biotech FBS. MDA-MB-231 cells showed similar growth with all batches of FBS, grew loosely on top of the scaffold and also resettled former crypts structures.

Furthermore, the expression of different markers characteristic for the molecular subsets of mamma carcinoma was investigated (Figure S 3). MCF-7 cells, representing the ER-positive subset of mamma carcinoma, showed strongest expression of the ER with PAN Biotech FBS and only very weak expression of HER2, which is characteristic for this subset of mamma carcinoma (Figure S 3 A). SKBR-3 cells, representing the HER2-overexpressing subset of mamma carcinoma, expressed HER2 with all batches of FBS whereas ER staining was absent (Figure S 3 C). And MDA-MB-231 cells, representing the TNBC subset, did not express ER or HER2 with any batch of FBS (Figure S 3 B).

According to the results of cell growth and marker expression under 3D culture conditions, the FBS batch PAN Biotech was determined to be the most suitable for the generation of a 3D mamma carcinoma test system representing the three molecular subsets of ER-positive, HER2-overexpressing and triple negative breast cancer and was therefore used for all further experiments.

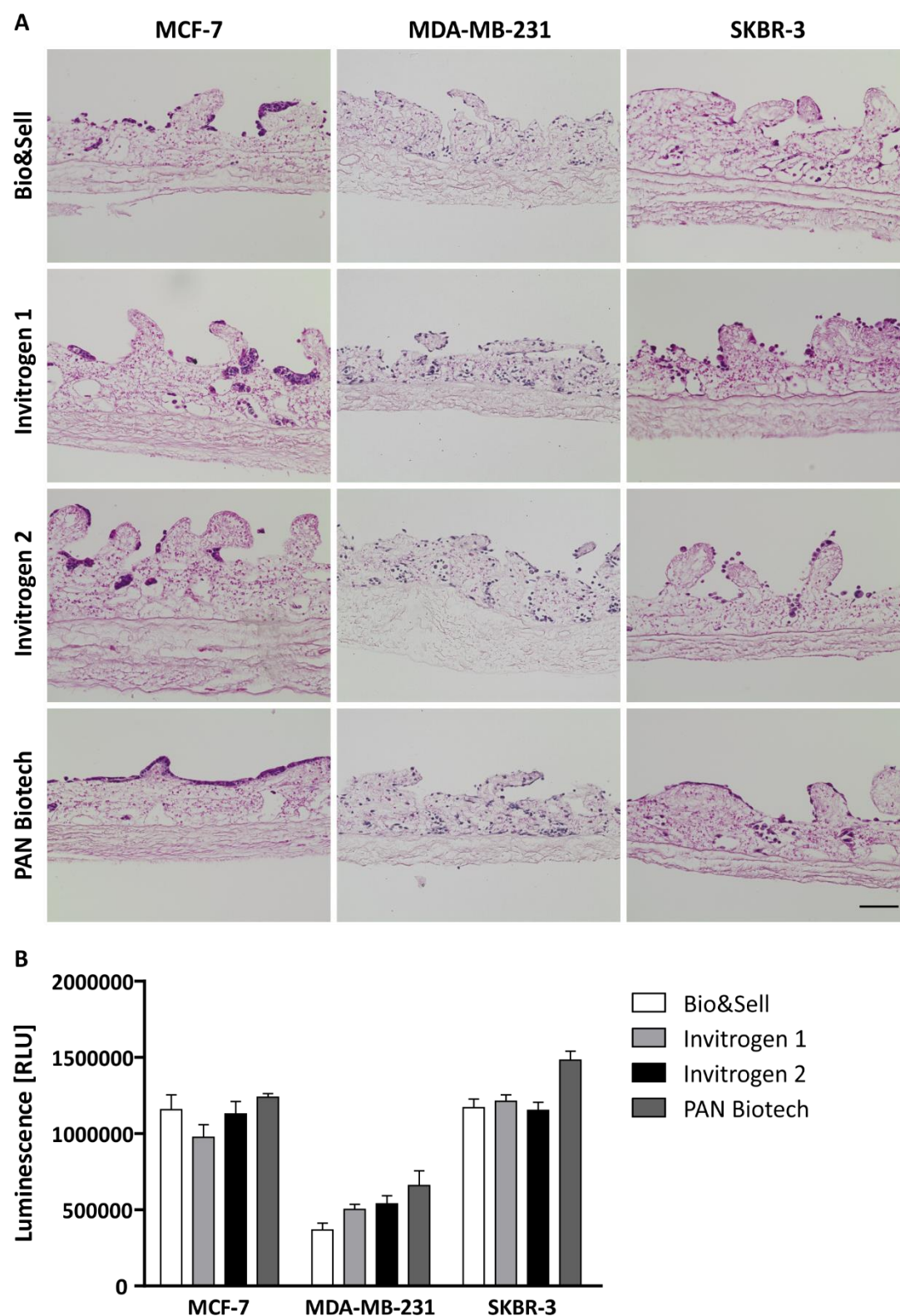


Figure 3: FBS batch testing

A: H&E staining of MCF-7 (left column), MDA-MB-231 (middle column) or SKBR-3 (right column) cultured for 14 days on SIS muc in their specific growth media supplemented with different batches of FBS (Bio&Sell, Invitrogen 1, Invitrogen 2, PAN Biotech). Scale bar: 100 μ m. B: Determination of cell proliferation and viability of the aforementioned cell lines in 2D cultured in cell-specific growth media supplemented with the different batches of FBS for 4 days with CellTiter-Glo[®] Luminescent Cell Viability Assay. RLU: relative light units.

4.1.2 Optimization of the HER2-overexpressing tumour model

As SKBR-3 cells showed the best adherence to the scaffold with the selected batch of FBS but still poor cell density, different media and culture conditions were tested for 3D cell culture of this cell line in order to optimize test system generation.

An increase in cell number on the scaffold could be achieved by culturing the models on an orbital shaker compared to standard static 3D culture (Figure 4 A and B). However, cell clusters showed poor adherence to the scaffold. Cell number and density further increased, when the culture medium was changed to DMEM medium instead of McCoy's 5A medium recommended by the supplier and models were cultured on an orbital shaker. Under these conditions, the cells grew in multiple layers on top of the scaffold, resettled former crypt structures and partially formed a denser network. Additionally, the expression of HER2, which is characteristic for the molecular subset represented by the SKBR-3 cell line, was preserved under these conditions (Figure 4 D). Therefore, all further experiments with SKBR-3 cells in 3D culture were performed in DMEM on an orbital shaker.

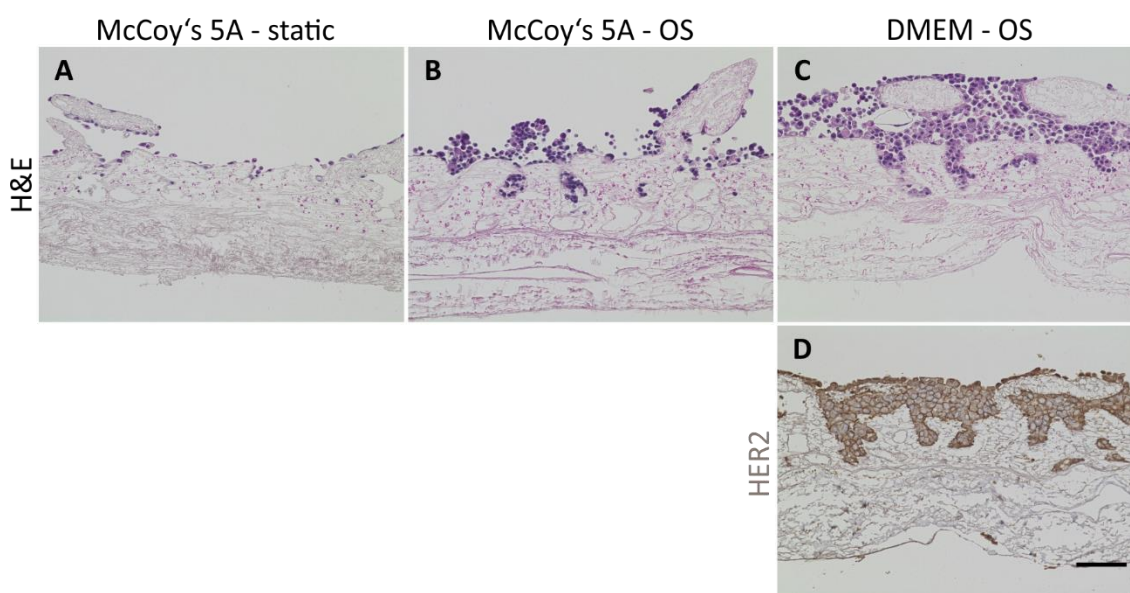


Figure 4: Optimization of SKBR-3 tumour models

H&E staining (A-C) and immunohistochemical staining against HER2 (D) of SKBR-3 tumour models cultured in McCoy's 5A under static conditions (A) or on an orbital shaker (OS; B) or in DMEM on an orbital shaker (C) for 14 days. Tumour cell number was increased in the tumour model cultured in McCoy's 5A medium on an orbital shaker (B) compared to static culture (A), but cells grew loosely on top of the SISmuc. Cell density was strongly increased in models cultured in DMEM on an orbital shaker (C+D) while characteristic HER2 expression was preserved (D). Scale bar: 100 μ m.

4.1.3 Determination of the optimum culture duration for compound testing

For reliable predictions of drug efficacy, it is crucial to determine the optimum culture duration for compound testing which is defined by a relatively steady morphology, constant proliferation rates and low basic endogenous apoptosis. In order to determine this optimum culture duration, 3D models of all three cell lines were cultured for up to 21 days and morphology as well as proliferation and apoptosis of the models was assessed at different time points. Morphologically,

in all models cell numbers strongly increased over time until day 11 or 12 of culture (Figure 5). After that, only minor changes in morphology and cell number could be observed until day 18. Between day 18 and 21, cell number seemed to slightly decrease in all models. These findings go in line with the proliferation data (Figure 6 A). MDA-MB-231 and SKBR-3 cells exhibited a higher proliferation rate in the beginning of culture at day 4 or until day 7, respectively. From day 7 or 11 onwards, proliferation index levelled off with a slight decrease at day 21. In MCF-7 models, proliferation index was relatively constant already from day 4 onwards. Furthermore, levels of apoptosis were assessed over culture period in order to avoid treatment at a time point, where basic apoptosis in the models is already high without any treatment (Figure 6 B). Apoptosis was low until day 14 in models of all cell lines. In MDA-MB-231 models, this low level of apoptosis was constant until day 21. In contrast, in models of MCF-7 and SKBR-3 a massive increase in apoptosis on day 21 was observed, indicating that the viability of the models already decreases at that time point. This goes in line with the proliferation and morphology data.

Taking together these results, the optimum time for drug screening lies between day 11 and day 14. Therefore, a culture duration of 14 days with treatment during the last days (depending on the compound) but starting no earlier than day 11 was chosen for all drug testing experiments in all three models. Based on these findings a standard operation procedure (SOP) for the establishment and treatment of 3D tumour models was generated and the method was published in the Journal of Visualized Experiments with equally contributing first authorship (Göttlich *et al.*, 2016).

4.2 Characterization of the mamma carcinoma test system

4.2.1 Comparison of the proliferation index

The proliferation index of tumours is a key feature when the efficacy of cytostatic compounds like chemotherapeutics is to be predicted as such compounds especially target the proliferating cells of the tumour.

Proliferation was assessed using immunofluorescence staining against Ki67, a marker that is expressed by all cells that are not in the G₀ phase of the cell cycle. All cell lines showed a reduced number of Ki67-positive cells when they were cultured on the matrix compared to conventional 2D cell culture (Figure 7 A-H). This was also quantified by counting the number of Ki-67-positive cells and total cells. A drastic decrease of proliferation compared to 2D cell culture was found for all cell lines when they were cultured on the matrix under static conditions or on an orbital shaker. The percentage of Ki67-positive cells decreased from 95.9 % in 2D culture to 43.5 % in 3D static culture for MCF-7, from 98.1 % in 2D culture to 19.1 % in 3D static culture for MDA-MB-231 cells and from 55.8 % in 2D culture to 23.7 % in 3D orbital shaker culture for SKBR-3, respectively (Figure 7 I). A further decrease in the proliferation index could be observed under 3D dynamic conditions for MCF-7 and MDA-MB-231 cells to 39.2 % and 13.3 %, respectively. 3D dynamic models of SKBR-3 cells in a flow bioreactor could not be established as cells were washed off the scaffold by the medium flow.

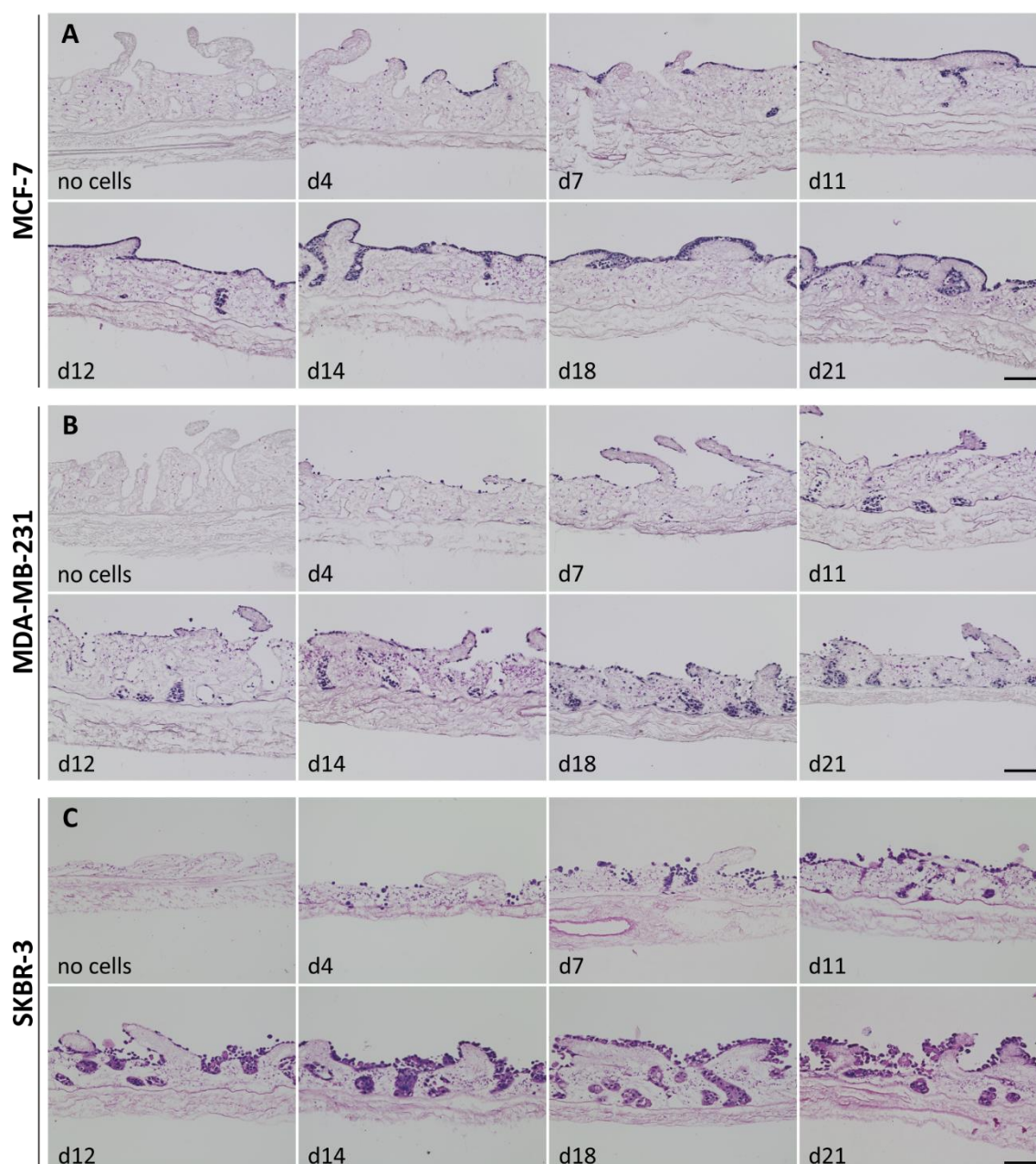


Figure 5: Determination of the optimum culture duration

H&E staining of mamma carcinoma models of MCF-7 (A), MDA-MB-231 (B) or SKBR-3 cells (C) cultured for 4 to 21 days under static conditions (MCF-7 and MDA-MB-231) or on an orbital shaker (SKBR-3). Cell density was increasing over time until day 11 or 12. Tumor models showed only minor changes in morphology between day 11 and day 18 for MCF-7 and MDA-MB-231 and between day 12 and 18 for SKBR-3, respectively, with a slight decrease in cell number at day 21 for models of all cell lines. Scale bar: 100 μ m.

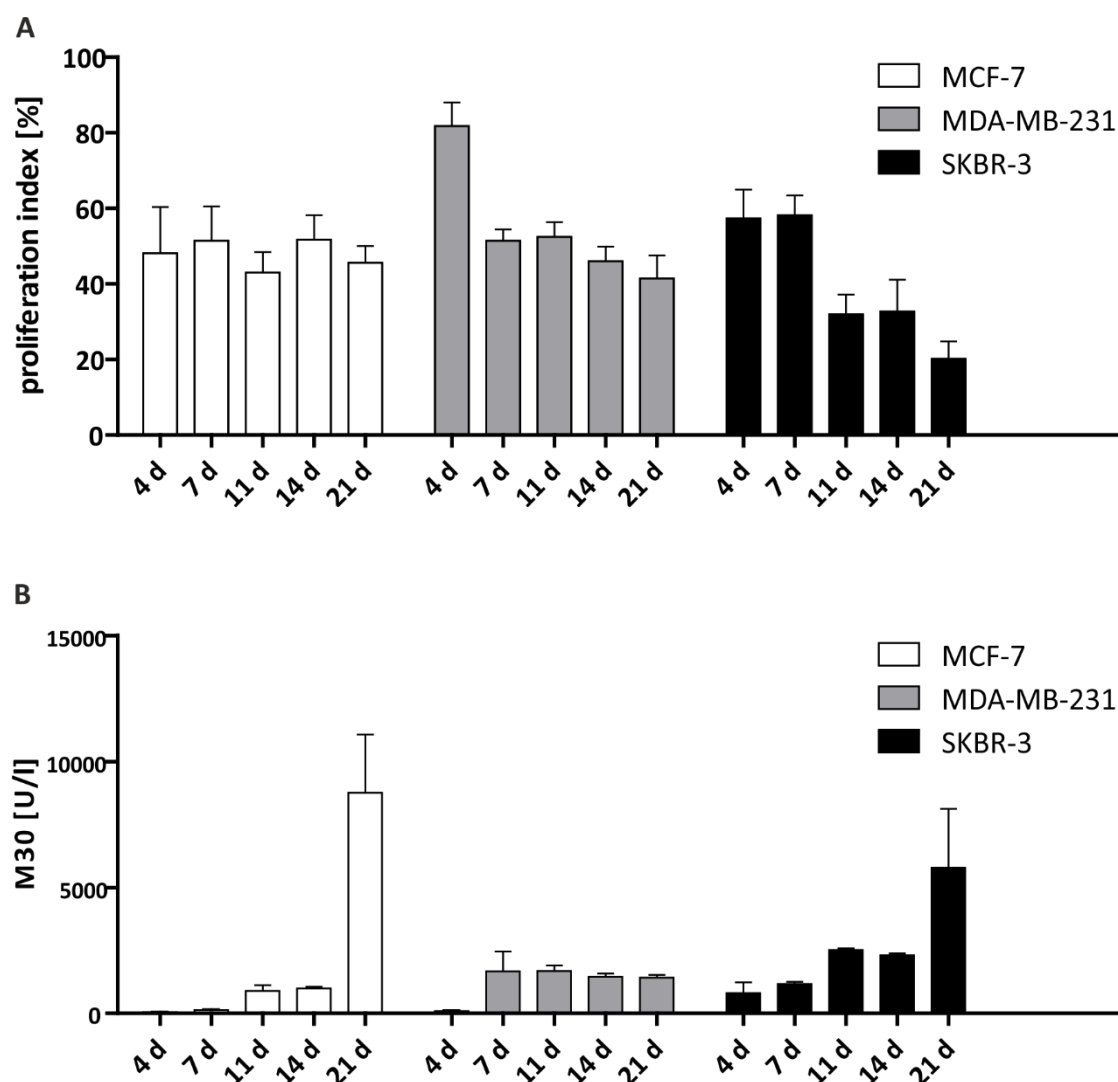


Figure 6: Proliferation and apoptosis over culture duration

A: Proliferation index (percent of proliferative cells per total cell number) was determined with the help of quantification of Ki67⁺ cells from immunofluorescence staining (10 images per condition) at different time points over 21 days of culture. Data are presented as arithmetic mean +SD (n=1). B: Tumour cell apoptosis was determined by quantification of M30 from tumour model supernatants collected at different time points after 24 h of medium change over 21 days of culture. Data are presented as arithmetic mean +SD (n=4). U/l: Units per litre.

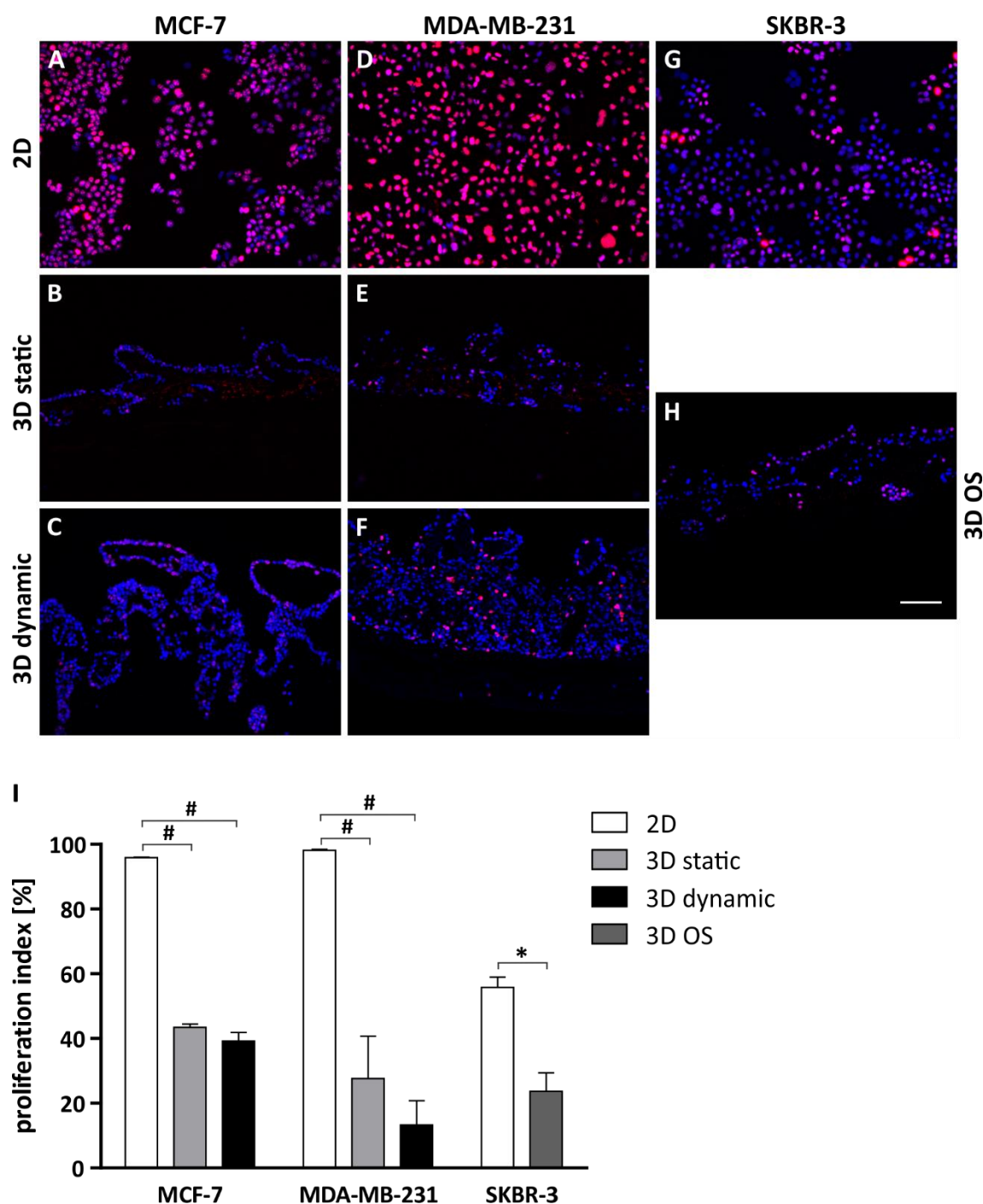


Figure 7: Comparison of proliferation index in different culture conditions

A-H: Immunofluorescence staining against Ki67 (red) of MCF-7 (A-C), MDA-MB-231 (D-F) and SKBR-3 cells (G-H) cultured under 2D, 3D static, 3D dynamic conditions or on an orbital shaker (OS). Nuclei are counterstained with DAPI (blue). Scale bar: 100 μ m. I: Proliferation index (percent of proliferative cells per total cell number) was determined with the help of quantification of Ki67⁺ cells from immunofluorescence staining (10 images per condition). Proliferation index was strongly decreased under 3D static, dynamic and OS condition compared to conventional 2D culture conditions. Data are presented as arithmetic mean \pm SD (n=4). Statistical significance values by pairwise Wilcoxon rank sum test with Bonferroni correction: # 0.05 < p < 0.1, * p < 0.05.

4.2.2 Markers of tumour biology in 2D and 3D models and xenografts

During epithelial tumour formation and progression, cells lose their polarized and differentiated phenotype. In some carcinomas the former epithelial cells also switch to a more mesenchymal phenotype. Therefore, markers of polarization (Muc-1), differentiation status (E-Cadherin and β -Catenin) and EMT (PCK and vimentin) were investigated in the cell lines cultured under different conditions and, if available, compared to xenograft material from the same cell lines.

MCF-7 cells grew in a tight monolayer on top of the matrix in 3D static conditions and filled the former crypts without crossing the basement membrane and invading into the scaffold. In some few areas, cells also grew in 2 or 3 layers (Figure 8). Under 3D dynamic conditions, cells formed multiple layers on top of the scaffold and also resettled the former crypt structures leading to the formation of tumour nodules inside the crypts that are surrounded by ECM without tumour cell migration into the scaffold. According to the marker expression, MCF-7 cells had a clear epithelial phenotype, strongly expressing PCK under all culture conditions, whereas the mesenchymal marker vimentin was absent (Figure 8 A-H). The strong expression of PCK and the absence of vimentin correlates well with the xenograft material, where only murine fibroblasts in the connective tissue that surround the PCK-positive tumour cell aggregates expressed vimentin. Also, MCF-7 cells were well differentiated, indicated by a colocalization of E-Cadherin and β -Catenin at the cell-cell contacts under all culture conditions which goes in line with the expression pattern of those markers in the xenograft material (Figure 8 I-P). Under 3D static conditions the cells were polarized according to the apical expression of the marker Muc-1. In the dynamic culture, the uppermost cell layer also showed this apical expression of Muc-1, while some cells in the deeper regions exhibited a diffuse expression indicating a loss of polarization of cells in those areas. In the xenograft material single cells also showed this depolarized phenotype, thereby strongly resembling the deeper regions of the 3D dynamic culture. In 2D culture it could not be determined where Muc-1 is localized, as cells can only be monitored from top view. Taken together, the expression of all here investigated markers in 3D models strongly correlated with the xenograft material and the tissue morphology of the 3D dynamic models showed strong similarities to the xenograft material (Figure 8 Q-X).

In contrast to MCF-7 cells, MDA-MB-231 cells displayed a more scattered growth on the scaffold without the formation of clear cell-cell contacts which goes in line with their more fibroblastoid morphology observed in the 2D cultures (Figure 9). Under 3D static conditions, cells grew loosely on top of the scaffold, resettled the former crypts and some single cells also migrated into the mucosal part of the scaffold. Under dynamic conditions, cells were distributed throughout the whole mucosal layer and the borders of the former crypts were partially not visible any more. The xenograft material exhibited the same scattered tumour tissue morphology. Concerning EMT-markers, MDA-MB-231 cells showed a heterogeneous expression of both PCK as well as vimentin under all culture conditions which was also the case in the xenograft material (Figure 9 A-H). Both E-Cadherin and β -Catenin were only weakly expressed and a colocalization of the markers could not be found in any of the models (Figure 9 I-P). Expression of E-Cadherin was slightly increased in the xenograft model, but here as well, no colocalization with β -Catenin could be detected. Also Muc-1 was only weakly expressed (Figure 9 Q-X). While it was absent under

2D culture conditions, some single cells in the 3D models diffusely expressed this marker, indicating their loss of polarization. The same expression pattern could be found in the xenograft material.

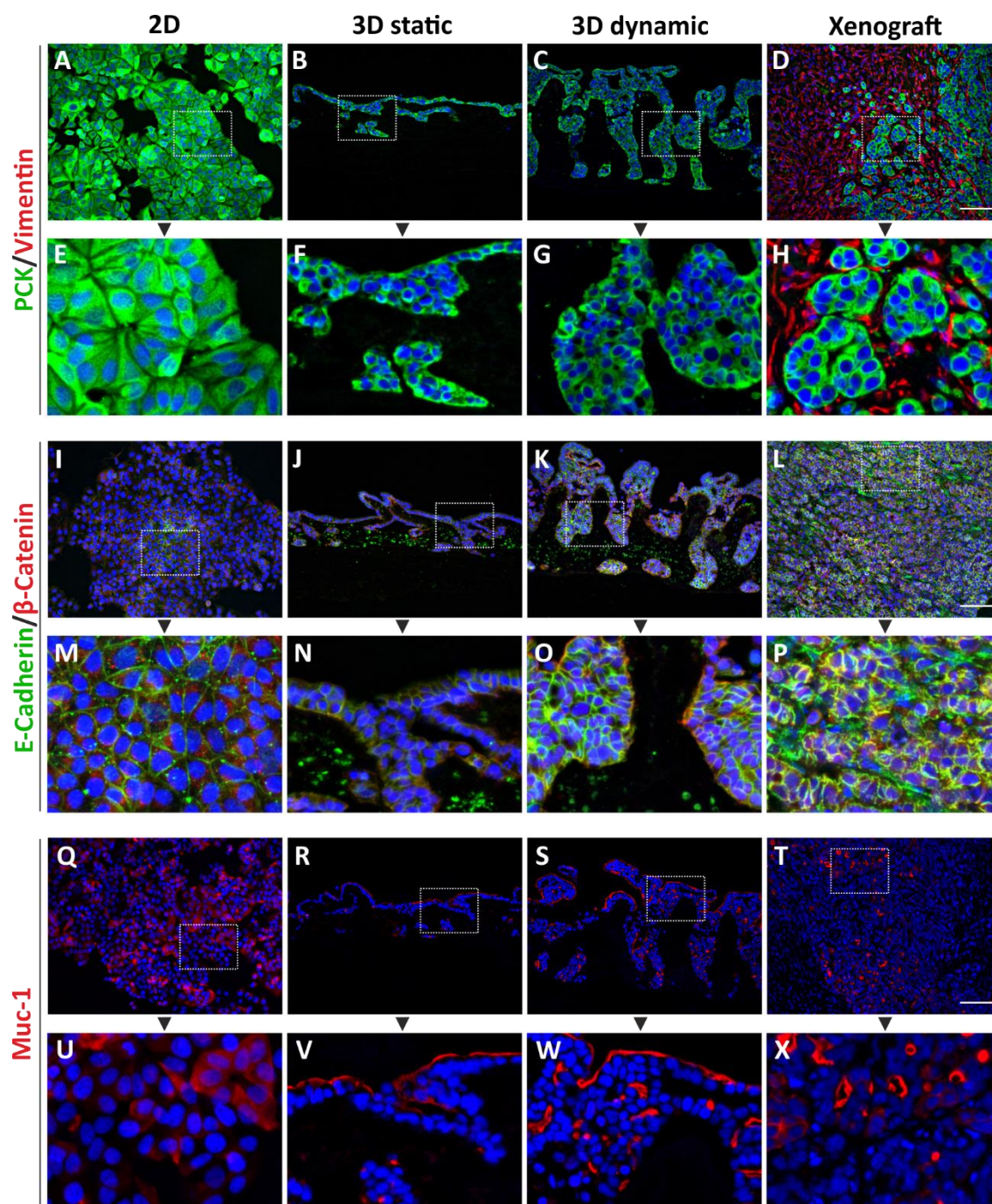


Figure 8: Expression of tumour biology markers in MCF-7 cells in 2D, 3D static, 3D dynamic or in a xenograft model

A-H: Immunofluorescence staining against pan cytokeratin (green) and vimentin (red) of MCF-7 cells cultured under 2D, 3D static, 3D dynamic conditions or in a xenograft model. I-P: Immunofluorescence staining against E-Cadherin (green) and β -Catenin (red). Q-X: Immunofluorescence staining against mucin-1 (red). Nuclei are counterstained with DAPI (blue). Scale bar: 100 μ m. Images E-H, M-P and U-X represent a magnification of the frames in the images above. Xenograft material was kindly provided by Oncotest (Charles River).

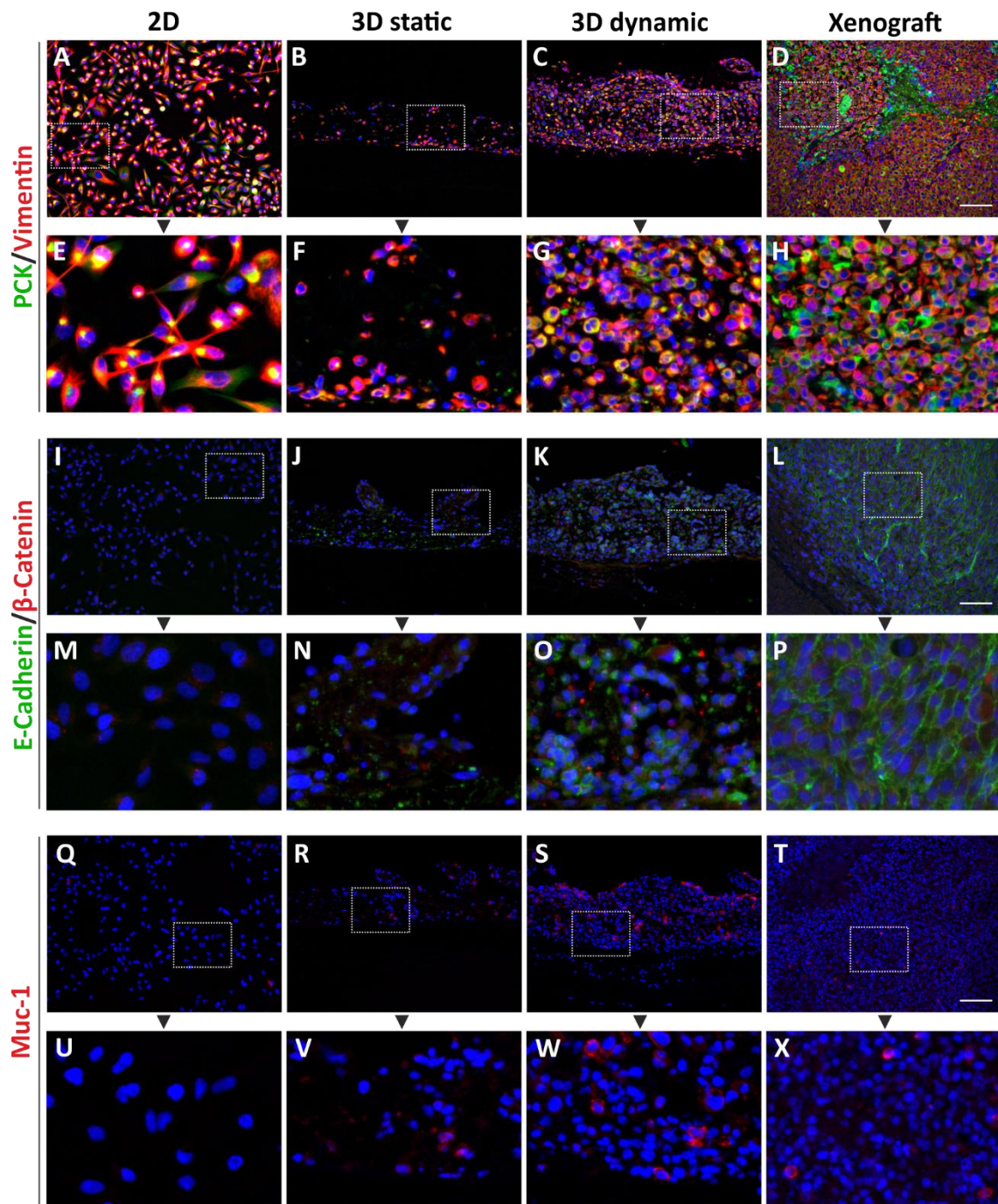


Figure 9: Expression of tumour biology markers in MDA-MB-231 cells in 2D, 3D static, 3D dynamic or in a xenograft model

A-H: Immunofluorescence staining against pan cytokeratin (green) and vimentin (red) of MDA-MB-231 cells cultured under 2D, 3D static, 3D dynamic conditions or in a xenograft model. I-P: Immunofluorescence staining against E-Cadherin (green) and β -Catenin (red). Q-X: Immunofluorescence staining against mucin-1 (red). Nuclei are counterstained with DAPI (blue). Scale bar: 100 μ m. Images E-H, M-P and U-X represent a magnification of the frames in the images above. Xenograft material was kindly provided by Oncotest (Charles River).

SKBR-3 cells strongly expressed epithelial PCK but lacked the mesenchymal vimentin under all culture conditions (Figure 10 A-D). Although cells grew in a close proximity to each other, they did not seem to form cell-cell-contacts neither in 2D nor in 3D conditions but had a rather rounded

shape. This goes in line with the fact that the cells did not express E-Cadherin, which is usually localized at epithelial cell-cell contacts. Only a weak and diffuse expression of β -Catenin could be observed (Figure 10 E-H). Like MDA-MB-231 cells, SKBR-3 cells only very weakly and diffusely expressed Muc-1 in some single cells both under 2D and 3D culture conditions (Figure 10 I-L). Taken together, this indicates, that SKBR-3 cells still have an epithelial phenotype but are already driven towards dedifferentiation and lost their polarity. Comparison to xenograft models was not possible, as xenograft material from this cell line was not available.

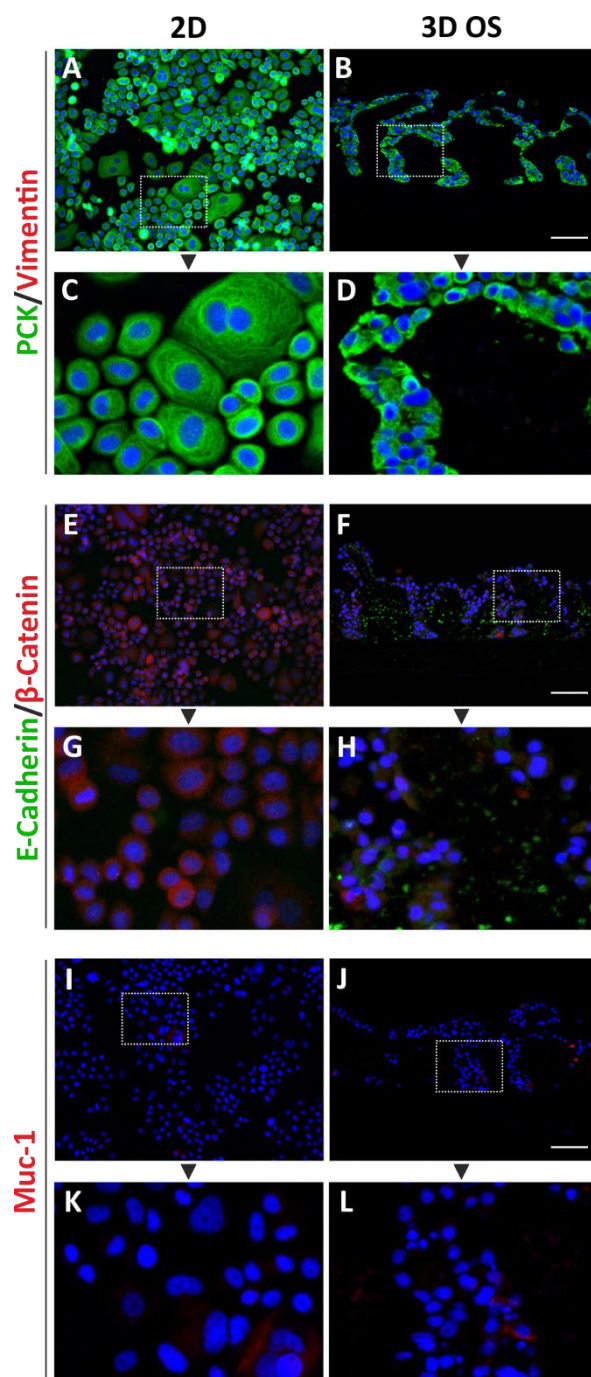


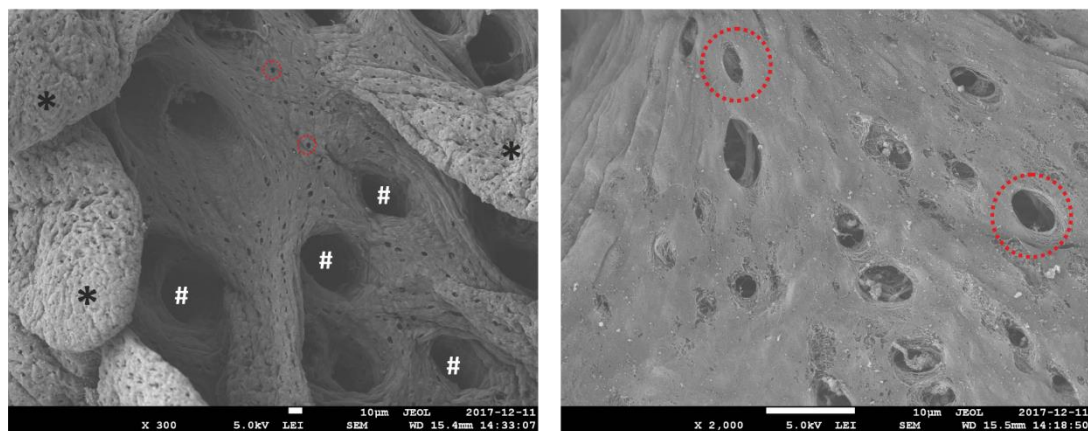
Figure 10: Expression of tumour biology markers in SKBR-3 cells in 2D and 3D OS culture conditions

A-D: Immunofluorescence staining against pan cytokeratin (green) and vimentin (red) of SKBR-3 cells cultured under 2D or 3D conditions on an orbital shaker (OS). E-H: Immunofluorescence staining against E-Cadherin (green) and β -Catenin (red). I-L: Immunofluorescence staining against mucin-1 (red). Nuclei are counterstained with DAPI (blue). Scale bar: 100 μ m. Images C-D, G-H and K-L represent a magnification of the frames in the images above.

4.2.3 Invasive behaviour of mamma carcinoma on the scaffold

Invasive growth of tumour cells is a prerequisite for metastasis formation. The first barrier a tumour cell derived from epithelial tissue has to cross, is the basement membrane underlying the epithelial cells in such tissues. For the 3D breast cancer models, the cell lines were cultured on SISmuc. In this decellularised scaffold the natural basement membrane is preserved to a great extent, indicated by the smooth structure lining the surface of the scaffold (Figure 11 A) observable in SEM images of the decellularised scaffold. In a higher magnification, small holes within this smooth lining of basement membrane became visible (Figure 11 A, red circles). These holes had a very sharp edged and rounded shape and the underlying collagen fibre network is absent beneath these holes, suggesting that these holes are naturally occurring pores rather than damages deriving from the decellularisation process.

A



B

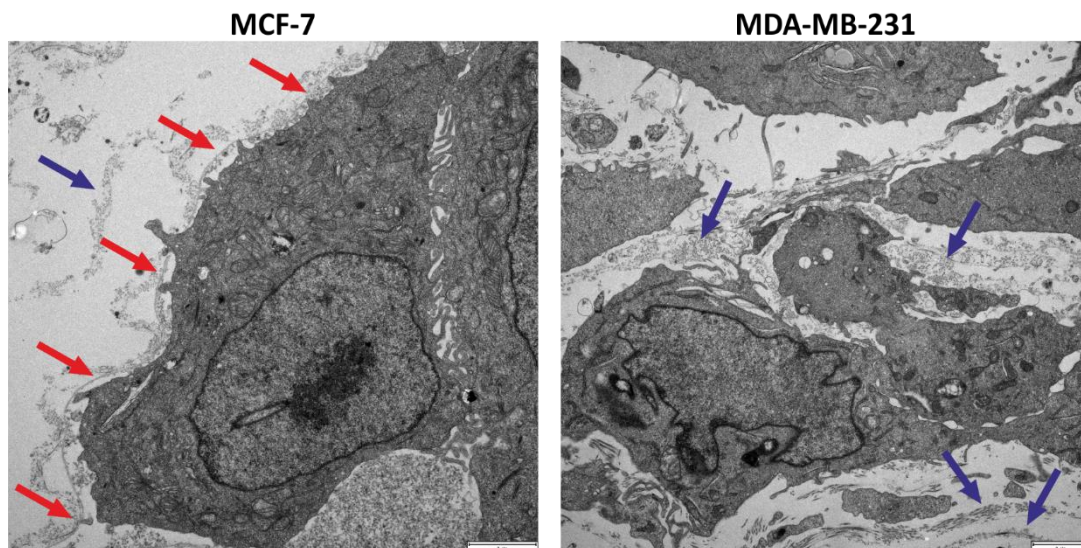


Figure 11: Preservation of basement membrane and invasive behaviour of tumour cells

A: SEM images of decellularised SISmuc scaffold in different magnifications. The smooth surface represents the preserved basement membrane structure with pores. * mark villi, # mark crypt structures, red circles mark pores. Scale bars: 10 µm. B: TEM images of MCF-7 and MDA-MB-231 3D models. MCF-7 cells were located on top of the basement membrane (red arrows), while MDA-MB-231 cells were located freely inside the collagen network (blue arrows) of the small intestinal mucosa.

As MCF-7 cells and MDA-MB-231 cells are described to be non-invasive and highly invasive, respectively (Sommers et al., 1991; Thompson et al., 1992), their invasive behaviour on the here used scaffold was analysed. As described before in 4.2.2, MCF-7 cells grew in monolayers or multiple layers on top of the SIS muc and inside the former crypt structures but without migrating into the scaffold under both 3D culture conditions. In contrast, single cells of the MDA-MB-231 cell line that had migrated into the mucosal layer could be observed under 3D static conditions and the whole mucosal layer was filled with cells when MDA-MB-231 cells were cultured in the dynamic flow bioreactor system. Moreover, former crypt structures partially disappeared under these culture conditions. In order to verify if MDA-MB-231 cells indeed have crossed the basement membrane, TEM images were taken from MCF-7 cells and MDA-MB-231 cells grown under 3D dynamic conditions (Figure 11 B). These images reveal, that MCF-7 cells were surrounded by a basement membrane structure (red arrows in Figure 11 B left image), whereas MDA-MB-231 cells seemed to be located freely in the network of collagen fibers of the small intestinal mucosa which are longitudinally and transversally cross-sectioned in this image (blue arrows in Figure 11 B). In contrast, a basement membrane structure surrounding the cells could not be found. This goes in line with the findings of collagen IV staining (Figure 12 A-D). Collagen IV is a major component of basement membranes and the immunofluorescence staining against this marker shows, that the surface of the scaffold as well as the former crypt structures in the cross section are lined with a collagen IV-positive layer representing the basement membrane. MCF-7 cells indeed do not overcome this barrier neither under static nor dynamic culture conditions but stay on top of the scaffold and inside the former crypts (Figure 12 A and B). In contrast, single MDA-MB-231 cells cross this basement membrane and migrate into the lamina propria mucosae part of the scaffold under 3D static culture conditions (Figure 12 C, white arrows). Under dynamic culture conditions, former crypt structures could not be observed anymore and cells dispersed throughout the whole mucosal layer, also starting to produce their own collagen IV (Figure 12 D). Some single cells could also be observed within the small intestinal submucosal layer, predominantly in former vessel structures. Additionally, the invasiveness of both cell lines was quantitatively assessed by counting the cells inside the matrix not surrounded by a collagen IV positive basement membrane structure under 3D static conditions (Figure 12 E). Here, a significant difference in invasiveness between the two cell lines could be found. Approx. 28 % of MDA-MB-231 cells were invading into the matrix compared to only 0.8 % of MCF-7 cells. Invasiveness in the dynamic models was not determined due to the lack of clear basement membrane structures and MDA-MB-231 cells producing their own collagen IV.

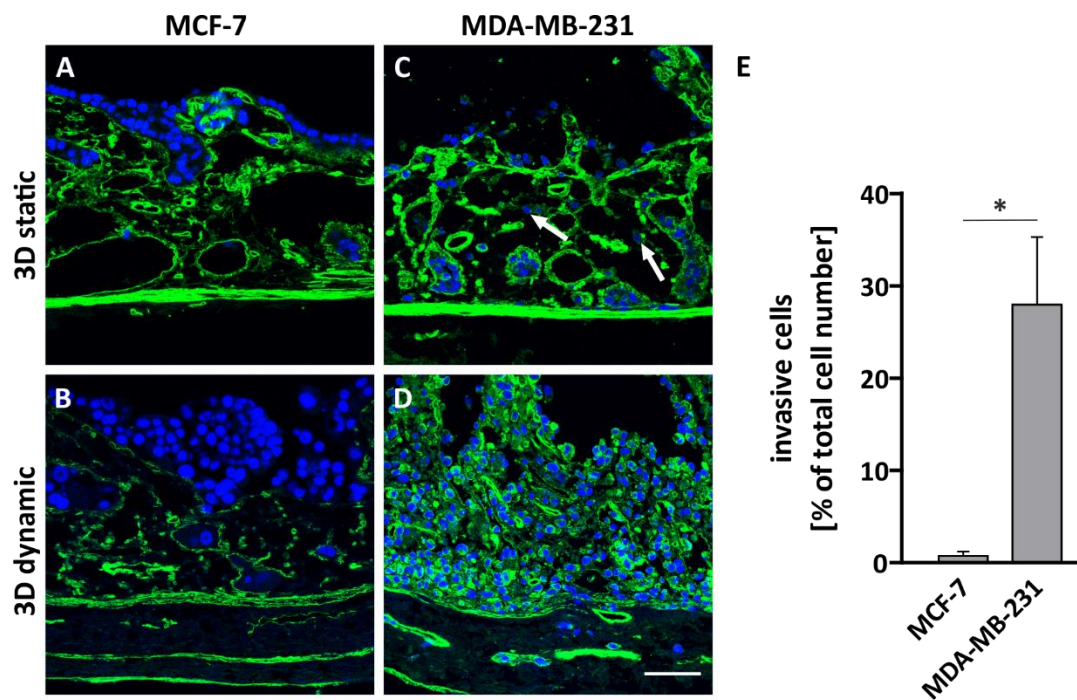


Figure 12: Differences in invasive behaviour of MCF-7 and MDA-MB-231 cells on SISmuc

A-D: Immunofluorescence staining against collagen IV (green) of MCF-7 or MDA-MB-231 models cultured under 3D static or 3D dynamic conditions. Single invasive MDA-MB-231 cells could be found in the scaffold under 3D static conditions (white arrows). Nuclei are counterstained with DAPI (blue). Scale bar: 100 μ m. E: Invasive cells in 3D static conditions (percent of invasive cells per total cell number) was determined with the help of quantification of collagen IV staining (10 images per condition). MDA-MB-231 cells showed significantly higher invasiveness compared to MCF-7 cells. Data are presented as arithmetic mean +SD (n=4). Statistical significance values by Wilcoxon rank sum test: * $p < 0.05$.

As described above, the basement membrane on the scaffold had pores. In order to investigate whether MDA-MB-231 cells use these pores for invasion or if the tumour cells actively alter the basement membrane structure, an ultrastructural analysis of the scaffold after 14 days of tumour cell culture was performed. For this purpose, SISmuc without any cells or seeded with either MCF-7 or MDA-MB-231 cells was cultured for 14 days and afterwards decellularised again. The cell-free scaffolds were then analysed by SEM imaging (Figure 13). Images were taken at the base of the scaffold and at the tips of the villi. After 14 days of static and dynamic incubation of the scaffold without cells, no changes could be observed in the basement membrane. The smooth surface with the sharp edged pores was still preserved under these conditions. While MCF-7 cells cultured on the scaffold under static conditions did not alter this appearance, smaller areas where the smooth structure of basement membrane was disrupted could be observed under dynamic culture conditions (Figure 13, red asterisk). In these areas, the underlying collagen fibre network was exposed, indicating that these holes are different from the pores described above. Such areas of disrupted basement membrane were already observed for MDA-MB-231 static models and were larger and more frequent compared to the MCF-7 dynamic model. When cultured under dynamic culture conditions, MDA-MB-231 cells strongly altered the basement membrane of the scaffold. Under these conditions, additionally, large holes could be found where no underlying collagen fibre network was visible (Figure 13, white hash signs). The same alterations could be

observed at the tips of the villi. Additionally, while the surface of the villi in the unseeded models was smoother, the cells seemed to ruffle the basement membrane in these areas.

The active alteration of the basement membrane structure and scaffold observed in ultrastructural analysis is underlined by data obtained from *in situ* zymography using a highly quenched fluorescently labelled substrate. This technique allows the spatially defined detection of the proteolytic activity of MMPs in a tissue and was established together with Tina Schmitt during her Master's thesis at the Chair of Tissue Engineering and Regenerative Medicine by adapting the method described by Duran-Vilaregut *et al.* and Agrawal *et al.* for the 3D test system (Agrawal *et al.*, 2006; Duran-Vilaregut *et al.*, 2011; Schmitt, 2017). By overlaying unfixed cryosections of tissues with a substrate - here a gelatine substrate - that is highly quenched fluorescently labelled, areas with proteolytic activity become visible after degradation of the substrate, thereby releasing the fluorescent signal in those areas. Using this technique, gelatinolytic activity could be detected in 3D tumour models of both cell lines under static and dynamic conditions and after 14 days of culture (Figure 14), suggesting that active MMPs are present in the tumour tissue especially where the tumour cells are located. For better orientation, *in situ* zymography was combined with immunofluorescence staining for collagen IV in order to visualize the scaffold.

Taken together, the differences in invasive behaviour described in literature for MCF-7 and MDA-MB-231 cells could be reproduced in the here presented model system using SISmuc as a scaffold. Furthermore, SEM and *in situ* zymography studies suggest an active alteration of the scaffold and its preserved basement membrane structure especially by the invasive cell line MDA-MB-231. This suggests that the here presented 3D models are suitable to analyse aspects of the invasive process.

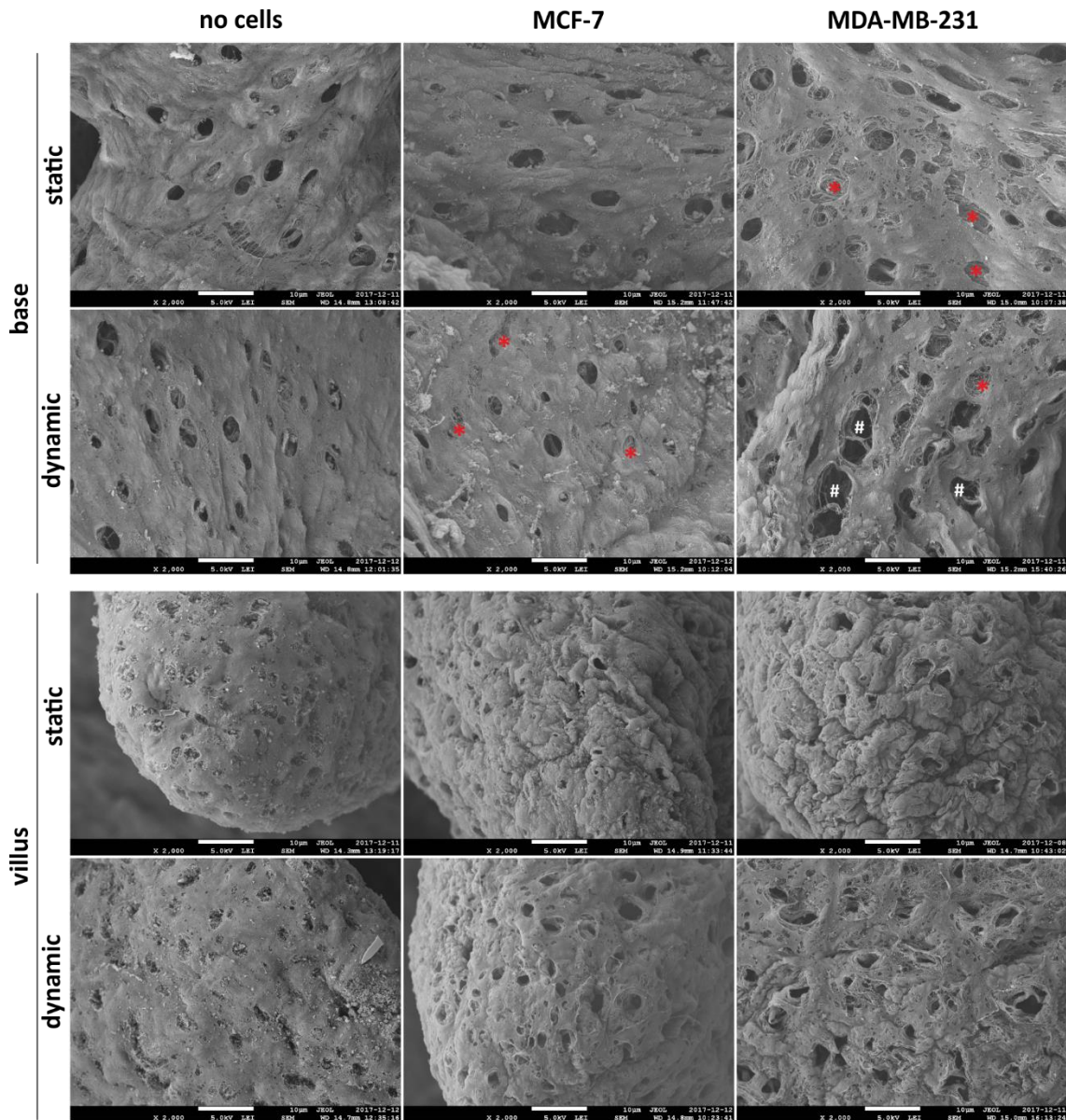


Figure 13: Structural analysis of scaffold SIS muc after tumour cell culture

SEM images of decellularised SIS muc scaffolds. The scaffolds were reseeded with no cells (left), MCF-7 (middle) or MDA-MB-231 cells (right) and cultured for 14 days under static or dynamic conditions. After this culture period, scaffolds were decellularised again and analysed by SEM imaging at the base (upper panel) of the SIS muc or at the tips of the villi (lower panel). *: Sites of destroyed basement membrane with visibility of underlying collagen network. #: Larger holes without visibility of the underlying collagen network. Scale bar: 10 μm.

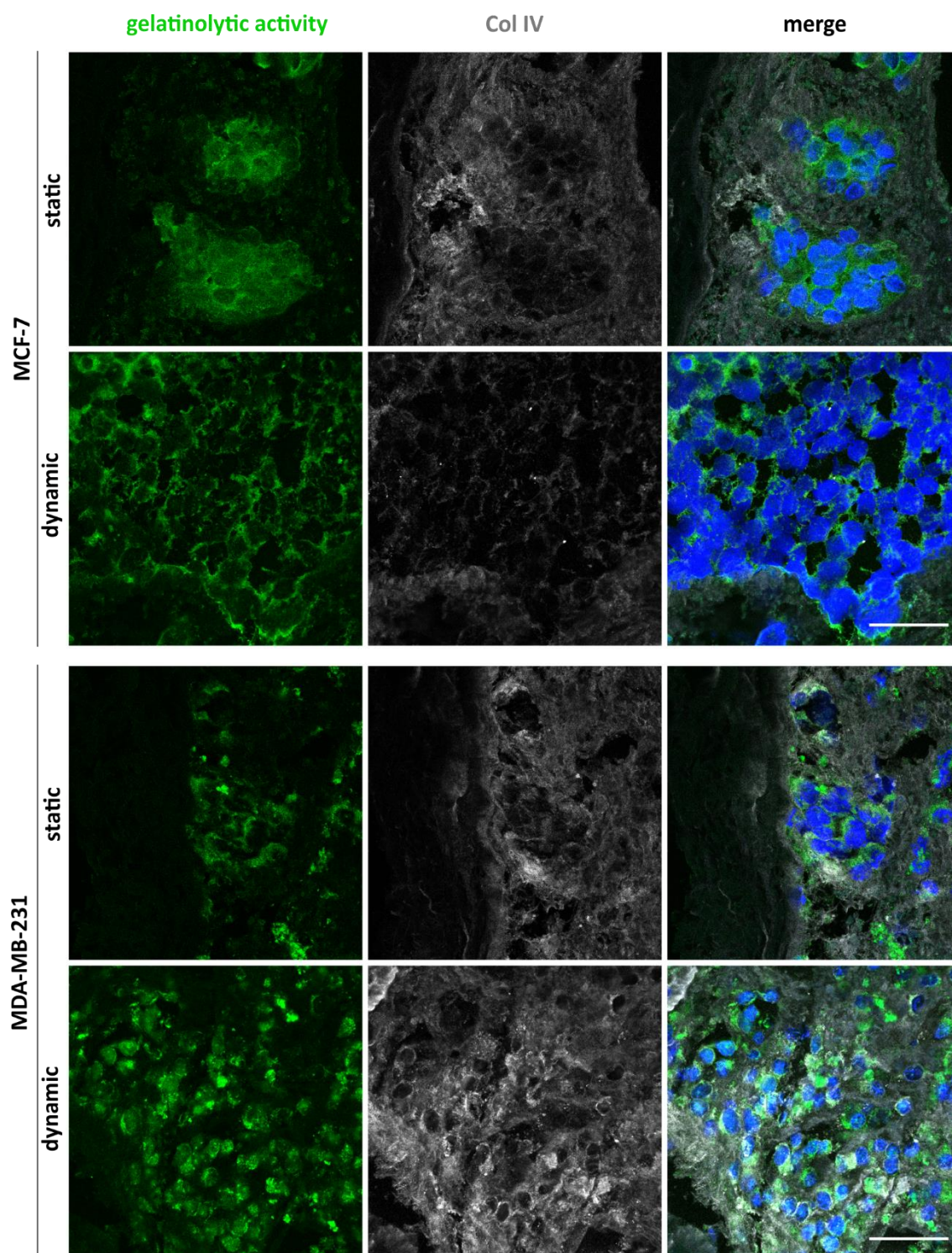


Figure 14: Gelatinolytic activity in 3D models of MCF-7 and MDA-MB-231 cells

In situ zymography combined with immunofluorescence staining against collagen IV (grey) of MCF-7 or MDA-MB-231 models cultured under 3D static or 3D dynamic conditions for 14 days. Signal of gelatinolytic activity (green) resulting from digest of DQTM gelatin. Nuclei are counterstained with DAPI (blue). Scale bar: 50 μ m. Experiment performed by Tina Schmitt.

4.3 Validation of the test system with a targeted therapy approach

After characterization of the 3D mamma carcinoma models, their ability to correctly predict therapy efficacy of compounds that are already well established in the clinical routine was investigated. For this, the targeted therapy approach with the humanized antibody trastuzumab (Herceptin®) was used, which is in routine clinical use for HER2/Neu-overexpressing mamma carcinomas but not for the molecular subsets of TNBC and ER-positive breast cancer as these subsets lack the expression of the target. As already introduced, several MOAs are discussed for trastuzumab that directly or indirectly suppress the tumour cells' growth, proliferation and survival.

At first, 2D and 3D static or orbital shaker cultures of MCF-7, MDA-MB-231 and SKBR-3 cells were treated with different concentrations of trastuzumab for 48 h. In 2D, SKBR-3 cells showed a slight decrease of cell viability for all concentrations applied with a minimum of 80.3 % after treatment with 5 µg/ml, while MCF-7 and MDA-MB-231 cells did not show any response to the treatment regardless of the dose administered (Figure 15 A). However, the observed decrease in cell viability of SKBR-3 cells was not significant compared to the untreated control. In 3D, no treatment effect on cell viability could be observed for any of the cell lines regardless of the trastuzumab concentration applied (Figure 15 B). These findings go in line with apoptosis data: Neither in 2D nor in 3D models a clear increase of apoptosis could be observed for any of the cell lines irrespective of the concentration applied (Figure 16 A and B).

As ADCC is also a discussed MOA of trastuzumab, it was then tested if this could be measured in the 3D models. For this purpose, an ADCC reporter gene assay was used and the original 2D protocol was adapted for the 3D model system. Indeed, the treatment of 3D SKBR-3 models with trastuzumab led to a potent induction of ADCC of up to 12.6-fold in SKBR-3 models according to the ADCC Reporter bioassay, while the induction of ADCC was low even for treatment with 30 µg/ml trastuzumab in MCF-7 and MDA-MB-231 models (Figure 17). However, the usage of this reporter assay is only an indirect method to measure ADCC induction via the activation of a reporter gene in an effector cell line engineered to express FcγRIIIa without any direct tumour cell killing being involved. Therefore, it was investigated if an immunological component in the form of PBMCs can be introduced into the 3D mamma carcinoma test system and whether this model can be used to directly measure ADCC via tumour cell apoptosis. PBMCs (Figure 18 A, black arrows) migrated into the tumour tissue of all three models and these immune cells were still viable after the treatment period of 48 h. Trastuzumab treatment of these models with included immunological component led to a dose-dependent decrease of tumour cell number in 3D SKBR-3 models according to H&E staining. In contrast, no clear effect was visible even for treatment with the highest concentration of 30 µg/ml trastuzumab in the MCF-7 and MDA-MB-231 cells (Figure 18 B). Treatment with 30 µg/ml isotype control antibody failed to induce a reduction of tumour cell number in models of all three cell lines, indicating that the effect of trastuzumab treatment observed in the SKBR-3 models is specific. These findings are underlined by the measurements of tumour cell apoptosis (Figure 19): In SKBR-3 models, a dose-dependent increase of apoptosis was observed. This was not the case for MDA-MB-231 models treated with the highest concentration of 30 µg/ml trastuzumab. MCF-7 models displayed a slight

increase of apoptosis in the first 24 h of treatment which goes in line with the weak expression of HER2 described in 4.1.1. Again, treatment with the isotype control antibody failed to induce apoptosis in models of all molecular subsets.

Taken together, biomarker-dependent therapy efficacy could be measured in the 3D mamma carcinoma models regarding ADCC, which was possible by the introduction of PBMCs as an immunological component into the 3D test system and correlated with the clinical response.

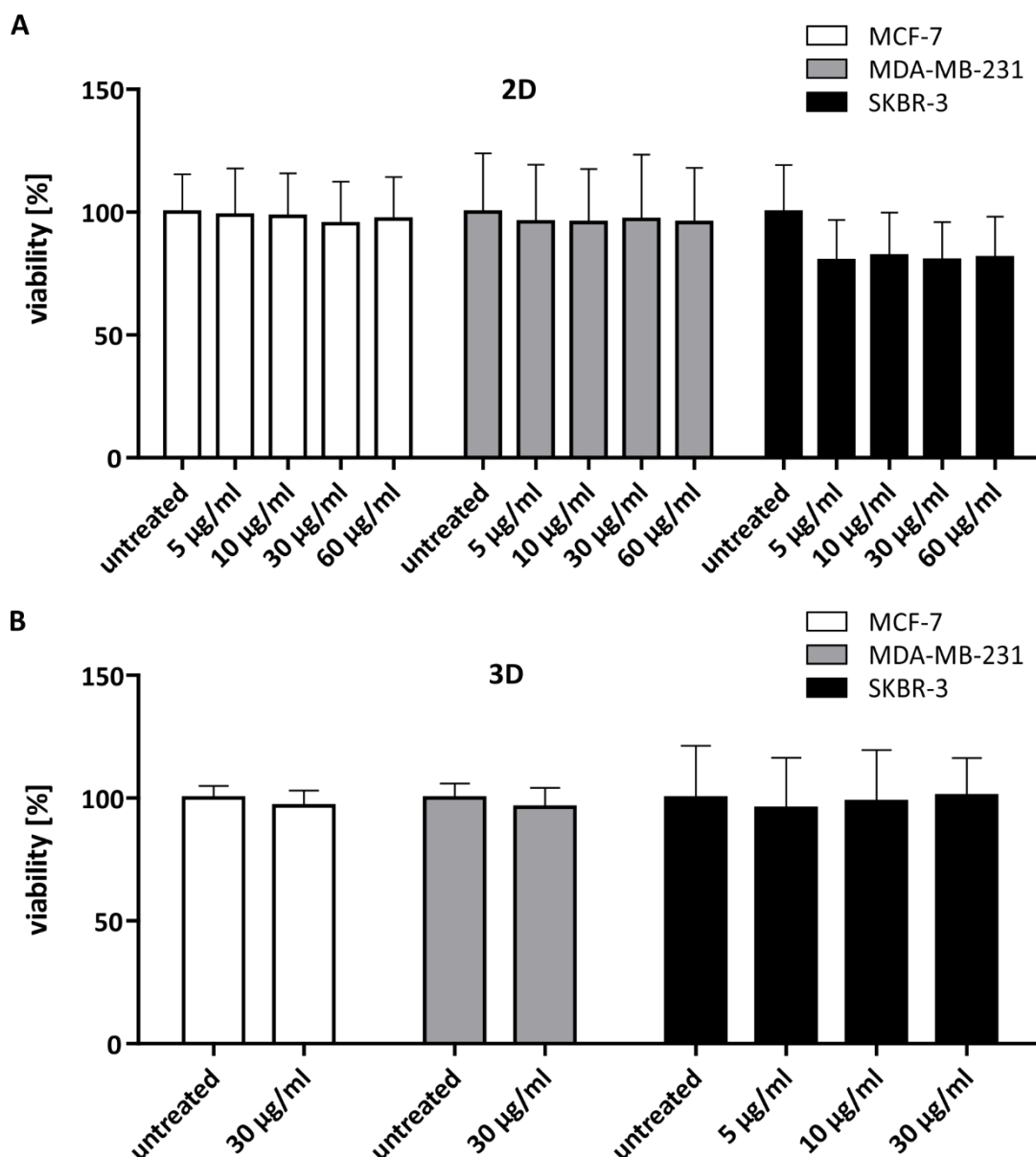


Figure 15: Cell viability after treatment with trastuzumab

Cell viability of MCF-7, MDA-MB-231 and SKBR-3 cells cultured under 2D (A) or 3D conditions (B) was determined by MTT assay after 48 h of treatment with indicated concentrations of trastuzumab. Cell viability was not significantly decreased upon treatment with trastuzumab irrespective of the concentration and culture method in any of the cell lines. Data are displayed as percentage of the untreated control and presented as arithmetic mean \pm SD (n=4). Statistical significance values by pairwise Wilcoxon rank sum test with Bonferroni correction.

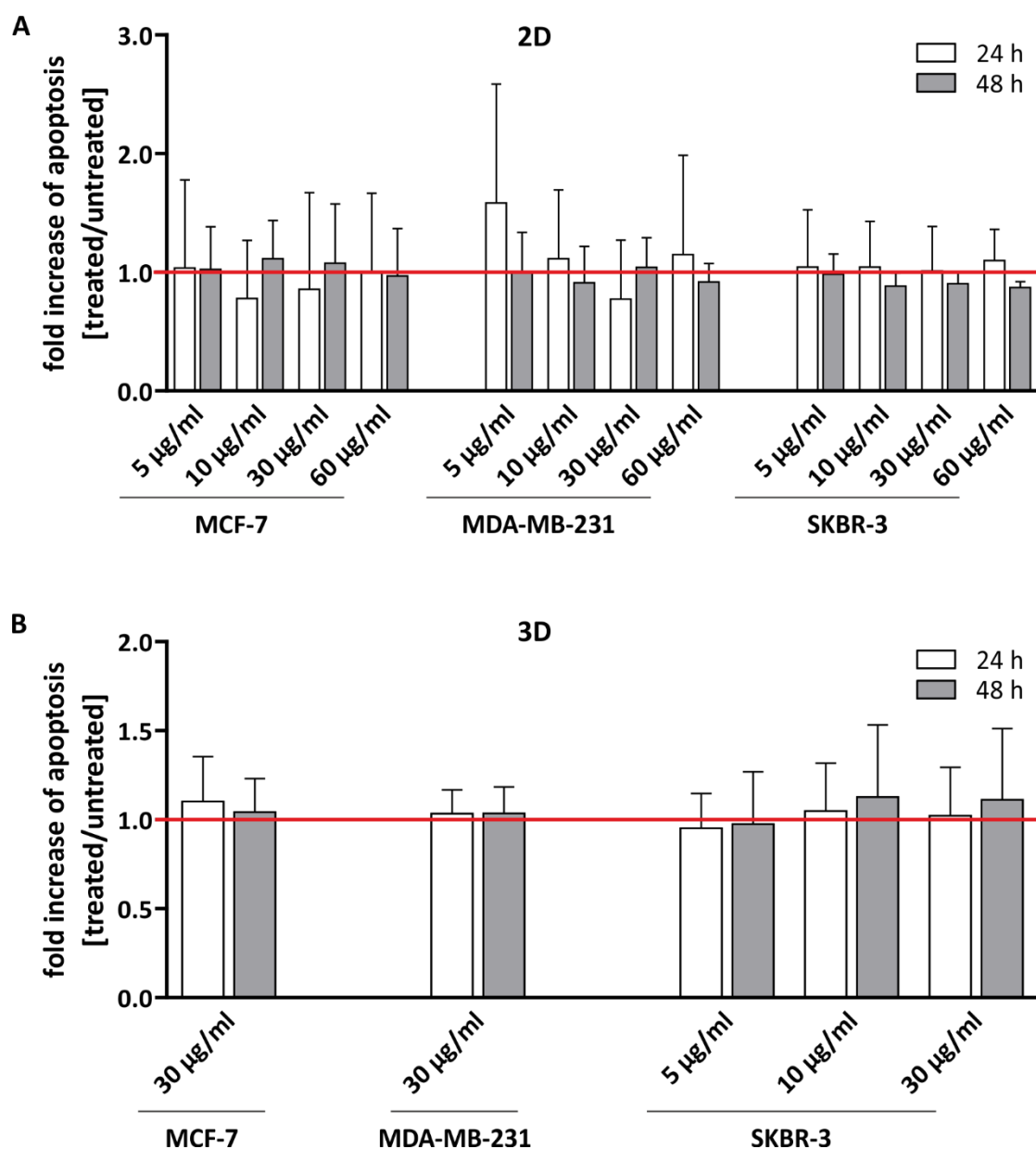


Figure 16: Apoptosis after treatment with trastuzumab

Fold increase of apoptosis of MCF-7, MDA-MB-231 and SKBR-3 cells cultured under 2D (A) or 3D conditions (B) after treatment with indicated concentrations of trastuzumab (determined by M30 Cytodeath™ ELISA). Apoptosis was not significantly increased irrespective of trastuzumab concentration and culture method in any of the cell lines. Data are normalized to the untreated control (red line) and presented as arithmetic mean +SD ($n \geq 4$). Statistical significance values by pairwise Wilcoxon rank sum test with Bonferroni correction.

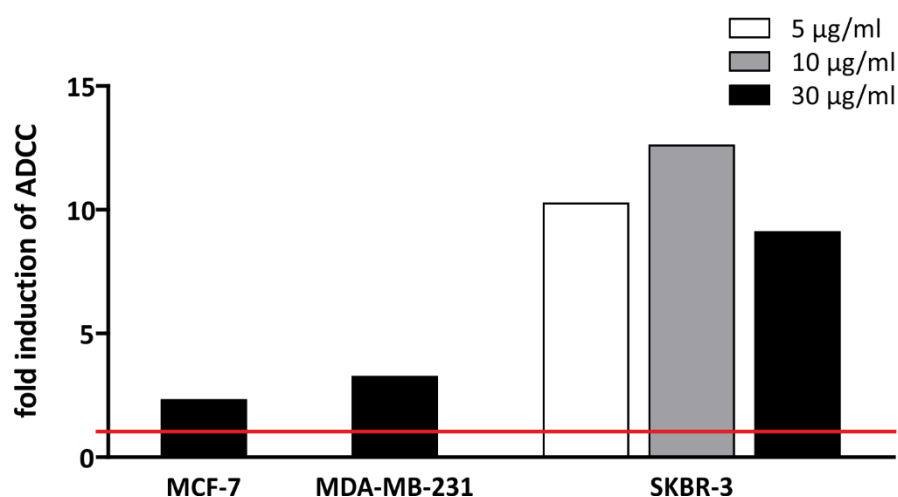


Figure 17: Antibody-dependent cell-mediated cytotoxicity after treatment with trastuzumab

Fold induction of ADCC in MCF-7, MDA-MB-231 and SKBR-3 cells cultured under 3D conditions was determined by ADCC Reporter Bioassay after 24 h of treatment with indicated concentrations of trastuzumab. Data are normalized to the untreated control (red line, $n=1$). ADCC was strongly increased irrespective of trastuzumab concentration in the SKBR-3 model compared to MCF-7 and MDA-MB-231 model.

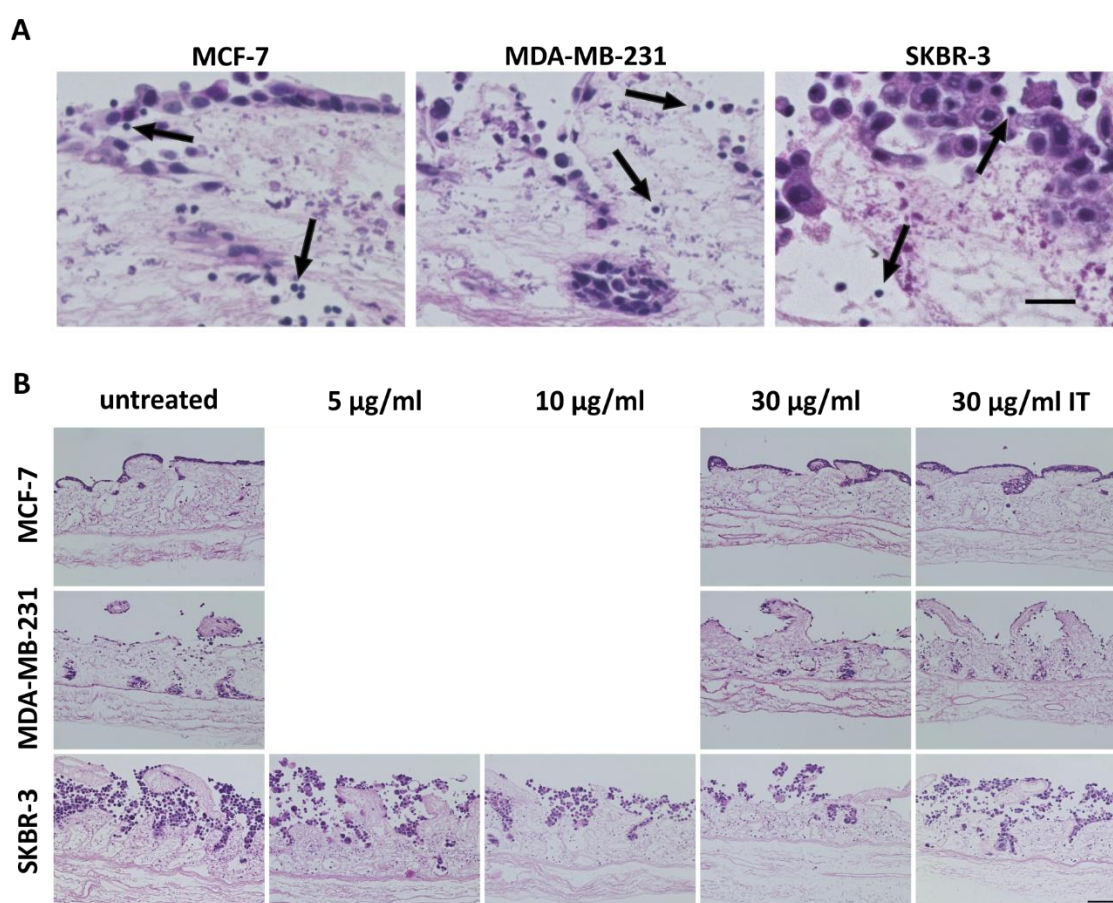


Figure 18: ADCC in 3D models with integrated immunological component

A: H&E staining of 3D models with PBMCs as an immunological component showed infiltration of PBMCs (black arrows) into the tumour cell mass and the scaffold in all models. Scale bar: 25 µm. B: H&E staining of 3D models with PBMCs as an immunological component treated with different concentrations of trastuzumab showed a decrease in tumour cell numbers only in the SKBR-3 model. IT: Isotype control. Scale bar: 100 µm.

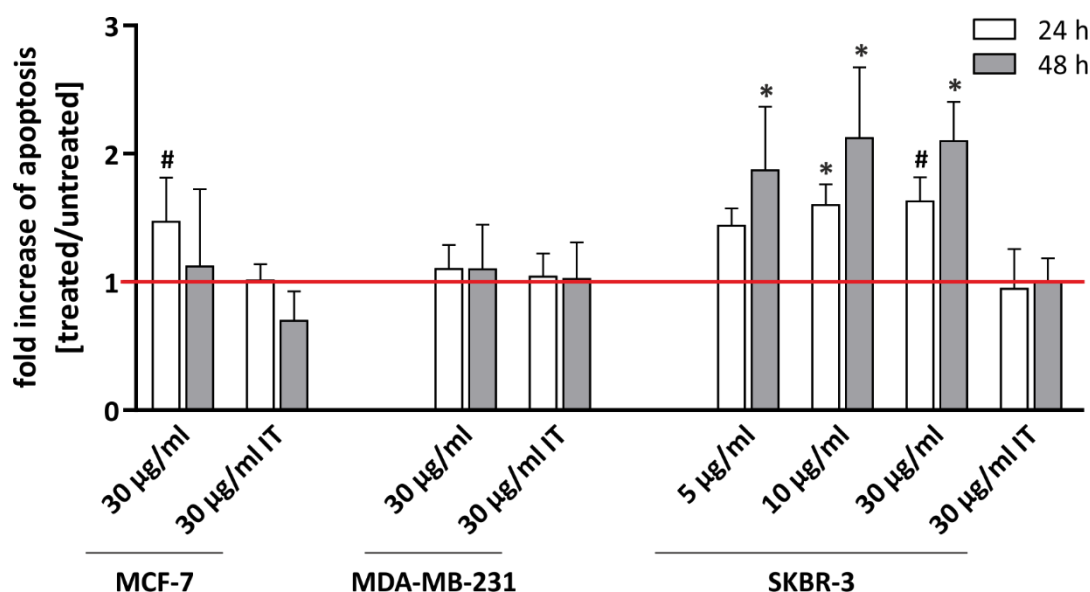


Figure 19: Apoptosis in 3D models with integrated immunological component

A: Fold increase of apoptosis of MCF-7, MDA-MB-231 and SKBR-3 cells cultured under 3D conditions was determined by M30 Cytodeath™ ELISA after treatment with indicated concentrations of trastuzumab and PBMCs as an immunological component. Apoptosis was significantly increased irrespective of trastuzumab concentration only in SKBR-3 models. IT: Isotype control. Data are normalized to the untreated control (red line) and presented as arithmetic mean +SD (n=6 with 3 different donors of PBMCs). Statistical significance values by pairwise Wilcoxon rank sum test with Bonferroni correction: # 0.05 < p < 0.1, * p < 0.05.

4.4 Application of the established test system

4.4.1 Evaluation of an innovative drug formulation strategy

A major obstacle in the development of novel anti-cancer drugs is the formulation of the compounds that are often poorly soluble in water in a way that allows effective dosage and treatment in patients. In order to overcome this obstacle, the development of excipients and innovative formulation strategies that improve the solubility, thereby increasing the bioavailability of such hydrophobic compounds, is necessary.

Here, an ultra-high loaded nanoformulation of the practically water-insoluble natural compound curcumin with the copolymer A-pPrOzi-A, was compared in 2D culture and in the 3D models of MDA-MB-231. The cytotoxic effects of the curcumin-loaded nanoformulation was compared with curcumin solved in DMSO. Bright field images of 2D cultures of MDA-MB-231 cells treated with increasing concentrations of up to 25 µM curcumin in the different formulations revealed a dose-dependent decrease of cell number for both formulations (Figure 20 A). In contrast, the same concentrations of curcumin in both formulations did not have an effect on the cell number in the 3D model of MDA-MB-231 cells as indicated by H&E staining (Figure 20 B). In the 3D context, higher doses of curcumin of 100 µM and higher were required to achieve a decrease in cell number. This goes in line with the viability data from MTT assay (Figure 21), illustrating a distinct reduction of tumour cell viability for concentrations of curcumin as low as 15 µM in 2D,

whereas no effect on cell viability for concentrations up to 25 μM curcumin was detected in the 3D model and concentrations of 100 μM and higher were necessary to reduce tumour cell viability. Furthermore, viability data demonstrated that there were no pronounced differences between the nanoformulation of curcumin with the copolymer A-pPrOzi-A and the DMSO-formulated control. These results are part of a manuscript that is posted as a preprint (Lübtow, Nelke, *et al.*, 2017).

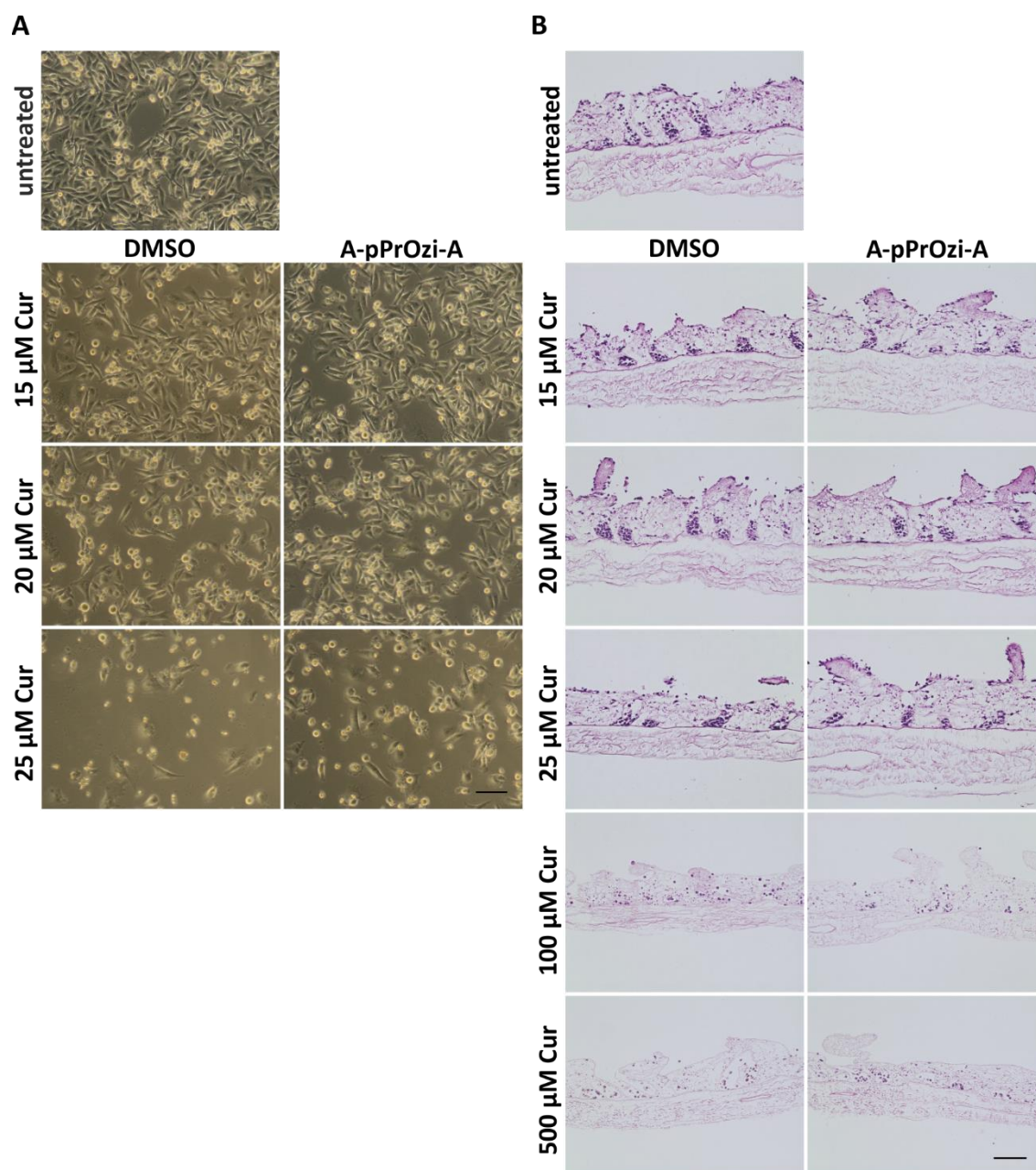


Figure 20: Treatment with curcumin in DMSO-formulation or with curcumin-loaded A-pPrOzi-A micelles under 2D and 3D conditions

Bright field images of MDA-MB-231 cells cultured under 2D (A) or H&E staining of MDA-MB-231 cultured under 3D conditions (B) treated with the indicated concentrations of curcumin (Cur) formulated in DMSO or A-pPrOzi-A for 72 h. MDA-MB-231 cells showed weaker response to both formulations when cultured under 3D conditions. Scale bar: 100 μm . Information from B is part of a preprint publication (Lübtow, Nelke, *et al.*, 2017).

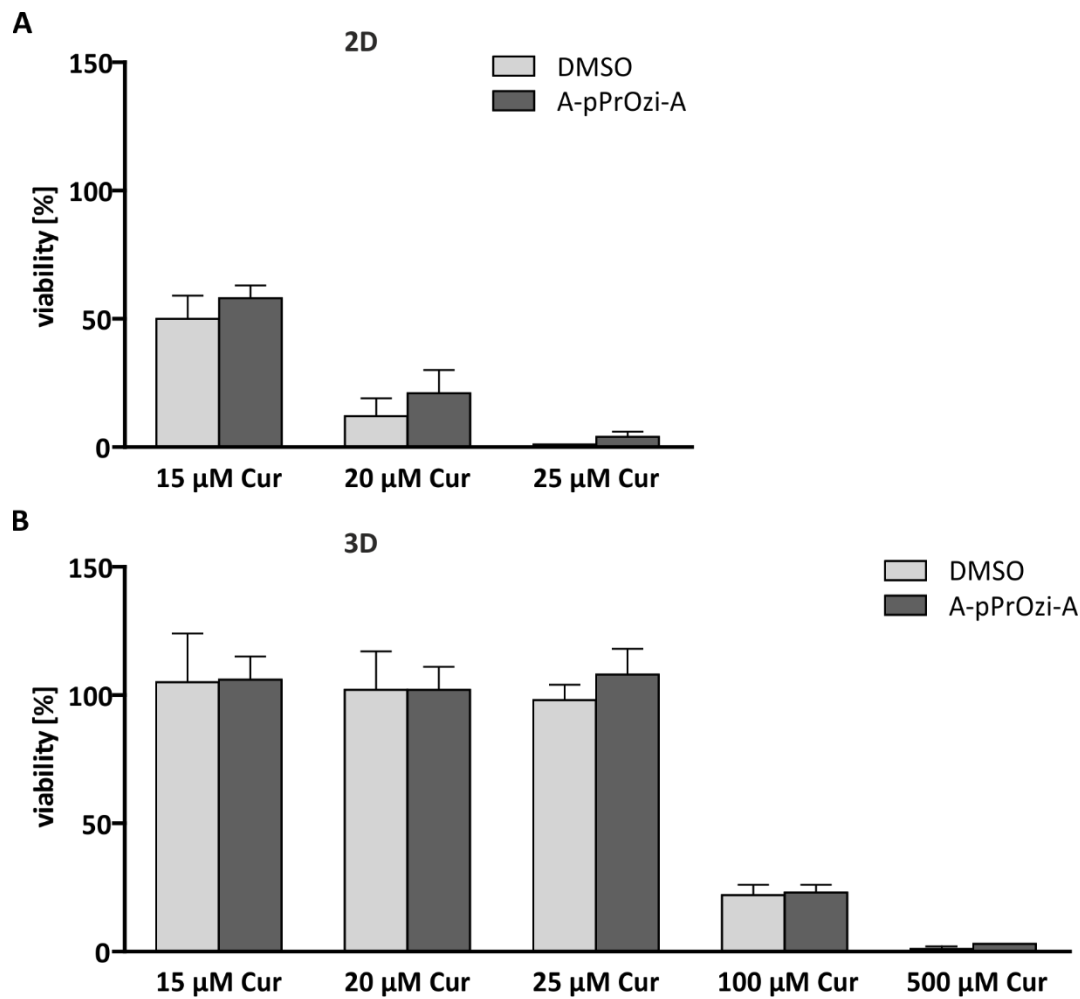


Figure 21: Cell viability after treatment with curcumin in DMSO-formulation or with curcumin-loaded A-pPrOzi-A micelles under 2D and 3D conditions

Cell viability of MDA-MB-231 cells cultured under 2D (A) or 3D conditions (B) was determined by MTT assay after 72 h of treatment with indicated concentrations of curcumin (Cur). Cell viability was strongly decreased upon treatment with curcumin in a dose-dependent manner in both formulations under 2D conditions. Under 3D conditions this response was alleviated and higher concentrations of curcumin were necessary to reduce cell viability. Data are displayed as percentage of the untreated control and presented as arithmetic mean \pm SD ($n=4$). Statistical significance values by pairwise Wilcoxon rank sum test with Bonferroni correction. Background correction of MTT-values was performed for treatment with 500 μ M curcumin, as minor assay interference was observed for this concentration. Information from this figure is part of a preprint publication (Lübtow, Nelke, *et al.*, 2017).

4.4.2 Testing of novel therapeutic strategies in the TNBC model

TNBC is the most aggressive molecular subset of mamma carcinoma and has the worst prognosis for patients. One of the reasons for this is that no targeted therapies are available for this subset so far. Therefore, testing of novel treatment strategies in this work focused on the TNBC model.

4.4.2.1 Combination therapy with doxorubicin and MK-1775

MK-1775 is a small molecule inhibitor of WEE1 kinase, a tyrosine kinase involved in cell cycle progression. Inhibition of this kinase impairs the G2 DNA-damage checkpoint. This checkpoint is especially important for *p53*-mutated cells, as these cells lack the G1 checkpoint. Annulment of the G2 checkpoint may therefore sensitize these cells for DNA-damaging therapies like chemotherapies. The *p53*-mutated background of the MDA-MB-231 cell line, makes it a candidate for this type of therapy which is in several clinical trials for different types of tumours at the moment. Therefore, therapy with MK-1775 alone and in combination with the DNA-damaging chemotherapeutic doxorubicin was tested in the model system.

Initially, the sensitivity of MDA-MB-231 cells towards different concentrations of doxorubicin and MK-1775 alone and in combination in 2D was determined by CellTiter-Glo® Luminescent Cell Viability Assay in order to identify synergistic effects and suitable concentrations for further testing (Figure 22). Treatment with 0.5 μ M MK-1775 alone led to a decrease in cell viability to 44 % which is close to the half maximal inhibitory concentration (IC50) and indicates a single-agent activity of MK-1775. The chemotherapeutic doxorubicin alone also led to a decrease in cell viability to 77 % and 44 % for a concentration of 0.1 and 0.5 μ M, respectively. The combination with 0.5 μ M MK-1775 further decreased cell viability to 33 % and 24 %, respectively. According to these results, doxorubicin concentrations of 0.1 and 0.5 μ M and MK-1775 concentration of 0.5 μ M was selected for further experiments. These results go in line with the phase contrast images (Figure 23, left panel) and viability data from MTT assay (Figure 24 A) of 2D cultures treated with the indicated concentrations of doxorubicin and MK-1775 alone or in combination. Here as well, a reduction in cell number and viability for treatment with doxorubicin and MK-1775 alone and a further decrease in combination therapy could be observed. In contrast, the same concentrations of doxorubicin and MK-1775 alone and in combination did neither lead to a clear reduction of tumour cell number (Figure 23, right panel) nor to a strong decrease of cell viability (Figure 24 B). These findings are corroborated by apoptosis data: Whereas in 2D a potent increase of apoptosis of up to 5.0-fold could be observed for treatment with MK-1775 and the combination therapies, the increase of apoptosis in the 3D model of MDA-MB-231 cells was as low as 1.7-fold compared to the untreated control (Figure 25).

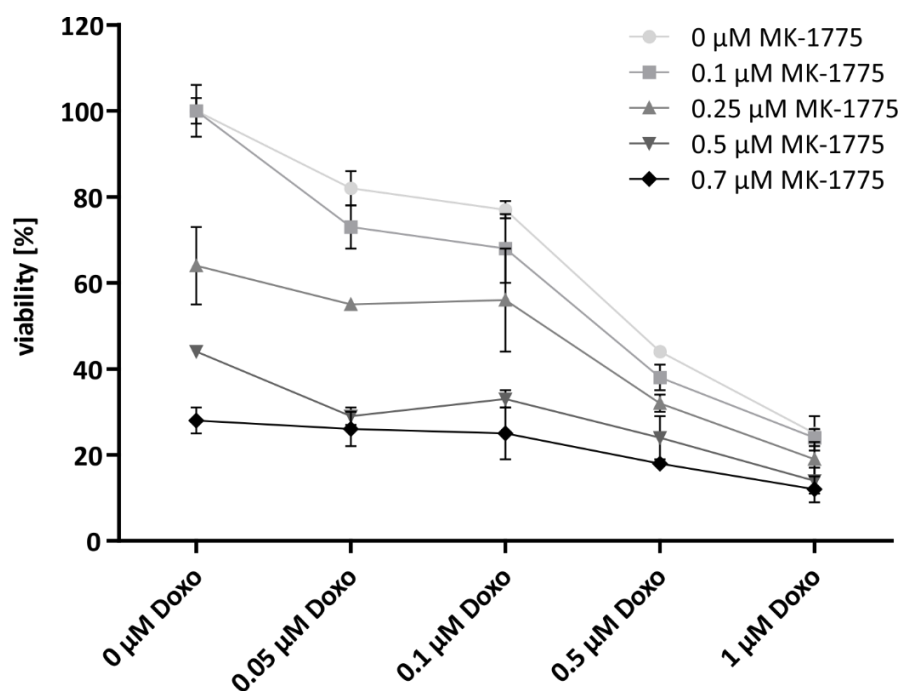


Figure 22: Cell viability of MDA-MB-231 cells treated with different doses of doxorubicin +/- MK-1775 in 2D conditions

Cell viability of MDA-MB-231 cells cultured under 2D conditions was determined by CellTiter-Glo® Luminescent Cell Viability Assay after 72 h of treatment with indicated concentrations of MK-1775, doxorubicin (Doxo) or a combination of both. Data are displayed as percentage of the untreated control and presented as arithmetic mean +SD (n=1).

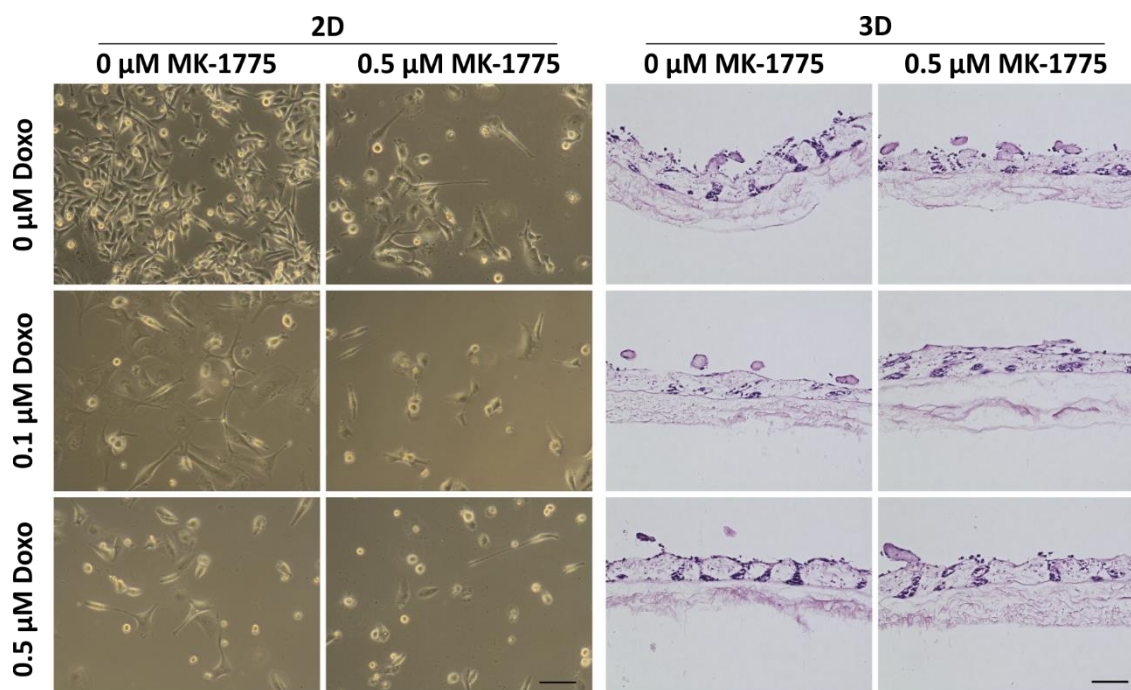


Figure 23: Treatment with doxorubicin +/- MK-1775 under 2D and 3D conditions

Bright field images of MDA-MB-231 cells cultured under 2D (left panel) or H&E staining of MDA-MB-231 cultured under 3D conditions (right panel) treated with the indicated concentrations of doxorubicin (Doxo) +/- MK-1775 for 72 h. MDA-MB-231 cells showed weaker response to doxorubicin, MK-1775 and combination therapy when cultured under 3D conditions. Scale bar: 100 μm.

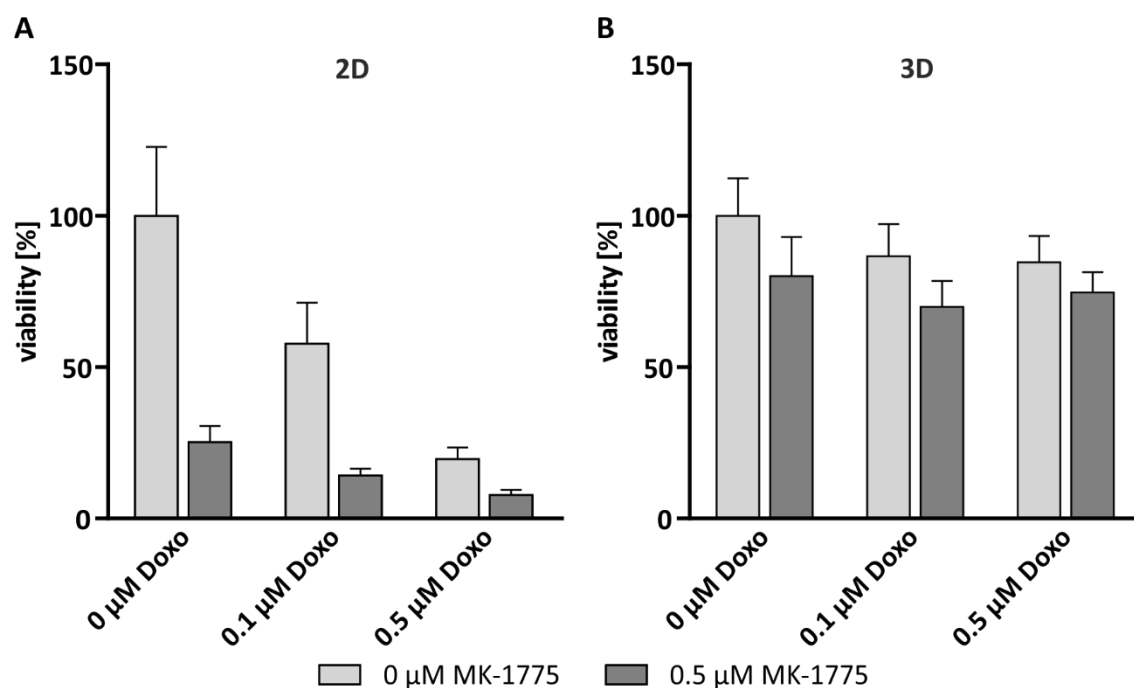


Figure 24: Cell viability after treatment with doxorubicin +/- MK-1775 under 2D and 3D conditions

Cell viability of MDA-MB-231 cells cultured under 2D (A) or 3D conditions (B) was determined by MTT assay after 72 h of treatment with indicated concentrations of doxorubicin (Doxo) +/- MK-1775. Cell viability was strongly decreased upon treatment with doxorubicin in a dose-dependent manner and upon treatment with MK-1775 under 2D conditions. Under 3D conditions this response was alleviated. Data are displayed as percentage of the untreated control and presented as arithmetic mean \pm SD ($n=5$ for A, $n=4$ for B). Statistical significance values by pairwise Wilcoxon rank sum test with Bonferroni correction.

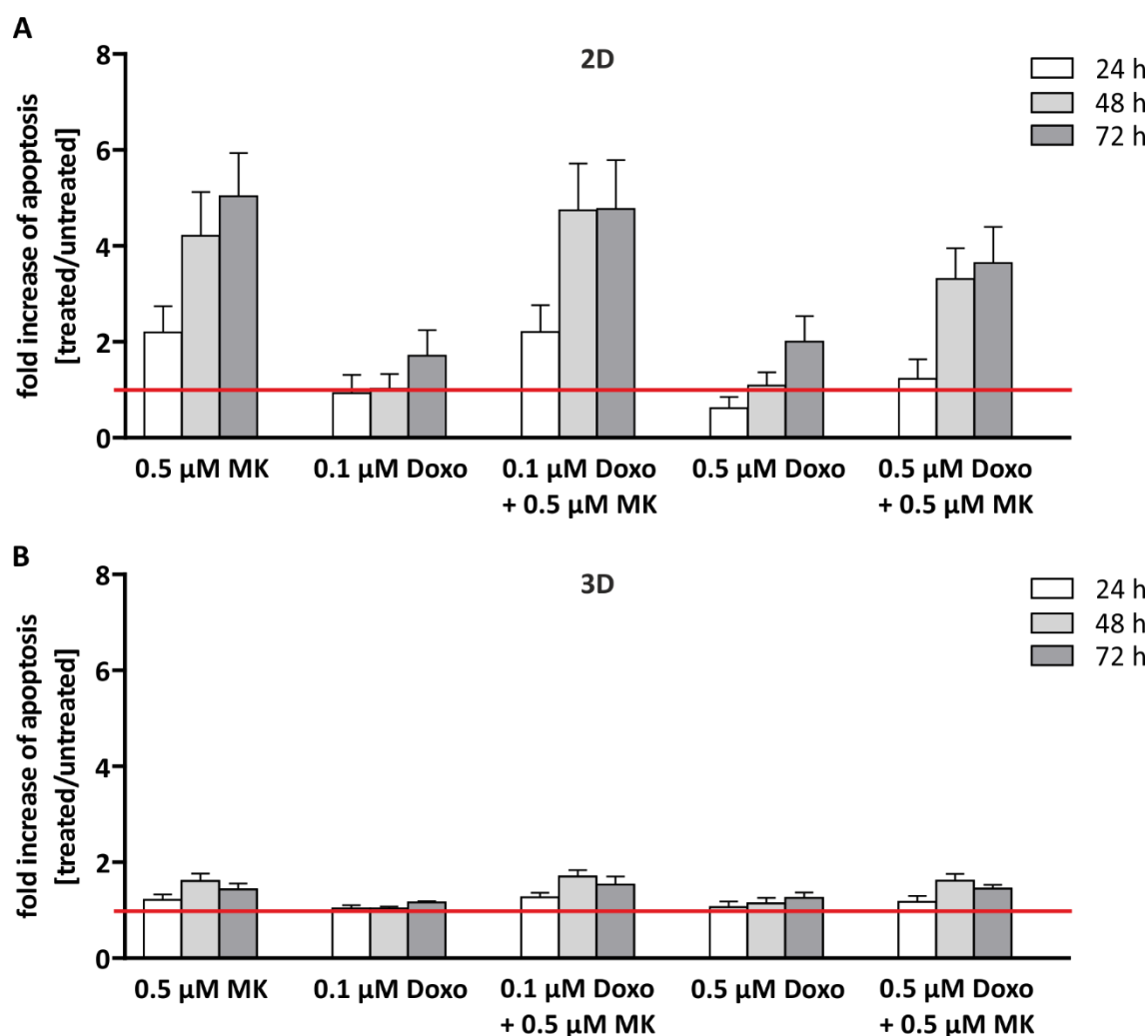


Figure 25: Apoptosis after treatment with doxorubicin +/- MK-1775 under 2D and 3D conditions

Fold increase of apoptosis of MDA-MB-231 cells cultured under 2D (A) or 3D conditions (B) was determined by M30 Cytodeath™ ELISA after treatment with indicated concentrations of doxorubicin (Doxo) +/- MK-1775 (MK). Data are normalized to the untreated control (red line) and presented as arithmetic mean \pm SD (n=5). Statistical significance values pairwise Wilcoxon rank sum test with Bonferroni correction.

4.4.2.2 ROR1-CAR T cell therapy as an alternative treatment strategy

A novel therapy strategy from the field of anti-cancer immunotherapies is CAR T cell therapy using the patients' own T cells to target the tumour. After the great success of this therapy in patients with haematological cancers, there are efforts to transfer this therapeutic strategy also to solid tumours (Newick *et al.*, 2016; B. L. Zhang *et al.*, 2016). However, for the evaluation of such therapies, suitable models with a complex tissue architecture and the option for perfusion are necessary in order to make reliable predictions. Therefore, it was tested if the here presented 3D TNBC model can be used for the evaluation of CAR T cell therapy efficacy in solid tumours. For this purpose T cells expressing the ROR1-CAR that had been generated in the laboratory of Dr. Michael Hudecek were used. At first, it was confirmed that MDA-MB-231 cells express ROR1 in 2D culture and that this expression is also preserved under 3D culture conditions (data not shown).

When conventional 2D cultures of MDA-MB-231 cells were treated with increasing concentrations of ROR1-CAR T cells or untransduced control T cells from the same donor, a potent killing of tumour cells and thereby a decrease in their number could be detected only for the treatment with CAR T cells but not with control T cells (Figure 26 A). This goes in line with a strong increase of tumour cell apoptosis upon treatment with CAR T cells that was significantly higher compared to treatment with control T cells. (Figure 26 B). These results indicate that ROR1-CAR T cells are able to efficiently lyse tumour cells that express the ROR1 antigen on their surface. However, it is not clear if this is also the case in tumours with a more complex tissue architecture, where the T cells have to migrate to the tumour cells. Therefore, ROR1-CAR T cell efficacy was then tested in the 3D static MDA-MB-231 model. A dose-dependent migration of CD45⁺ T cells into the models and an interaction with the tumour cells could be observed for both ROR1-CAR and control T cells (Figure 27 A-I). However, only ROR1-CAR T cells were able to potently induce a dose-dependent tumour cell apoptosis in the 3D static models (Figure 27 K) and proliferation of CAR T cells was significantly higher compared to the control T cells (Figure 27 J). This goes in line with a stronger activation of ROR1-CAR T cells compared to control cells according to CD25 and CD69 expression assessed by flow cytometry after re-isolation of T cells from the tumour tissue (Hudecek group, data not shown).

As the T cells were applied to the medium on top of the tumour model, migration had to occur along the z-axis. Therefore, it could not be excluded, that T cell migration into the 3D static tumour models is mainly gravity-driven. Therefore, the 3D dynamic tumour models were used to investigate if CAR T cells manage to actively adhere to and migrate into the tumour to elicit their effector functions. To test this, the T cells were applied to the medium reservoir of the bioreactor system, thereby circulating through the tubing system and bypassing the tumour tissue. The H&E overview staining revealed a decrease in tumour cell number after treatment with ROR1-CAR but not with control T cells (Figure 28 A-C). The CD45 immunofluorescence staining shows that both ROR1-CAR as well as control T cells were indeed able to adhere to the tumour cells and deeply migrate into the tumour tissue despite the medium flow. However, the proliferation of ROR1-CAR T cells was significantly higher compared to control T cells (Figure 28 G). Also, the increase of tumour cell apoptosis was significantly higher after ROR1-CAR T cell treatment (Figure 28 H). Furthermore, the here presented tumour models also allowed the further investigation of T cells and their functions after treatment: ROR1-CAR T cells showed a stronger activation according to CD25 and CD69 expression assessed via flow cytometry and a significantly higher secretion of the cytokines IL-2 and IFN γ to the medium (Hudecek group, data not shown).

Taken together, it could be shown that ROR1-CAR T cells could efficiently lyse complex tumour tissues and that the here presented tumour model is a powerful tool for the investigation of such therapy approaches.

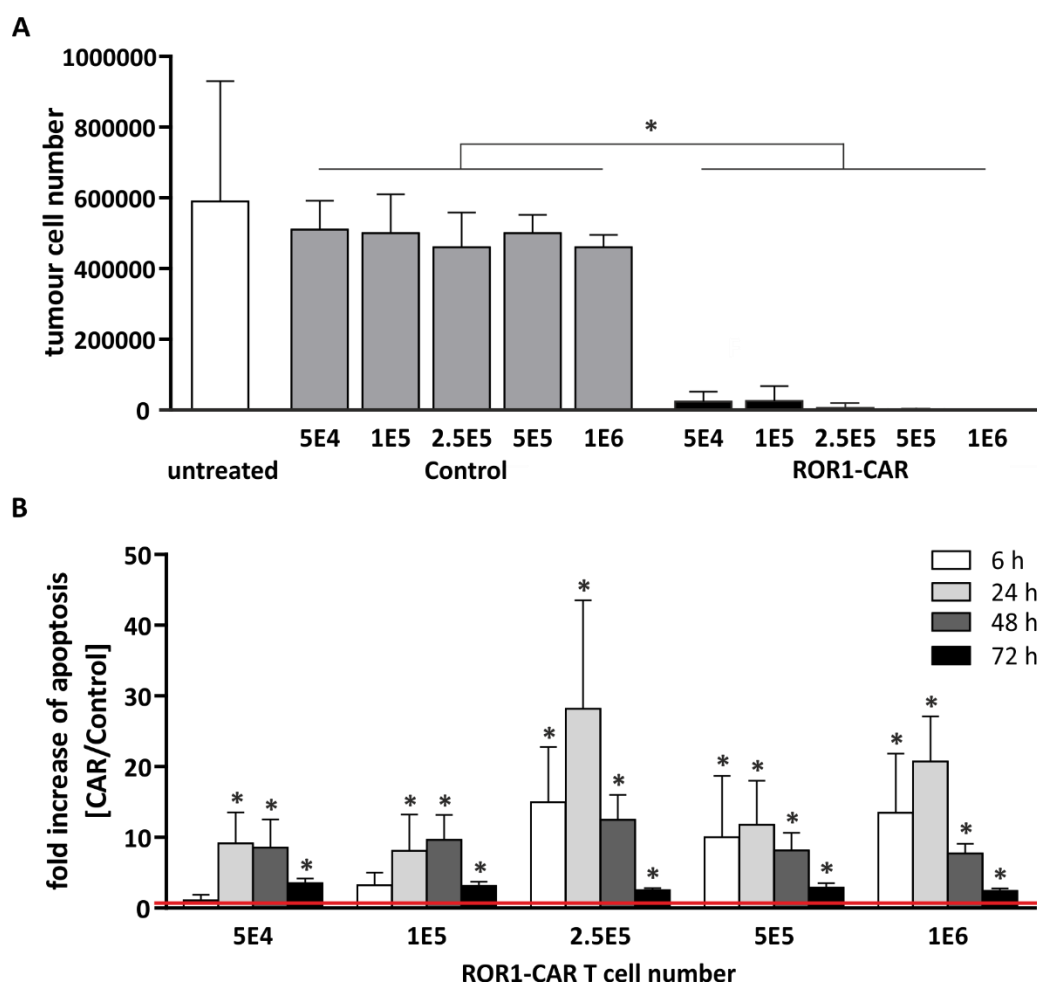


Figure 26: Treatment with ROR1-CAR T cells under 2D conditions

A: MDA-MB-231 cell number per 6-well after 72 h of treatment with the indicated cell number of ROR1-CAR T cells or untransduced control T cells (Control) under 2D conditions. Cell number of surviving tumour cells was significantly decreased upon treatment with ROR1-CAR T cells compared to treatment with corresponding control T cells. Data is presented as arithmetic mean \pm SD (n=4). Statistical significance values by Wilcoxon rank sum test: * p<0.05. B: Fold increase of apoptosis of MDA-MB-231 cells cultured under 2D conditions was determined by M30 Cytodeath™ ELISA after treatment with indicated cell number of ROR1-CAR T cells for 72 h. Tumour cell apoptosis was significantly increased upon treatment with ROR1-CAR T cells compared to control T cells. Data are normalized to the corresponding values of untransduced control T cells (red line) and presented as arithmetic mean \pm SD (n=4). Statistical significance values by Wilcoxon rank sum test: * p<0.05.

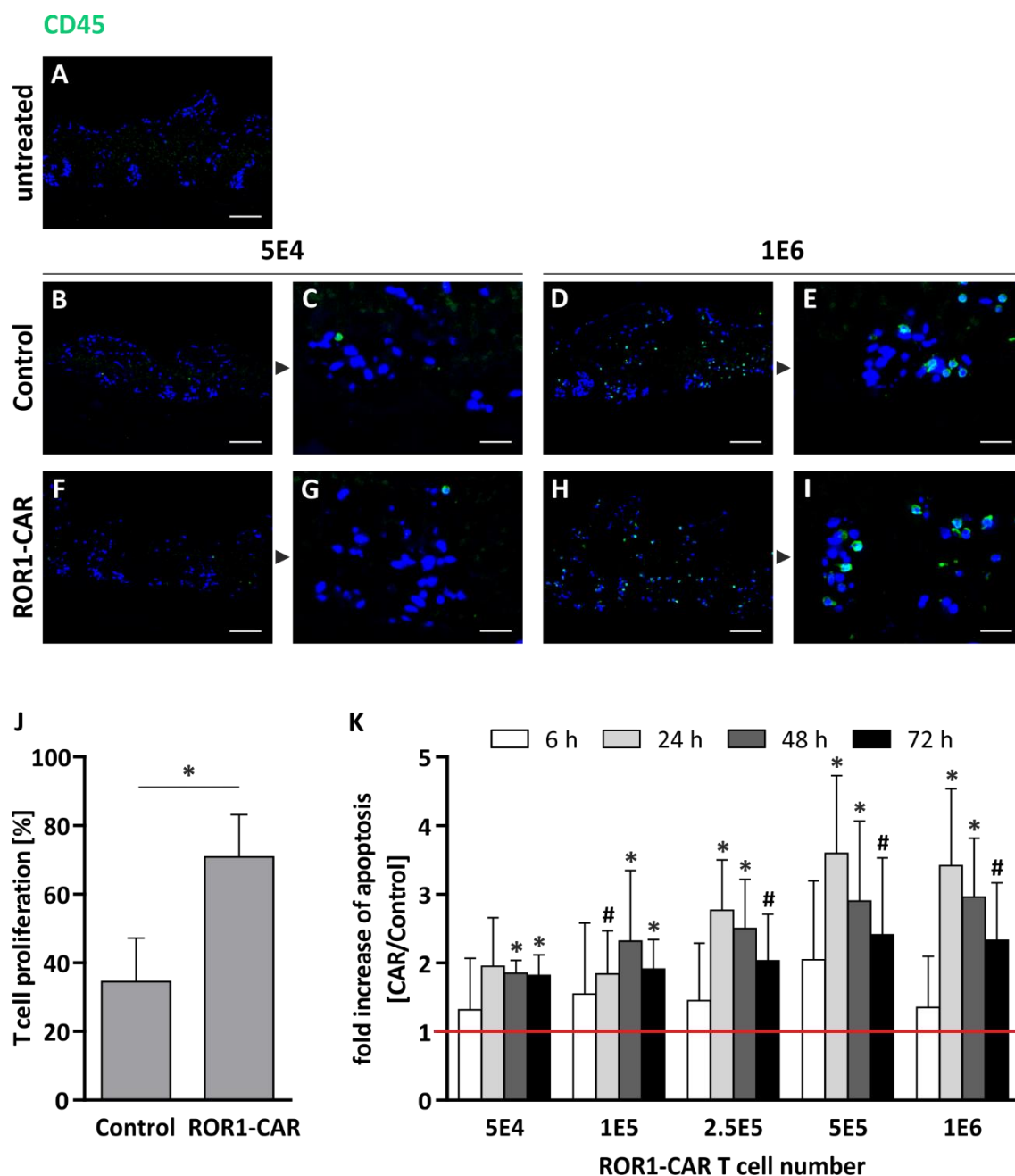


Figure 27: Treatment with ROR1-CAR T cells under 3D static conditions

3D static models of MDA-MB-231 cells were treated for 72 h with different cell numbers of ROR1-CAR or untransduced control T cells (Control). A-I: Immunofluorescence staining against CD45 (green). Nuclei are counterstained with DAPI (blue). Images C, G, E and I represent a magnification of the images on the left. Scale bar: 100 μ m (A, B, F, D, H) and 25 μ m (C, G, E, I). Staining shows a dose-dependent migration of ROR1-CAR and control T-cells into the tumour tissue. J: Proliferation of untransduced control or ROR1-CAR T cells was determined with the help of quantification of Ki67⁺/CD45⁺ cells from immunofluorescence staining (10 images per condition). Proliferation of ROR1-CAR T cells was significantly higher after 72 h of contact to 3D tumour models compared to control T cells. Data are presented as arithmetic mean \pm SD (n=4). Statistical significance values by Wilcoxon rank sum test: * p<0.05. K: Fold increase of apoptosis of MDA-MB-231 cells cultured under 3D conditions was determined by M30 CytodeathTM ELISA after treatment with indicated cell number of ROR1-CAR T cells. Tumour cell apoptosis was increased upon treatment with ROR1-CAR T cells compared to control T cells. Data are normalized to the corresponding values of untransduced control T cells (red line) and presented as arithmetic mean \pm SD (n=4). Statistical significance values by Wilcoxon rank sum test: # 0.05<p<0.1, * p<0.05.

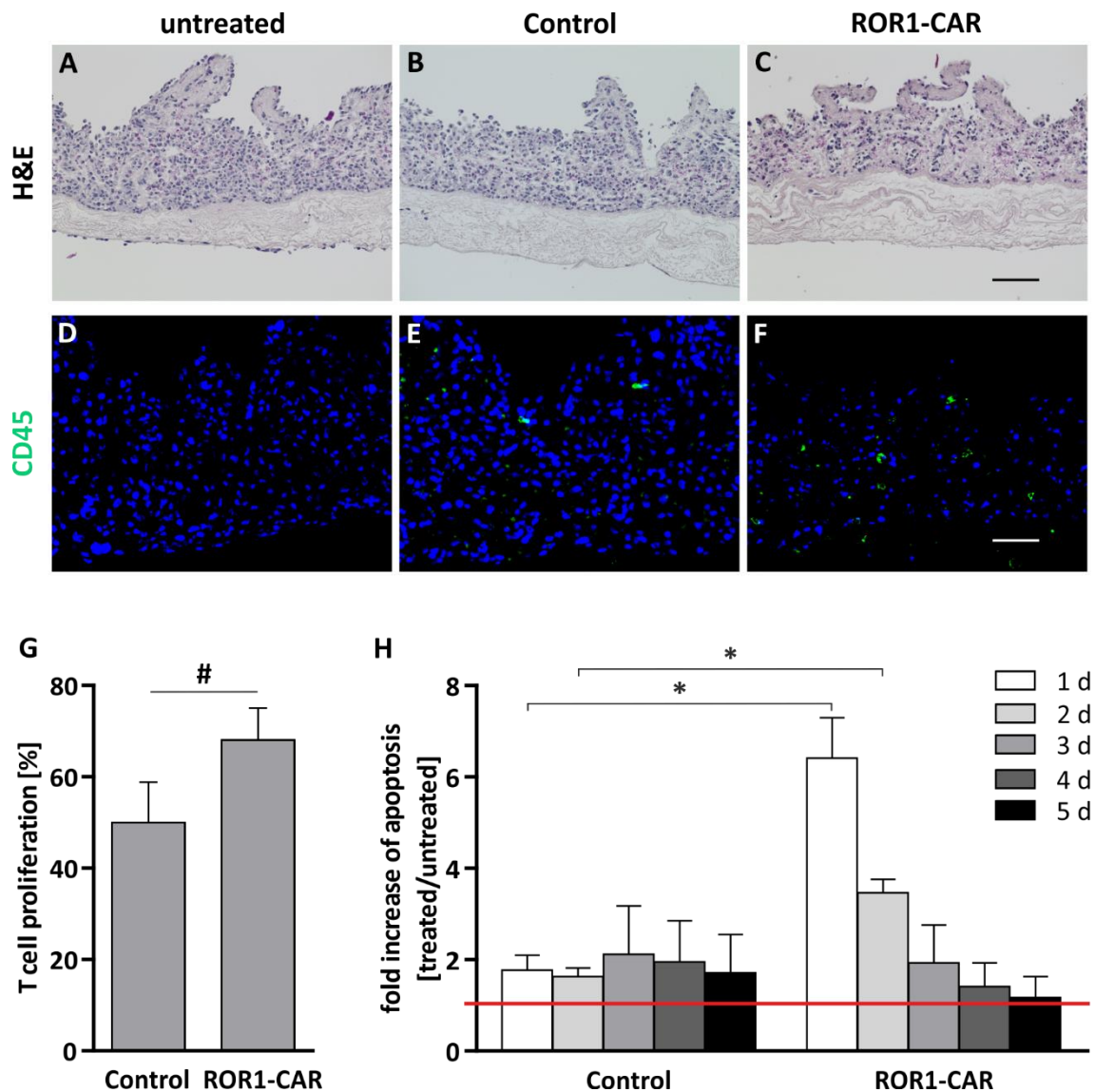


Figure 28: Treatment with ROR1-CAR T cells under 3D dynamic conditions

3D dynamic models of MDA-MB-231 cells were treated for 5 d with ROR1-CAR or untransduced control T cells (Control). A-C: H&E staining shows decrease of tumour cell number upon treatment with ROR1-CAR T cells. Scale bar: 100 μ m. D-F: Immunofluorescence staining against CD45 (green). Nuclei are counterstained with DAPI (blue). Scale bar: 50 μ m. Staining shows migration of ROR1-CAR and control T-cells into the tumour tissue. G: Proliferation of untransduced control or ROR1-CAR T cells was determined with the help of quantification of Ki67⁺/CD45⁺ cells from immunofluorescence staining (6 images per condition). Proliferation of ROR1-CAR T cells is higher after 5 d of contact to 3D dynamic tumour models compared to control T cells. Data are presented as arithmetic mean \pm SD (n=4). Statistical significance values by Wilcoxon rank sum test: # 0.05 < p < 0.1. H: Fold increase of apoptosis of MDA-MB-231 cells cultured under 3D conditions was determined by M30 CytodeathTM ELISA after treatment with untransduced control or ROR1-CAR T cells. Tumour cell apoptosis was increased upon treatment with ROR1-CAR T cells compared to control T cells. Data are normalized to the untreated control (red line) and presented as arithmetic mean \pm SD (n=4). Statistical significance values by Wilcoxon rank sum test: * p < 0.05.

4.5 Establishment of coculture models

It is well known that tumour cells are influenced by various other cell types like fibroblasts, endothelial cells, immune cells and many others. In the context of mamma carcinomas, adipocytes also play an important role as the breast is an adipose tissue and adipocytes are in close vicinity to tumour cells. In order to expand the complexity of the mamma carcinoma test system, coculture models with fibroblasts and hASCs were established.

4.5.1 Coculture with dermal fibroblasts

For the integration of a stromal compartment to the models, dermal fibroblasts were cocultured with the tumour cell lines MCF-7 and MDA-MB-231 on the scaffold SISmuc. When dermal fibroblasts were cultured on SISmuc alone, they remodelled the scaffold, thereby smoothing its surface, so that former villi could not be observed anymore (Figure 29 A). The fibroblasts in monoculture were negative for the epithelial marker PCK and positive for the mesenchymal marker vimentin (Figure 29 B and C). However, when cultured alone under 3D static conditions, they did not express fibroblast activation protein (FAP), a marker for activated fibroblasts and CAFs (Figure 29 C). The smoothing of the matrix by fibroblasts could also be observed in the coculture models with MCF-7 and MDA-MB-231 cells. While MCF-7 cells in monoculture formed a closed monolayer on top of the scaffold and resettled former crypt structures, they began to grow in 2 or 3 layers on top of the scaffold and did not form aggregates in deeper crypt structures when they were cocultured under static 3D conditions with fibroblasts (Figure 30, upper panel). In contrast, MDA-MB-231 cells that loosely grew on top of the scaffold and resettled former crypts in the monoculture, mixed with fibroblasts in the mucosal layer (Figure 30, lower panel) in the coculture model. Under dynamic culture conditions, MCF-7 cells that formed a bulky tumour mass on top of the scaffold and resettled former crypt structures in monoculture, formed high pillars of cells on top of the smoothed scaffold and large tumour aggregates in the mucosal layer in the coculture (Figure 31, upper panel). While a partial disintegration of the former crypt structures could already be observed in the MDA-MB-231 dynamic monoculture, the crypt structures were completely dissolved in the coculture with dermal fibroblasts and cells were dispersed in the complete mucosal layer of the scaffold (Figure 31, lower panel). Some cells also crossed the lamina muscularis mucosae and migrated into the small intestinal submucosa in the coculture model.

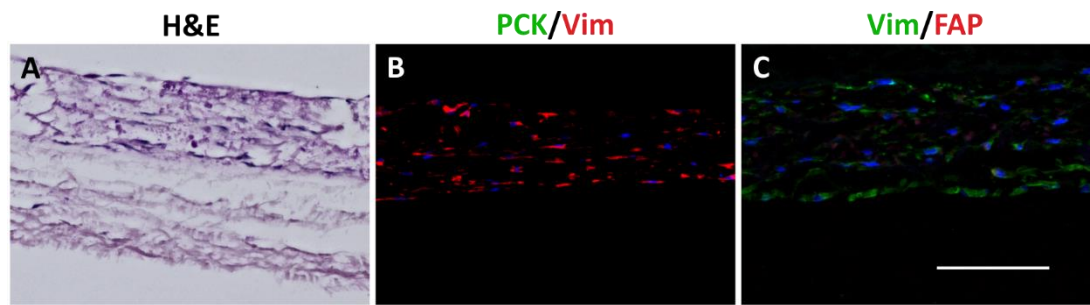


Figure 29: Monoculture of dermal fibroblasts cultured on SISmuc

H&E staining (A), immunofluorescence staining against pan cytokeratin (green) and vimentin (red; B) and immunofluorescence staining against vimentin (green) and FAP (red; C) of dermal fibroblasts cultured under 3D static conditions for 14 days. Nuclei are counterstained with DAPI (blue; B and C). Scale bar: 100 μ m.

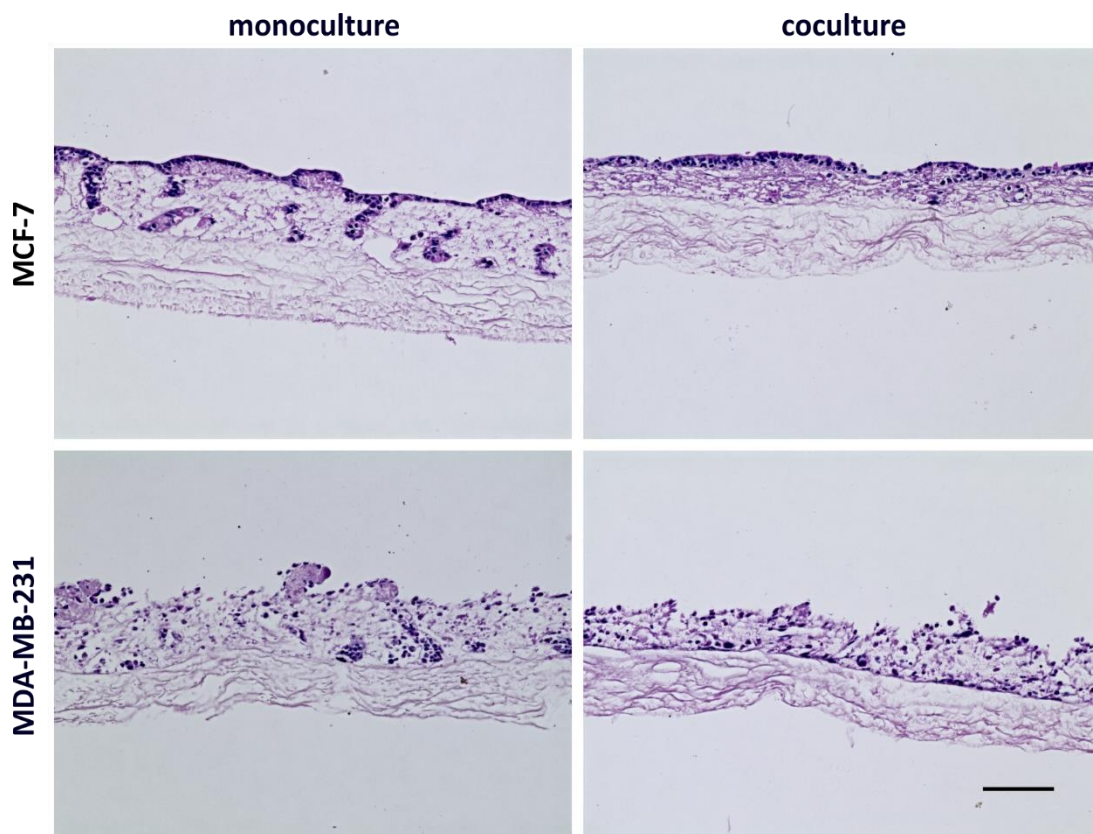


Figure 30: Static mono- and coculture models of MCF-7 and MDA-MB-231 cells with dermal fibroblasts

H&E staining of MCF-7 and MDA-MB-231 cells cultured under static conditions alone (left) or in coculture with dermal fibroblasts (right). Scale bar: 100 μ m.

Additionally, coculture models were further characterized by immunohistochemical staining and compared to xenograft material of MCF-7 and MDA-MB-231 cells. In comparison to the monoculture, only few PCK-positive MCF-7 cell aggregates in former crypts could be detected and they were small in size in static coculture. The vimentin-positive fibroblasts could be found

in a small number in the mucosal compartment only (Figure 32 A and B). Under dynamic culture conditions, the PCK-positive MCF-7 cells formed larger aggregates inside the mucosal layer in coculture with fibroblasts compared to monoculture. These aggregates were surrounded by a large number of vimentin-positive fibroblasts that were distributed throughout the complete mucosal part and established a close contact to the tumour cells. This closely resembles the xenograft material, where PCK-positive tumour cell aggregates are closely surrounded by vimentin-positive murine fibroblasts. In coculture models with MDA-MB-231 cells, tumour cells and fibroblasts could not easily be discriminated, as MDA-MB-231 cells also expressed vimentin in mono- and in cocultures (Figure 33). Some few cells are also positive for PCK. These double-positive cells are therefore MDA-MB-231 cells. As already described earlier, MDA-MB-231 cells mixed with fibroblasts both under static and dynamic culture conditions and the former crypt structures in dynamic culture conditions were completely dissolved in the dynamic coculture model. Here, single cells that crossed the lamina muscularis mucosae, thereby resettling the small intestinal submucosa, seemed to be a mixture of both cell types as well, as some PCK-positive cells could also be identified in this area (Figure 33, white arrows in magnification). Also in the xenograft material, a clear distinction between fibroblasts and tumour cells could not be made.

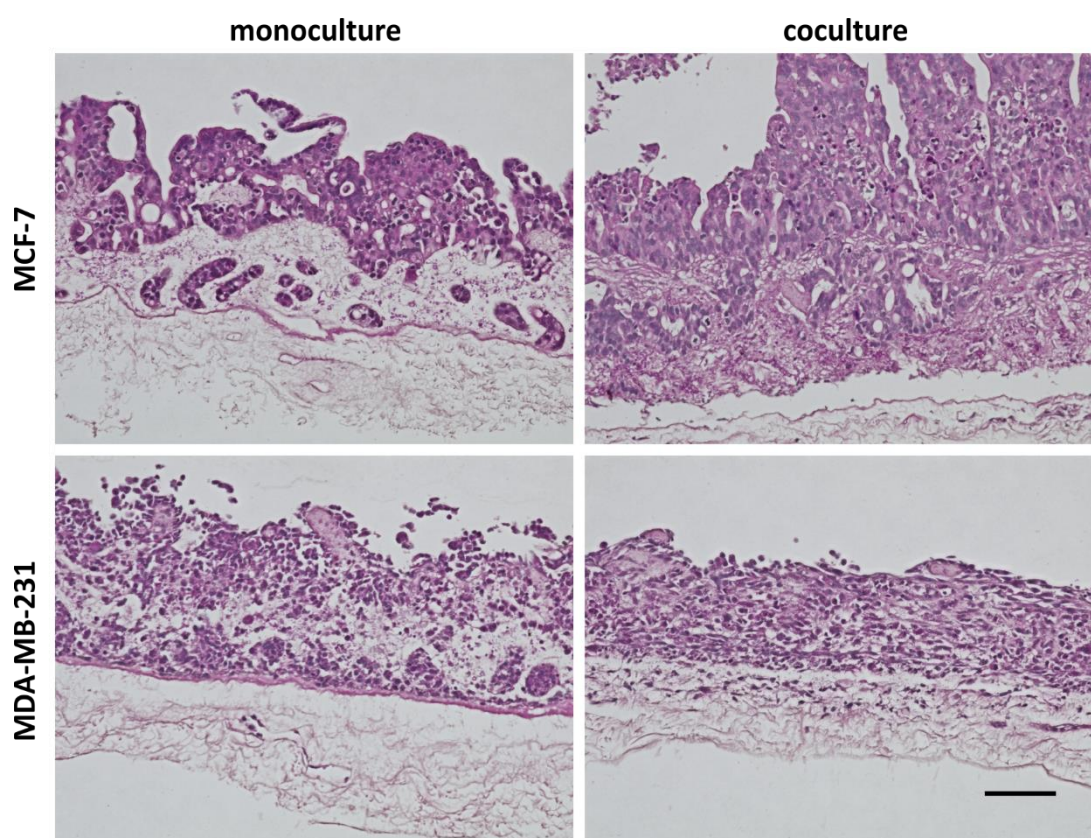


Figure 31: Dynamic mono- and coculture models of MCF-7 and MDA-MB-231 cells with dermal fibroblasts
H&E staining of MCF-7 and MDA-MB-231 cells cultured under dynamic conditions alone (left) or in coculture with dermal fibroblasts (right). Scale bar: 100 μ m.

To investigate whether the dermal fibroblasts that were not activated in monoculture (Figure 29 C), are activated by the tumour cells and thereby transformed to CAFs, a double-staining against PCK and FAP was performed (Figure 34). While under static culture conditions all fibroblasts were FAP-negative, they were strongly activated under dynamic culture conditions in coculture with both MCF-7 and MDA-MB-231 cells indicated by FAP-positive staining. In the dynamic MCF-7 coculture model a lot of FAP-positive fibroblasts that surrounded the PCK-positive tumour cell aggregates could be found and also in the xenograft material, the murine fibroblasts were FAP-positive. In contrast, only few FAP-positive fibroblasts could be determined in the dynamic MDA-MB-231 coculture model and the xenograft of this cell line.

Taken together, coculture models with fibroblasts were successfully established. The fibroblasts remodelled the scaffold and influenced the tumour tissue morphology. Especially the dynamic coculture models resembled the xenograft material and a transformation to CAFs in these models could be observed.

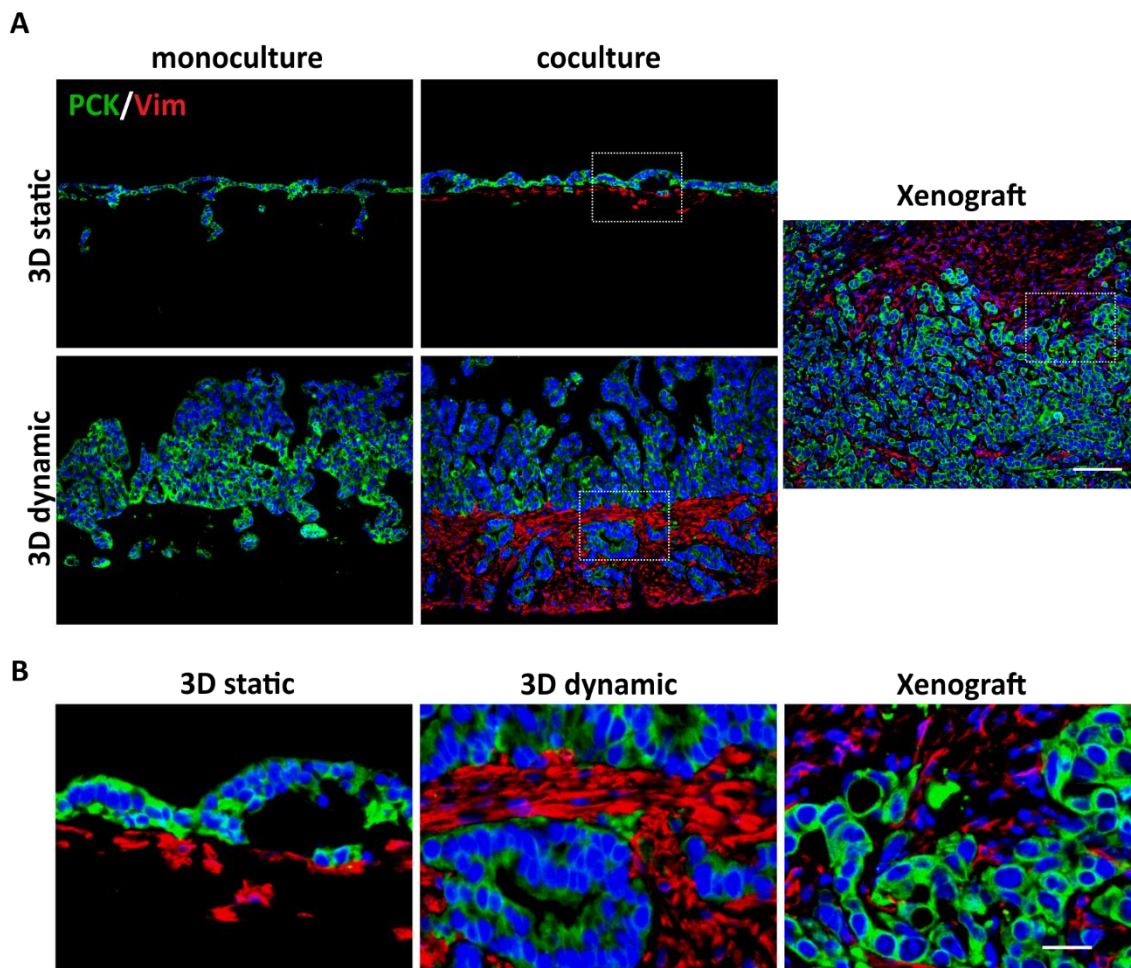


Figure 32: Static and dynamic mono- and coculture models of MCF-7 cells with dermal fibroblasts – PCK-Vim staining

A: Immunofluorescence staining against pan cytokeratin (green) and vimentin (red) of MCF-7 cells cultured under 3D static, 3D dynamic conditions alone (left) or in a coculture with dermal fibroblasts (middle) and of a xenograft model (right). Nuclei are counterstained with DAPI (blue). Scale bar: 100 μ m. B: Magnification of the frames in the images from A. Scale bar: 25 μ m. Xenograft material was kindly provided by Oncotest (Charles River).

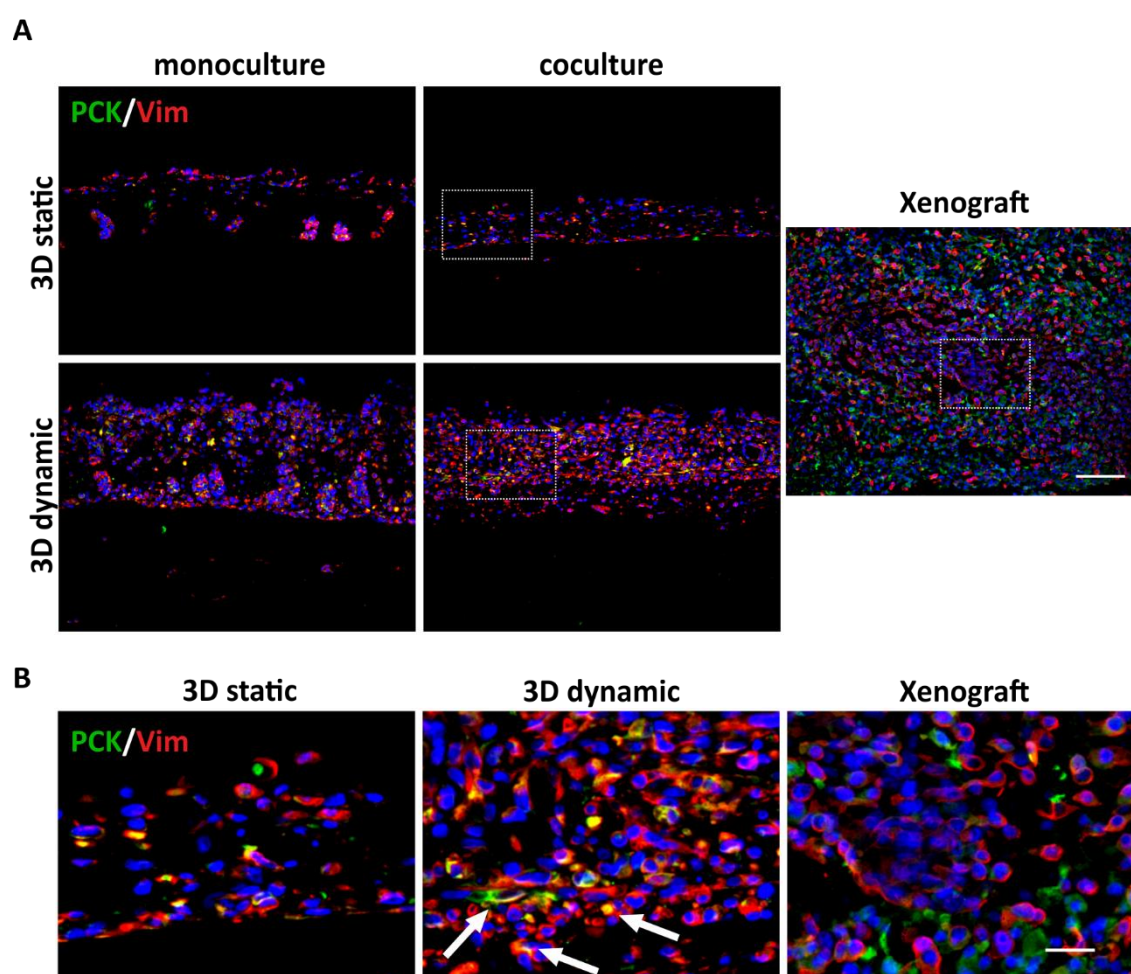


Figure 33: Static and dynamic mono- and coculture models of MDA-MB-231 cells with dermal fibroblasts – PCK-Vim staining

A: Immunofluorescence staining against pan cytokeratin (green) and vimentin (red) of MDA-MB-231 cells cultured under 3D static, 3D dynamic conditions alone (left) or in a coculture with dermal fibroblasts (middle) and of a xenograft model (right). Nuclei are counterstained with DAPI (blue). Scale bar: 100 μ m. B: Magnification of the frames in the images from A. Fibroblasts as well as PCK-positive MDA-MB-231 cells (white arrows) crossed the lamina muscularis mucosae under 3D dynamic conditions. Scale bar: 25 μ m. Xenograft material was kindly provided by Oncotest (Charles River).

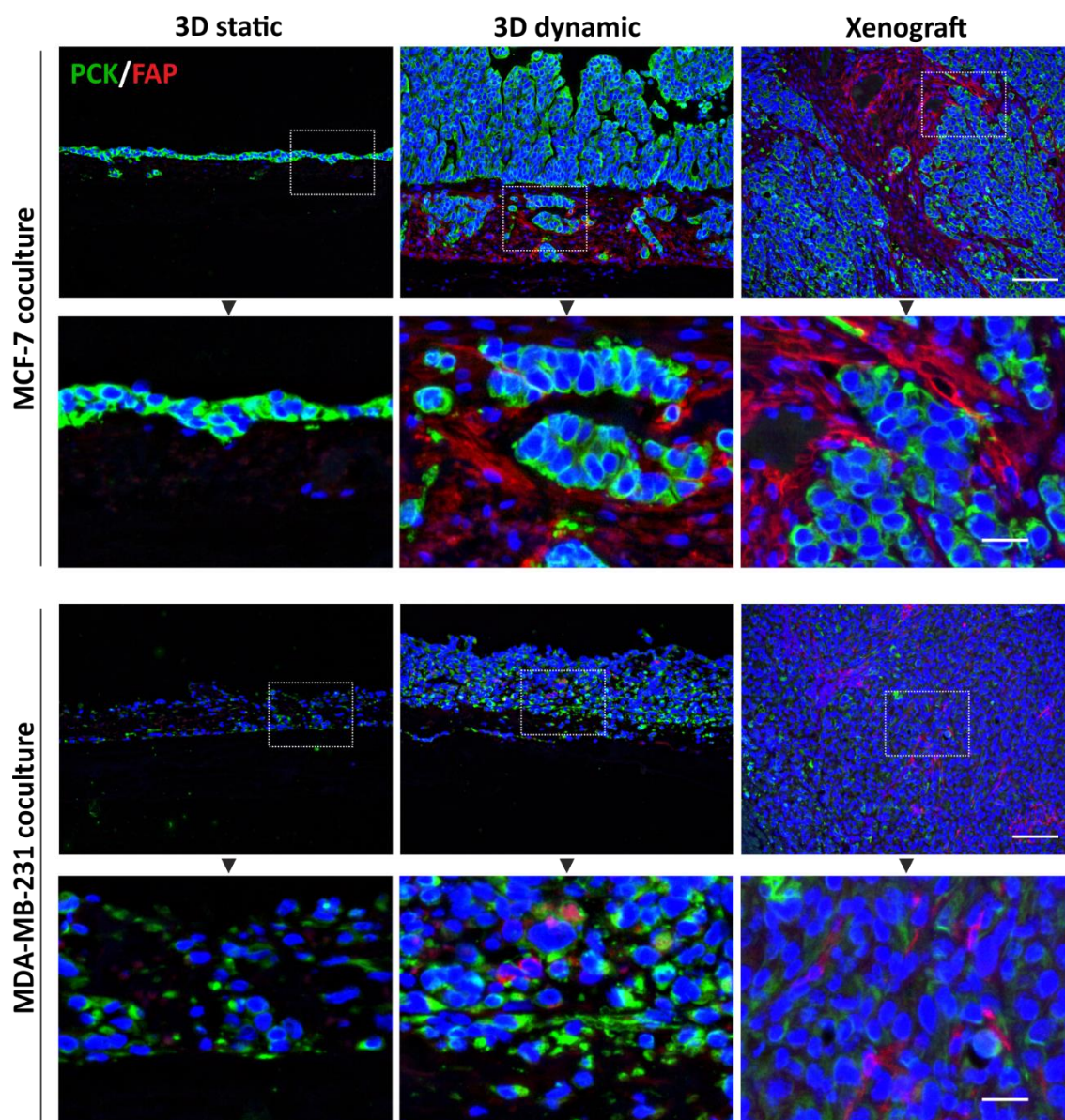


Figure 34: Static and dynamic coculture models of MCF-7 and MDA-MB-231 cells with dermal fibroblasts – PCK-FAP staining

Immunofluorescence staining against pan cytokeratin (green) and FAP (red) of MCF-7 (upper panel) and MDA-MB-231 cells (lower panel) cultured under 3D static (left), 3D dynamic conditions (middle) in a coculture with dermal fibroblasts and of a xenograft model (right). Nuclei are counterstained with DAPI (blue). Scale bar: 100 μm . Images in the second row of each panel represent a magnification of the frames in the images above. Scale bar: 25 μm . Xenograft material was kindly provided by Oncotest (Charles River).

4.5.2 Coculture with adipogenically differentiated hASCs

For the establishment of coculture with adipocytes, adipogenic differentiation of hASCs was performed. At first, it was tested whether sufficient tumour cell growth can be achieved in the presence of the inducers necessary for adipogenic differentiation. While growth of MCF-7 cells was drastically impaired by the addition of inducers in all tested media, MDA-MB-231 growth was not affected by the inducers (Figure 35 A). Therefore, MCF-7 cells were omitted from the

further experiments. Next, the potential of the isolated hASCs to differentiate along the adipogenic lineage in different media was investigated. For this purpose, the hASCs were seeded in different media without inducers and after two days (referred to as day 0) differentiation was started by the addition of adipogenic inducers. The differentiation of hASCs was histologically analysed with Oil Red O staining of accumulated lipid droplets after 0 and 9 days of culture in induction medium. Non-induced 2D monolayers, cultured in media without inducers during the whole time, served as controls. No difference of hASC growth in the different media could be observed at day 0 before the induction of adipogenic differentiation (Figure 35 B, d 0). While under control conditions (Figure 35 B, d 9 –I) no adipogenesis occurred in all media, an efficient differentiation along the adipogenic lineage could be observed by Oil Red O staining of the accumulated lipid droplets in 2D monolayers after 9 days when inducers were added (Figure 35 B, d 9 +I). Quantitative analysis of differentiation was additionally performed by determination of the triglyceride content and normalization to the DNA content. Histological observations could be confirmed by the quantification of the triglyceride contents. An increase in the triglyceride content could be measured 9 days after induction for all media tested compared to non-induced controls (Figure 35 C). In conclusion, all tested media are suitable to induce adipogenic differentiation and MDA-MB-231 cells showed sufficient growth in all media. Therefore, mixed medium of PBM and MDA-MB-231 cell-specific medium was used for further experiments.

Subsequently, it was investigated whether adipogenic differentiation of hASCs can also be achieved in 3D culture on the scaffold SISmuc. For this purpose, 1×10^5 or 5×10^5 hASCs for static culture conditions and 5×10^5 hASCs for dynamic culture conditions were seeded on the scaffold and cultured for 14 days in induction medium. For dynamic culture conditions, cells were allowed to attach for 3 days before dynamic culture started. The differentiation of hASCs was histologically analysed with Oil Red O and BODIPY 493/503 staining of accumulated lipid droplets in cryosections of the 3D models. Successful differentiation of hASCs along the adipose lineage could be achieved for all cell numbers and under all culture conditions as indicated by the presence of lipid droplets (Figure 36). However, only a small number of adipogenically differentiated hASCs could be detected under static conditions, when 1×10^5 cells were seeded. The cell density was improved for the higher seeding number and even more increased under 3D dynamic conditions. Therefore, 5×10^5 hASCs were used for coculture experiments with MDA-MB-231 cells.

For the establishment of these coculture models, tumour cells and hASCs were simultaneously seeded on the scaffold SISmuc in induction medium and cultured for 14 days under static or dynamic conditions as described above. Under static culture conditions, a mixture of adipogenically differentiated hASCs and MDA-MB-231 cells could be found on top of the scaffold in multiple layers but also in former crypt structures (Figure 37). Cell numbers of both cell types increased under dynamic conditions leading to enhanced proximity of the cell types.

Taken together, it was possible to induce the adipogenic differentiation of hASCs in 3D culture on the scaffold SISmuc and to establish 3D coculture models with MDA-MB-231 cells. However, a further characterization of these coculture models in the future is necessary.

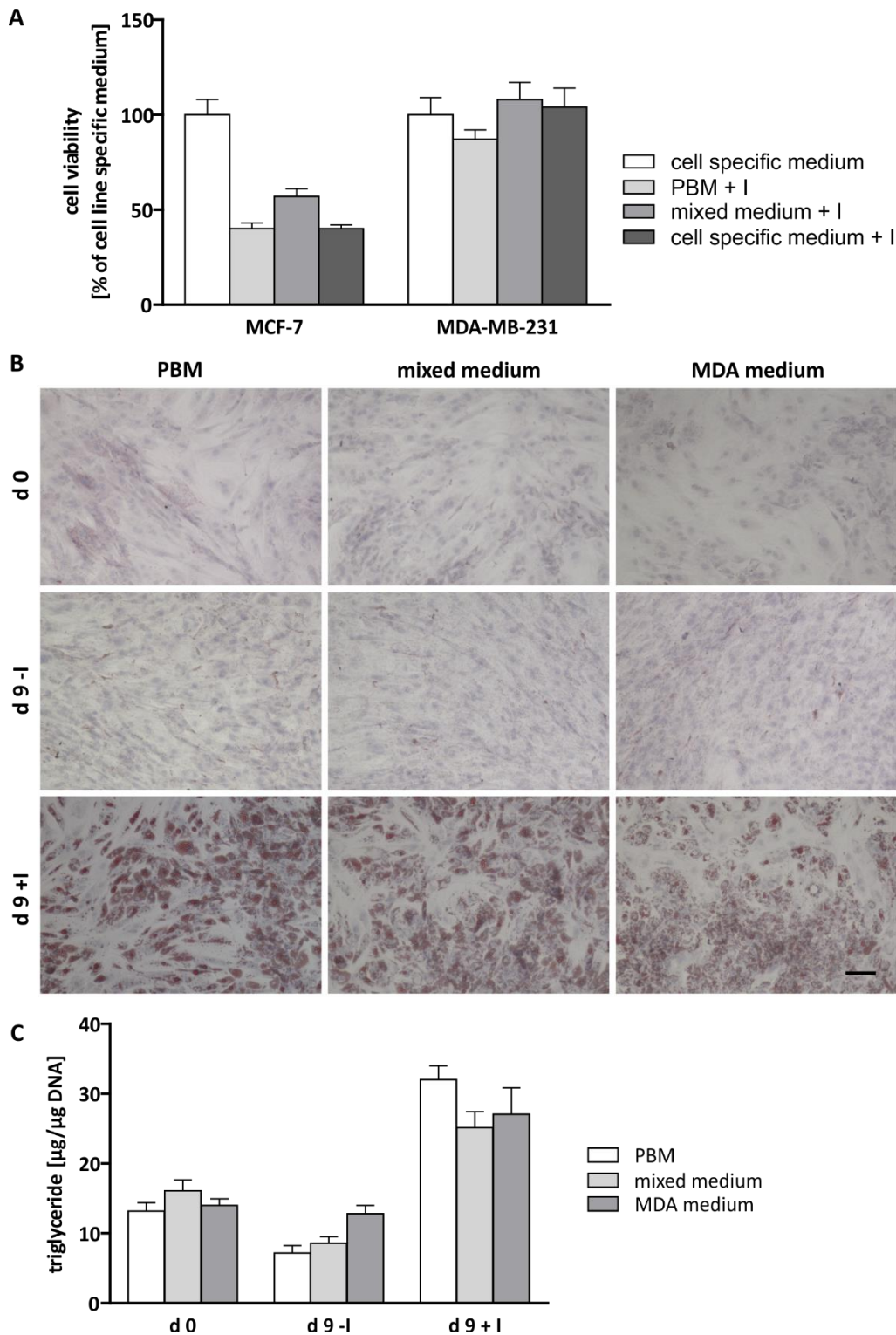


Figure 35: Media testing for hASC differentiation

A: Cell viability of MCF-7 and MDA-MB-231 cells cultured under 2D conditions in different media was determined by CellTiter-Glo® Luminescent Cell Viability Assay. Data are normalized to the cell specific medium control without inducers. +I: addition of inducers for adipogenic differentiation. B: Oil red O staining (red) of hASCs cultured under 2D conditions in different media with or without the addition of inducers (+/-I). Cells were seeded on day -2 and inducers were added from day 0. C: Triglyceride content of hASCs on day 0 and day 9 with or without the addition of inducers (+/-I) from day 2 to the different media normalized to the DNA content per well. hASCs were kindly provided by the group of Prof. Dr. Blunk (Klinik und Poliklinik für Unfall-, Hand-, Plastische und Wiederherstellungschirurgie, University Hospital Würzburg).

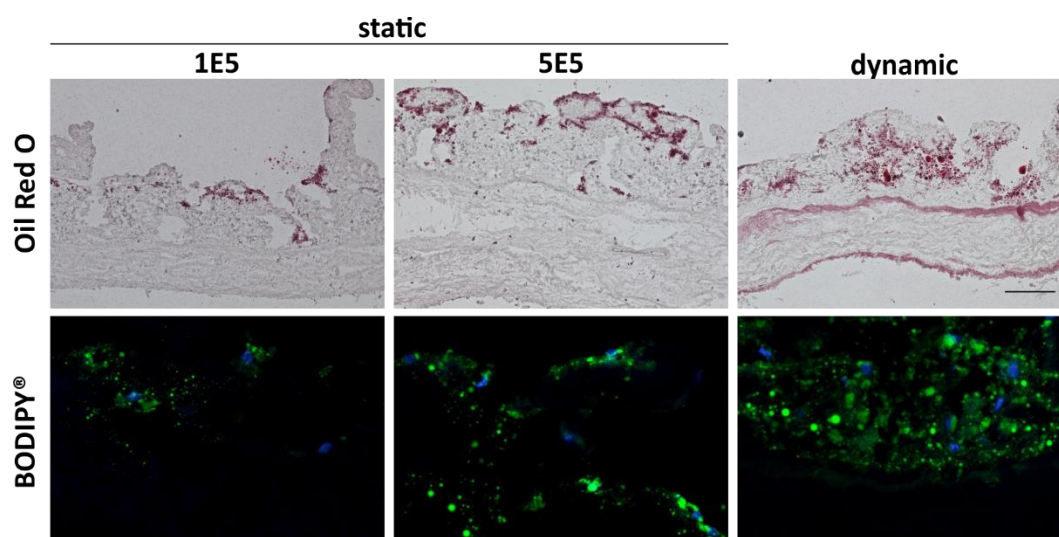


Figure 36: hASC adipogenic differentiation on SIS muc

hASCs were seeded on the scaffold in different numbers (1×10^5 or 5×10^5 hASCs per cell crown for static and 5×10^5 hASCs for dynamic model) and cultured for 14 days in mixed medium with inducers under static or dynamic culture conditions. Adipogenic differentiation was determined by staining of the lipid droplets with Oil Red O (red, upper panel) and BODIPY® 493/503 (green, lower panel). Nuclei are counterstained with DAPI in lower panel. Scale bar: 100 μ m. hASCs were kindly provided by the group of Prof. Dr. Blunk (Klinik und Poliklinik für Unfall-, Hand-, Plastische und Wiederherstellungschirurgie, University Hospital Würzburg).

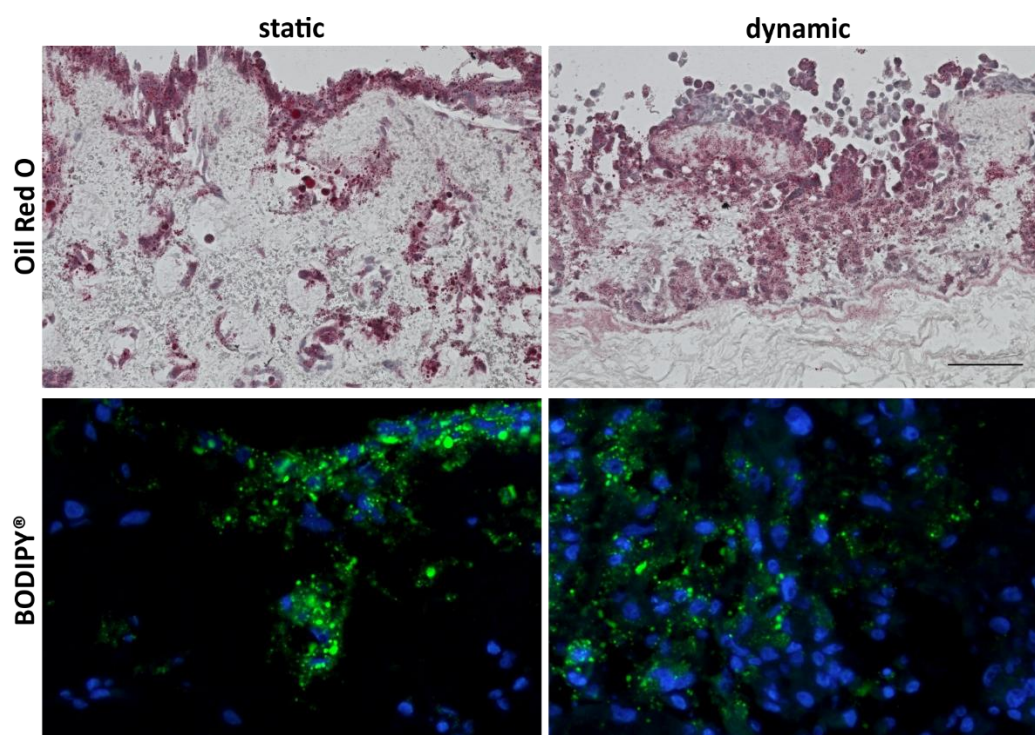


Figure 37: Coculture of MDA-MB-231 cells with hASCs on SIS muc

MDA-MB-231 cells and hASCs were simultaneously seeded on the scaffold SIS muc and cocultured for 14 days in mixed medium with inducers under static or dynamic culture conditions. Adipogenic differentiation was determined by staining of the lipid droplets with Oil Red O (red, upper panel) and BODIPY® 493/503 (green, lower panel). Nuclei are counterstained with DAPI in lower panel. Scale bar: 100 μ m. hASCs were kindly provided by the group of Prof. Dr. Blunk (Klinik und Poliklinik für Unfall-, Hand-, Plastische und Wiederherstellungschirurgie, University Hospital Würzburg).

5 Discussion

The process of drug development is highly inefficient, especially in the field of oncology where attritions rates are as high as 95 % (Hutchinson & Kirk, 2011; Bhattacharjee, 2012). Approximately 60 % of the drug candidates that had been tested to be promising candidates for therapy in the preclinical stage fail in the clinical phases I to III due to the lack of efficacy (Arrowsmith & Miller, 2013). One of the reasons for this, is the usage of inadequate test systems in the early stage of drug development that do not sufficiently represent *in vivo* tumours. Therefore, there is an urgent need for novel human tumour test systems that allow reliable predictions of the clinical response to potential drug candidates.

In this work, a mamma carcinoma test system representing the different molecular subsets of breast cancer was established and optimized for the preclinical application of compound testing using a tissue engineering approach. The employment of a natural tissue matrix as a scaffold resulted in the generation of models that reflect tumour relevant characteristics and correspond well with *in vivo* tumours from xenografts with respect to tumour cell proliferation and expression of relevant markers of tumour biology. Furthermore, the possibility to study the process of invasion in these models was demonstrated. The suitability of these models as a test system for compound screening was confirmed by the prediction of the efficacy of a biomarker-guided targeted therapy approach with trastuzumab that correlated with the clinical situation. In order to analyse ADCC in this context, an immunological component was introduced into the models. Moreover, the TNBC model was applied to evaluate an innovative formulation strategy for poorly soluble compounds and to assess the efficacy of different novel therapeutic strategies for the treatment of TNBC: Treatment with the small molecule inhibitor of WEE1 kinase MK-1775 alone and in combination with the chemotherapeutic agent doxorubicin did not show efficacy in the 3D model in contrast to 2D culture. On the other hand, the innovative treatment approach with ROR1-CAR T cells revealed promising results in the 3D model, thereby confirming the suitability of the test system for the evaluation and optimization of such alternative anti-cancer strategies from the field of cancer immunotherapies. In the last part, the model was expanded by the introduction of a stromal component by the integration of fibroblasts or adipogenically differentiated hASCs in order to provide a more realistic model for future compound testing as well as for the mechanistic investigation of the interplay between tumour and stroma.

5.1 Establishment and optimization of a 3D mamma carcinoma test system

The 3D mamma carcinoma test system was established on the basis of SISmuc. This scaffold is derived from the BioVaSc[®], a decellularised section of the porcine small intestine that has a preserved vascular structure (Mertsching *et al.*, 2005) and allows the generation and long term culture of vascularized tissue constructs (Linke *et al.*, 2007). In contrast, in SISmuc the vessel system is removed and the scaffold is comprised of the small intestinal submucosa (SIS) and the mucosal layer (muc) and mainly composed of elastin and different collagens (Schultheiss *et al.*, 2005; Mertsching *et al.*, 2009). These ECM components and the scaffold's complex architecture with preserved villi and crypt structures allow the generation of organized tissues from a single or more cell types. Furthermore, Stratmann *et al.* showed that the basement membrane underlying

the former small intestinal epithelium is preserved in this scaffold, thereby providing the first natural barrier tumour cells derived from epithelia have to cross on their way to metastasis formation (Stratmann *et al.*, 2014). In addition, the usage of this scaffold provides the option for expansion of the test system by vascularization in later stages, when the more complex scaffold BioVaSc® is used.

For the generation of the mamma carcinoma test system, human breast cancer cell lines were used. The usage of cell lines in cancer research has been critically discussed for several years as genetic and phenotypic drift may occur during long term culture and subpopulations might be selected leading to a drift away from the originating tumour. On the other hand, Wang and colleagues were able to show that 51 of 59 NCI60 cell lines analysed in their study represented their tumour of origin (H. Wang *et al.*, 2006). Wistuba and colleagues compared 18 human breast cancer cell lines to their corresponding archival tumour tissues and found excellent consensus in terms of morphological characteristics, expression of tumour markers like ER, HER2 and PR as well as the presence of aneuploidy and *p53* mutation after long term culture (Wistuba *et al.*, 1998). Additionally, cancer cell lines also have major advantages over primary cell culture (Cree *et al.*, 2010): Cell lines are easily available, mostly well characterized in terms of behaviour, mutational status and biomarker expression as well as easy to handle. These factors critically contribute to reproducibility which is a key factor in the establishment of standardized test systems. Therefore, the usage of cell lines is advantageous especially during the initial establishment of such test systems while in later stages, the usage of primary cells might be beneficial.

Recently, there is evidence that cell lines cultured under 3D conditions better simulate the clinical setting and 3D culturing techniques might therefore be a promising tool for preclinical drug screening, thereby bridging the gap between simplistic 2D monolayers of cell lines and complex *in vivo* tumours (Yamada & Cukierman, 2007; Breslin & O'Driscoll, 2013; Lovitt *et al.*, 2014; Weigelt *et al.*, 2014)

Here, three breast cancer cell lines representing three different molecular subsets of mamma carcinoma were used. The expression of the three biomarkers ER, PR and HER2/Neu are routinely assessed in the clinical practice to stratify invasive breast cancer as the expression or absence of these biomarkers provides a prognostic value and is decisive over the therapeutic approach chosen for the patient, like anti-hormonal therapy for ER-positive BC or anti-cancer immunotherapy with trastuzumab or pertuzumab for HER2/Neu-amplified or overexpressing BC patients (Vuong *et al.*, 2014).

Standard cell culture relies on the supplementation of medium with FBS in order to provide the cells with growth factors and nutrients. However, as FBS has a poorly defined composition, a high batch-to-batch variability and bears the risk of bacterial, viral or mycoplasma contamination, it is a very critical component of cell culture that might highly influence the reproducibility of results. This is especially detrimental for test systems. For instance, Sikora and colleagues found, that the differing hormone content of FBS strongly influenced the outcome of drug response tests in breast cancer cell lines (Sikora *et al.*, 2016). The comparison of different batches of FBS in 2D and 3D cultures of breast cancer cell lines in this work revealed major differences in cell growth and morphology only under 3D culture conditions. Additionally, FBS influenced the adherence

to the scaffold, tissue morphology as well as biomarker expression, which might strongly affect the test results of drug compound screening. Therefore, as long as FBS cannot be properly replaced by defined growth stimulating substances, a careful and proper testing of batches is necessary. For test systems, criteria should be defined that should be met by culture with a certain batch of FBS. For the here presented test system, these criteria comprised sufficient adhesion and growth on the scaffold, tissue morphology and expression of biomarkers for the stratification of tumours into molecular subsets (ER, HER2 or missing expression for TNBC). Furthermore, the results indicate, that testing of these defined criteria in 2D cultures only might not be sufficient as cells in 2D seem to better tolerate variations in the cell culture medium compared to 3D. This higher sensitivity of 3D cultures was also reported by Vidi *et al.* (Vidi *et al.*, 2013).

Even with the usage of the best matched FBS batch (PAN Biotech), a reproducible and appropriate growth of the HER2 model could not be achieved under 3D static culture conditions and the models were therefore not suitable for compound testing. Therefore, the 3D culture conditions for this cell line needed to be optimized. As it is well known that cell growth can be improved in dynamic culture systems (Zhao *et al.*, 2009; Mishra *et al.*, 2012; Hansmann *et al.*, 2013), culture of the 3D models on an orbital shaker was investigated. This is a simplistic approach of dynamic culture without losing the possibility of scale-up like in more complex bioreactor systems, as the models can still be cultured in the 12 well plate format. The incubation on the orbital shaker leads to the movement of media, causing better nutrient supply and waste management due to a more homogenous distribution of nutrients and waste products in comparison to static culture conditions. Shear stress might also play a role and provide a growth stimulus. These culture conditions indeed resulted in enhanced growth of the tumour cells, whereas adherence to the scaffold remained poor. A change of culture medium in combination with the incubation on an orbital shaker led to reproducible and sufficient growth of SKBR-3 cells on the scaffold with improved adherence and sustained expression of the key biomarker HER2. With the help of these changes, compound testing was possible in the HER2 model.

Another important factor that influences the reproducibility of a test system is the culture duration. While tumour cell number on the scaffold is still strongly increasing until day 11, a kind of tissue homeostasis can be found between day 11 and day 18 in the models. For MDA-MB-231 and SKBR-3 this goes in line with the proliferation index that levels off to a more or less constant value in the same time span, whereas in the initial stage the proliferation index is clearly higher. The parameter of proliferation index is especially important for the treatment with cytostatic compounds that primarily affect proliferating cells (Cree *et al.*, 2010). Therefore, a constant proliferative index that is close to the *in vivo* situation is crucial for significant and reproducible results in drug testing experiments. Next to tumour cell number and tissue morphology as well as proliferation index, apoptosis in the tumour tissue is a major factor for the validity of a test system. Here it was shown that the basic apoptosis without the addition of any test compound drastically increased in two of the 3 models after day 14. Such high basic apoptosis values would interfere with the measurement of drug induced apoptosis during compound testing. Therefore, a culture period of 14 days and treatment during the last days of culture beginning no earlier than day 11 of culture were defined to be ideal for a reliable and reproducible prediction of drug sensitivity in the here presented test system.

5.2 Characterization of the mamma carcinoma test system

For the characterization of the 3D mamma carcinoma test system, parameters like proliferation and the expression of markers of tumour biology in comparison to xenograft material were assessed and the invasive behaviour of the cells was investigated.

The proliferation index or Ki67 index is the proportion of proliferating cells in a tumour and is usually determined with the marker Ki67. This nuclear antigen was first described by Gerdes *et al.* in the 1980s and is expressed by cells in the cell cycle phases S, G1, G2 and M phase but not in the G0 phase (Gerdes *et al.*, 1984; Scholzen & Gerdes, 2000). With the help of immunohistochemical staining against Ki67, the growth fraction of neoplastic cell populations in tumour biopsies can be assessed. However, as there is no standard operating procedure and no standard defined cut-off definition, the interlaboratory and interstudy comparability of Ki67 is limited (Yerushalmi *et al.*, 2010; Luporsi *et al.*, 2012). Additionally, several studies controversially discuss the prognostic value of the Ki67 index. Therefore, Ki67 so far is not implemented in standard routine pathology but is widely determined in biopsies of mamma carcinoma patients in the clinic for treatment decision especially for adjuvant treatment strategies (Inwald *et al.*, 2013). One of the reasons for this is that it is well known that cytostatic compounds like chemotherapies primarily target proliferating cells (Cree *et al.*, 2010). Therefore, the proliferation index of tumour test systems should well correlate with clinical values in order to reliably predict sensitivity towards such compounds. Here, it was shown that tumour cell lines in 2D culture had a very high proliferation index that does not represent *in vivo* tumours. In contrast, the Ki67 index was significantly decreased in the 3D test system. This has previously been reported from our group for colon and lung cancer models but from other groups as well (Fallica *et al.*, 2012; Luca *et al.*, 2013; Stratmann *et al.*, 2014; Göttlich *et al.*, 2016; Nietzer *et al.*, 2016) and indicates a better representation of the clinical setting. In the case of mamma carcinoma, the Ki67 index strongly varies between the different molecular subsets. Inwald *et al.* reported mean proliferation indices of 17% (± 14) for ER-positive, 34-42 % (± 24) for triple negative and 27 % (± 19) for HER2/Neu-overexpressing breast cancer patients (Inwald *et al.*, 2013). While the proliferation index of the 3D SKBR-3 model with 23.7 % is very close to HER2/Neu-overexpressing mamma carcinomas, the index of the 3D MDA-MB-231 model (19.9 %) is lower compared to its clinical subset but still lies in the range when the standard deviation in this subset is regarded. Only the proliferation index of the 3D MCF-7 model with 43.5 % is considerably higher compared to the index of ER-positive mamma carcinomas. In general, the proliferation rates of the 3D models were closer to the clinical values compared to the artificially high indices of 2D cultures, outlining the potential of these models for more reliable predictions of drug sensitivity.

Next to Ki67, other markers of tumour biology were investigated in the 3D static and dynamic test systems and their expression was compared to 2D cultures and xenograft material of the same cell lines, if available. Dynamic culture conditions, both on an orbital shaker as well as in a flow bioreactor system, drastically improved the growth of all cell lines on the scaffold and led to the

formation of more complex tumour tissues. The dynamic culture conditions leads to a more homogenous distribution of nutrients as well as waste products compared to static culture, where periodic fluctuations in the context of medium changes occur (Hansmann *et al.*, 2013). Additionally, physical stimuli like shear stress can contribute to a more *in vivo* like morphology. For instance, Hirt *et al.* compared static and dynamic cultures of a colorectal cancer cell line and observed the formation of tissue-like structures in the perfusion bioreactor that more closely resembled the tissue architecture and morphology of xenografts (Hirt *et al.*, 2015). Similar observations were made in the here presented work: Both tissue morphology, i.e. formation of tumour nodules surrounded by ECM for MCF-7 cells and more scattered tumour tissue formation for MDA-MB-231 cells, as well as expression of all investigated biomarkers in 3D dynamic culture showed very strong similarities with the corresponding xenograft material of MCF-7 as well as MDA-MB-231 cells. This indicates a strong correlation of 3D dynamic models and the xenograft models with the advantage of reduced costs and time requirements. Only an apical expression of Muc-1 like in the uppermost layer of MCF-7 dynamic and static models could not be found in the corresponding xenograft material, which is probably due to the fact that for the generation of these, the tumour cells were subcutaneously injected into the connective tissue of the mice, which is no physiological environment for epithelial tumours. In contrast, the epithelial tissue architecture and preserved basement membrane of the scaffold SIS_{muc} allow the formation of polarized or partially polarized tumour tissues. This has already been reported for the 3D lung carcinoma test system (Stratmann *et al.*, 2014) and could be confirmed here for the ER-positive MCF-7 breast cancer model.

For SKBR-3 cells, no xenograft material was available so that a comparison was not possible. In general, xenografts of this cell line are not easy to establish due to the poor tumourigenic potential of the cell line (Holliday & Speirs, 2011).

Taken together, according to marker expression and tissue morphology, MCF-7 cells formed rather well-differentiated tumour tissues with a partial loss of polarization that was more prominent in the 3D dynamic model. SKBR-3 cells still exhibited an epithelial phenotype in 3D culture but were only moderately differentiated and lacked polarity. And MDA-MB-231 cells in 3D models represent a poorly differentiated tumour with complete loss of polarity and a shift towards the mesenchymal phenotype. These findings go in line with the study of Sommers *et al.* that characterized the cell lines and made similar observations and classifications according to marker expression and tissue morphology in Matrigel (Sommers *et al.*, 1994).

For further characterization, the potential of invading into the scaffold was analysed in 3D models of MCF-7 and MDA-MB-231 cells. Invasive growth is a prerequisite for the formation of metastasis at distant sites of the body, which leads to a poor prognosis for patients and decreased survival. The first barrier a tumour cell that derived from an epithelial tissue like the breast epithelium has to cross is the basement membrane, a naturally occurring barrier underlying all epithelial cells of the body. As demonstrated with SEM imaging, the basement membrane of the SIS_{muc} derived from porcine small intestine is preserved and lines the former villi and crypt structures of the scaffold. This has already been reported earlier (Stratmann *et al.*, 2014) and could be verified in this work. In larger magnifications, sharp-edged holes with a rounded shape were observed in this basement membrane structure. This manifestation and the fact that no collagen

fibre network could be observed underneath these holes, implies that these holes are pores that naturally occur in the basement membrane of the small intestine rather than damages from decellularisation. Indeed, such pores in the basement membrane of the small intestine have already been described for rats and pigs and are suggested to permit the passage of intercellular fluid between epithelium and lamina propria mucosae as well as the passage of cells like immune cells (McClugage & Low, 1984; Komuro, 1985; Lowden & Heath, 1994). It remains unclear if the basement membrane in the breast tissue shares this feature of pores but nevertheless different degrees of invasiveness of MCF-7 and MDA-MB-231 could clearly be observed after culture on SISmuc. While MCF-7 did not cross the basement membrane in 3D static and dynamic culture, the invasive phenotype of MDA-MB-231 cells observed in 3D static culture was even strongly enhanced under 3D dynamic conditions. These differences in invasive behaviour between the two cell lines go in line with literature, where MCF-7 cells were described as non-invasive and MDA-MB-231 as invasive cell line according to data from conventional invasion assays like Matrigel-based Boyden chamber invasion assay and sprouting assay in Matrigel (Sommers *et al.*, 1991; Thompson *et al.*, 1992; Bae *et al.*, 1993). The assays for the evaluation of invasive potential described in these publications are using Matrigel as a mimic of basement membrane. However, this artificial basement membrane substratum is primarily comprised of a laminin isoform that is rarely found in the basement membrane of adult tissues (Virtanen *et al.*, 2000). Furthermore, it has been shown that it does not recapitulate the complex mix of covalent cross-links that are characteristic for the type IV collagen polymers found *in vivo* (Kleinman *et al.*, 1986; Even-Ram & Yamada, 2005). Therefore, it is not clear if Matrigel as a mimic of basement membrane better represents the breast-specific basement membrane.

It has long been assumed that a shift towards the mesenchymal phenotype during the process of EMT is the prerequisite for invasion and metastasis formation. The fact that distant metastases have an epithelial phenotype was explained by the reverse process of mesenchymal-epithelial transition (MET). This would explain the higher invasive potential of MDA-MB-231 cells as they exhibit this EMT phenotype. At the moment, however, it is controversially discussed if EMT and MET is required for metastasis formation or an epiphenomenon of cancer cell resistance (Fischer *et al.*, 2015; Maheswaran & Haber, 2015; X. Zheng *et al.*, 2015). Fischer and colleagues showed in animal experiments that cells found in distant metastases did not undergo an EMT and MET process during metastasis formation (Fischer *et al.*, 2015), while Zheng and colleagues found that deletion of Twist or Snail, two key transcription factors responsible for EMT, did not impair dissemination and metastasis formation in mouse models of pancreatic cancer (X. Zheng *et al.*, 2015). However, in both publications a link of EMT and chemoresistance was found. Further research will shed new light on this debate in the future.

The presence of pores in the basement membrane structure of SISmuc raises the question whether the MDA-MB-231 cells can use these pores for invasion or if they have to actively alter the scaffold for invasion. Recently, it was reported that MDA-MB-231 cells can squeeze through small constrictions by temporarily dissolving their nuclear membrane (Denais *et al.*, 2016). In samples of breast cancer patients with invasive carcinoma, however, the basement membrane was observed to be disrupted by the tumour cells in most cases (Wetzels *et al.*, 1989). Therefore, it was investigated via SEM imaging whether the preserved basement membrane of SISmuc is

altered by the tumour cells. Indeed, the occurrence of holes in the basement membrane in the MDA-MB-231 static and in the MCF-7 3D dynamic model suggests an active alteration of the scaffold by the tumour cells. Underneath these holes, the collagen fibre network of the underlying ECM was visible, indicating that these differed from the pores described before. In 3D dynamic MDA-MB-231 models, where a very high invasiveness was observed according to the collagen IV staining, these alterations are even more drastic and include the existence of enlarged pores without an underlying ECM fibre network. These changes might be caused by MMPs. It is well known that such enzymes regulate the tumour microenvironment and that their expression and secretion is upregulated in most cancers compared to healthy tissues (Egeblad & Werb, 2002). This is often associated with worse prognosis and reduced survival. Next to their role in the development of cancer they are associated with cancer cell invasion and metastasis formation. With the help of *in situ* zymography it was possible to demonstrate that MMPs also play a role in the here presented tumour models. *In situ* zymography is an elegant method to visualize the activity of endogenous enzymes in their biological context (Yan & Blomme, 2003). This technique does not only provide information about the location of MMP activity but also allows the detection of the net proteolytic activity in a tissue, meaning that only active MMPs are detected but not their inactive proforms or their active forms that are inhibited by inhibitor-complexes in the tissue. In contrast, during gel zymography both the inhibitory segment of propeptide domains are pushed away from the catalytic site as well as non-covalently bound complexes like TIMP-MMP complexes are dissociated, resulting in the measurement of the potential enzymatic activity rather than the net enzymatic activity in the sample (Vandooren *et al.*, 2013). Apart from gelatine substrates, more specific substrates like collagen IV, a major component of basement membrane and therefore of special interest regarding invasive processes of tumour cells, can be used in order to investigate if proteolytic activity against these substrates is present in the tissue. A drawback of *in situ* zymography is that it cannot detect which type of MMP is active in the tissue. This can be narrowed down by the usage of substrates that are more specific for degradation by certain MMPs as well as by the addition of inhibitors of specific MMPs (Snoek-van Beurden & Von den Hoff, 2005; Vandooren *et al.*, 2013). In the future, with the help of this technique combined with other methods like gel zymography, that also allows the detection of secreted MMPs, and immunohistochemical staining of MMPs, the here presented 3D models could be used to investigate invasive processes in a mechanistic way. In mamma carcinoma, MMP-9 is of special interest as it is strongly associated with aggressive and metastatic breast cancer and is correlated with poor prognosis according to breast cancer DNA microarray datasets (McGowan & Duffy, 2008). One of the substrates of MMP-9 is collagen IV. Mehner and colleagues showed that MMP-9 is most highly expressed in human triple-negative and basal-like tumours (Mehner *et al.*, 2014). According to MMP-9 silencing experiments performed by this group, cancer-cell produced MMP-9 is required for invasion in cell culture as well as metastasis formation in the lungs in a mouse orthotopic xenograft model of MDA-MB-231 cells representing this subtype of cancer. Therefore, the investigation of the role of MMPs, in particular MMP-9, in our test system would be interesting in the future.

Taken together, the here presented tumour model based on the decellularised scaffold SISmuc with its preserved natural basement membrane structure is suitable to recapitulate invasive behaviour and is therefore an alternative for existing invasion assays. Furthermore, it holds the

potential to mechanistically investigate the process of invasion e.g. the involvement of MMPs, to determine compound efficacy on tumour cells of different progression stages and to test novel anti-metastatic therapy strategies that target the process of cancer cell invasion.

5.3 Validation of the test system with a targeted therapy approach

For the evaluation of the clinical relevance of the here presented mamma carcinoma test system, a targeted therapy approach that is already in clinical application was tested in these models and compared to 2D culture. Treatment with the therapeutic antibody trastuzumab is in routine clinical application since 2000 in Europe. After trastuzumab monotherapy was shown to be active against HER2-overexpressing metastatic breast cancer in clinical studies, it was approved by the FDA in 1998 for this subset of breast cancer patients (Baselga *et al.*, 1996; Cobleigh *et al.*, 1999; Vogel *et al.*, 2002).

Despite the fact, that trastuzumab is well established in the clinical routine, its relevant MOA is still not well defined. Different possible MOAs are discussed and scientific data support each theory, but observations *in vitro* and *in vivo* often diverge (Morris & Carey, 2006; Nahta *et al.*, 2006). For instance, the downregulation of HER2 protein by internalization and degradation after trastuzumab therapy, thereby leading to anti-proliferative and pro-apoptotic effects, was observed *in vitro* (Cuello *et al.*, 2001), but this observation could not be confirmed *in vivo* (Gennari *et al.*, 2004; Mohsin *et al.*, 2005). As HER2 acts via multiple signalling cascades like MAPK and PI3K/Akt pathway, which are leading to increased proliferation and survival, treatment with trastuzumab was assumed to decrease proliferation, inhibit growth and induce apoptosis via decrease in HER2 signalling. However, in *in vivo* studies where neoadjuvant trastuzumab was applied to HER2-positive breast cancer patients and biopsy material was compared before and after treatment, neither a downregulation of HER2 nor a reduction in proliferation was observed (Gennari *et al.*, 2004; Mohsin *et al.*, 2005). In contrast, the induction of apoptosis was observed in both studies. While Gennari *et al.* clearly relate this induction of apoptosis to the occurrence of ADCC, Mohsin *et al.* did not investigate the mechanism of ADCC. Therefore, it remains unclear in this study whether apoptosis is signalling- or ADCC-dependent or a combination of both.

No direct effect of trastuzumab on cell viability and survival of SKBR-3 cells according to MTT and apoptosis data could be observed neither in 2D nor in 3D culture conditions in this work. While Nakajima *et al.* also did not observe a decrease in cell viability according to MTT assay in 2D cultures of three HER2-overexpressing breast cancer cell lines including SKBR-3 (Nakajima *et al.*, 2008), other studies described anti-proliferative as well as apoptotic effects in 2D cultures (Cuello *et al.*, 2001; Yakes *et al.*, 2002). In these studies, however, doses of trastuzumab applied to the cells were considerably higher and treatment time was longer compared to the experiments in this dissertation. In contrast to this absent therapy response to trastuzumab treatment in a setting without immunological component, a clear induction of ADCC in the 3D models of SKBR-3 cells could be observed both in a reporter-based assay as well as via the introduction of PBMCs as an immunological component into the test system. This effect of trastuzumab via ADCC could be observed already after 24 h and even for low concentrations, suggesting that ADCC might be a major MOA of trastuzumab. In contrast to the SKBR-3 models, no induction of ADCC by

trastuzumab could be observed for the MCF-7 and MDA-MB-231 models lacking the overexpression of HER2. This correlates well with preliminary data of the phase III clinical trial NSABP B-47 where breast cancer patients with HER2-low and -negative status were tested for trastuzumab efficacy in combination with chemotherapy and no benefit for those patients could be observed (Fehrenbacher L. *et al.*, 2017). Taken together, the here presented tumour test system representing different molecular subtypes of breast cancer successfully simulated the clinical situation regarding the targeted therapy approach with trastuzumab. Furthermore, an immunological component in the form of PBMCs was successfully introduced into these models and tumour cell apoptosis measurement could be used as a read-out parameter for ADCC. This allows testing of other immunotherapies that rely on immunological cells in the future.

Further validation of the test system with the help of compounds that had been tested to be effective in preclinical studies in 2D *in vitro* models and/or *in vivo* mouse models but failed in clinical trials would be beneficial in the future. However, the identification of such compounds is often difficult due to insufficiently published data of clinical trials that were unsuccessful. Furthermore, patient cohorts in such trials are often not sufficiently stratified for proper interpretation of the data according to tumour entities or biomarkers and compounds that failed are rarely commercially available.

5.4 Application of the established test system

5.4.1 Evaluation of an innovative drug formulation strategy

Besides the identification of novel targets and compounds for anti-cancer therapy, a main challenge for pharmaceutical industry is the appropriate formulation of the promising compounds for application in the patient (Ali & Kolter, 2012). This is especially challenging for compounds that are poorly soluble in water which accounts for 40-60% of all new chemical entities developed in pharmaceutical industry (Giliyar *et al.*, 2006; Merisko-Liversidge & Liversidge, 2008). In order to improve the water solubility, thereby increasing the bioavailability of hydrophobic therapeutic agents, novel drug formulation strategies and excipients are urgently needed as they can help to unfold the therapeutic potential of such compounds.

Curcumin, a bright yellow phenolic chemical produced by several plants, is one of such compounds with extremely low solubility in water and reduced bioavailability (Anand *et al.*, 2007). Even though several preclinical studies suggest that curcumin has a variety of activities that are beneficial for health like cardio-protective, anti-inflammatory and anti-tumour activity (Miriya *et al.*, 2007; Jurenka, 2009; X. Yang *et al.*, 2015), these benefits could not translate into clinical success (Nelson *et al.*, 2017) and therefore it has not been approved as a drug for human use. Its extremely low solubility in water, poor bioavailability and stability, however, make it an excellent candidate to study the potential of novel formulation strategies for drug delivery. Recently, Lübtow *et al.* reported that the copolymer A-pPrOzi-A is able to drastically enhance the solubility of curcumin (Lübtow, Hahn, *et al.*, 2017). As there is growing evidence, that 3D tumour models better reflect the complex *in vivo* situation compared to conventional 2D culture, this nanoformulation of curcumin was tested in the MDA-MB-231 3D model and compared to

2D culture. Indeed, cells in the 3D context were more resistant to curcumin therapy and required higher doses of the compound to achieve a cytotoxic effect. As this is a problem in the clinical context especially for poorly soluble substances like curcumin, this provides the rationale for the development of novel strategies for the formulation and application of such insoluble compounds. The finding that there was no difference between the effects of nanoformulated curcumin and the DMSO-formulation indicates that nanoformulated curcumin is fully bioactive.

Taken together, the test system was successfully used to evaluate the use of the copolymer A-pPrOzi-A for the application of the highly hydrophobic substance curcumin by the formation of ultra-high loaded nanoformulations. These nanoformulations might therefore help to fully unfold the therapeutic potential of insoluble compounds and to reach cancer therapy relevant concentrations in patients.

5.4.2 Testing of novel therapeutic strategies in the TNBC model

As already described before, no targeted therapies are available for the triple negative subset of breast cancer patients so far (Brenton *et al.*, 2005). Therefore, TNBC tumours are predominantly treated with non-specific and highly toxic chemotherapy or radiation (Chen & Russo, 2009). The lack of validated molecular targets leads to a poor prognosis and outcome for TNBC compared to other subtypes of breast cancer (Anders & Carey, 2009). This results in a pressing need for the better understanding of this breast cancer subset, the identification of novel targets and the development of alternative therapy strategies in order to improve the prognosis for TNBC patients. Therefore, the testing of compounds and novel therapy strategies in the presented test system focused on the TNBC model.

5.4.2.1 Combination therapy with doxorubicin and MK-1775

The mutation or loss of *p53* is occurring in approximately 70 % of TNBC (Cerami *et al.*, 2012; Gao *et al.*, 2013). This led to the exploration of approaches to target mutated *p53* in TNBC. As cells without *p53* function lack *p53*-dependent cell cycle checkpoint, they rely on the G2-M checkpoint when DNA-damages occur. The abrogation of this checkpoint leads to the premature entry of the cells into mitosis and in case of DNA-damage to mitotic catastrophe and apoptosis (Bucher & Britten, 2008). One option to exploit this, is the inhibition of WEE1 kinase which is needed to prevent the premature entry into mitosis. This led to the investigation of WEE1 inhibitors in combination with DNA-damaging chemotherapy. MK-1775 (AZD1775) is a potent WEE1 kinase inhibitor that demonstrated enhanced efficacy in *p53*-mutant or deficient cell lines of different entities in combination with DNA-damaging agents (Hirai *et al.*, 2009; Hirai *et al.*, 2010) and its efficacy was investigated in the MDA-MB-231 TNBC model.

According to data from 2D experiments, treatment with MK-1775 alone showed efficacy as assessed by viability and apoptosis measurements and only weak synergistic effects in combination with doxorubicin were observed. This is corroborated by previous findings of Krehling and colleagues who made similar observations in sarcoma cell lines (Krehling *et al.*, 2012) and Guertin and colleagues who showed single-agent efficacy of MK-1775 that is *p53*-independent in various cell lines and xenograft models (Guertin *et al.*, 2013). They claimed this

to be a consequence of DNA-damage during S-phase rather than premature entry into mitosis, as they found an increase in DNA-damage after treatment with MK-1775 (Guertin *et al.*, 2013). This can be explained by the fact that WEE1 also plays a critical role in the regulation of appropriate initiation and progression of DNA replication forks. Therefore WEE1 inhibition leads to an increase in DNA double strand breaks, thereby inducing apoptosis (Beck *et al.*, 2010; Dominguez-Kelly *et al.*, 2011; Beck *et al.*, 2012).

However, in the 3D test system neither a single-agent efficacy of MK-1775 nor an effect of combination therapy with doxorubicin could be observed for the same concentrations according to viability and apoptosis measurements. This suggests, that the tumour cells in the 3D environment have a higher chemoresistance to both MK-1775 and doxorubicin compared to MDA-MB-231 cells grown under 2D conditions. It is possible, that higher concentrations of the compound can cause anti-tumour effects. However this is unlikely, as an MK-1775 plasma drug concentration of 240 nM (compared to 0.5 μ M used in the 3D experiments) was associated with maximal efficacy in rat tumour xenografts and is therefore used as the pharmacokinetic target of plasma drug concentration in clinical trials (Leijen, van Geel, Pavlick, *et al.*, 2016). According to the data from the 3D test system, a recommendation for treatment of *p53*-mutated TNBC with MK-1775 with and without doxorubicin cannot be made. If this correlates with the treatment of *in vivo* tumours of patients, is not clear yet. In phase I studies MK-1775 was well tolerated and demonstrated manageable toxicity. In a phase I study that evaluated MK-1775 in combination with gemcitabine, cisplatin or carboplatin in patients with advanced solid tumours, 10 % of the patients enrolled had a partial response and 53 % had stable disease. However, as patients treated with the chemotherapeutic agent alone were not included in this study, it is not clear yet if patients benefit from the addition of MK-1775 to chemotherapeutic treatment (Leijen, van Geel, Pavlick, *et al.*, 2016). First results from a phase II clinical study evaluating MK-1775 in combination with carboplatin in patients with *p53*-mutated ovarian cancer that had been refractory or resistant to platinum first-line therapy indicate that MK-1775 enhances carboplatin efficacy in those patients. Five percent of the patients enrolled had a complete response and 38 % a partial response. As these patients were refractory or resistant to carboplatin treatment alone, the anti-tumour effect observed under re-exposure to carboplatin with MK-1775 can be interpreted as beneficial (Leijen, van Geel, Sonke, *et al.*, 2016). However, further phase II and III clinical trials with larger patient cohorts are needed to confirm the effects observed in this study. Currently, 49 clinical trials investigating MK-1775 as a single-agent or in combination with other compounds are listed on clinicaltrials.gov. Of these, 5 have been terminated early by the responsible party, 1 was withdrawn before enrolment started and 2 are suspended. Only 2 of the trials have been completed so far and 29 are recruiting or not yet recruiting patients for evaluation. One of these studies investigates the efficacy of cisplatin and MK-1775 in metastatic TNBC (NCT03012477). However, recruiting started in January 2017 and the estimated primary completion date is September 2020. The results of these studies will shed light on the question whether patients will benefit from MK-1775 as a monotherapy or in combination with other compounds and if this is also the case for TNBC patients.

5.4.2.2 ROR1-CAR T cell therapy

Next to targeted kinase inhibitors, the field of immunotherapies has also advanced for the treatment of cancer in the recent years and novel therapy strategies have been developed that are successfully applied in the clinical setting. A relatively new field is the therapy of cancer with adoptive transfer of immune cells. The transfer of patient-derived T cells that had been genetically engineered to express a tumour targeting CAR was a huge success for the therapy of haematological cancers with high rates of sustained complete remissions (Kochenderfer *et al.*, 2012; Brentjens *et al.*, 2013; Maude *et al.*, 2015). This success in clinical studies led to FDA approval of CD19-CAR T cell therapy, the first gene therapy to be approved for clinical use (P. P. Zheng *et al.*, 2018). The transfer of CAR T cell therapy to solid tumours is one of the major objectives in the field, but the treatment of such malignancies provides additional challenges for CAR T cells like migration from blood stream to tumour site, the infiltration of stromal tissue to reach the cancer cells and the survival in the immunosuppressive tumour microenvironment (Newick *et al.*, 2016; B. L. Zhang *et al.*, 2016). Therefore, suitable tumour test systems are required that appropriately reflect the conditions found in such tumours, thereby allowing a reliable prediction of CAR T cell efficacy. As such alternative treatment strategies might also be beneficial for TNBC patients, it was tested whether the here presented 3D *in vitro* test system is suitable for the evaluation of efficacy of such therapies. In order to keep the off-tumour effects causing severe side-effects as low as possible, an appropriate target on the tumour cells for CAR T cell therapy is necessary (Kalaitidou *et al.*, 2015). Such targets should be highly expressed on tumour cells but preferably be absent or only weakly expressed on healthy cells of the body. Here, the surface protein ROR1 was used as a target for CAR T cells. While it is expressed in a plethora of tissues during embryogenesis as well as in several human carcinomas like breast carcinomas (Zhang, Chen, Cui, *et al.*, 2012; Zhang, Chen, Wang-Rodriguez, *et al.*, 2012), it is only very weakly expressed in adult tissues like lung, pancreas, B cell precursors and adipocytes (Hudecek *et al.*, 2010). The TNBC cell line MDA-MB-231 is suitable as a target since it expresses the ROR1 antigen both in 2D and 3D culture and should therefore respond to treatment with ROR1-CAR T cells. Indeed, a dose-dependent anti-tumour effect of CAR T cells was observed in 2D experiments, whereas untransduced control T cells from the same donor did not have an effect on the tumour cells. This goes in line with previously published results of Hudecek and colleagues who observed a substantial reactivity of ROR1-CAR T cells against lung and TNBC cell lines (Hudecek *et al.*, 2013). However, such conventional 2D models do not adequately reflect complex tumour tissues as they lack physiological tissue architecture with cell-cell and cell-matrix interactions and do not provide the necessity for CAR T cells to migrate into a complex tissue. In contrast, the 2D cultured cells are easily accessible for the T cells and long term effects of immunotherapy can hardly be analysed.

Therefore, the 3D static TNBC model was applied to test whether CAR T cells are capable to specifically lyse tumour cells in the context of tissue architecture *in vitro*. Indeed, dose-dependent migration of CD45+ ROR1-CAR and control T cells was observed, whereas efficient tumour cell lysis was restricted to ROR1-CAR T cells. As T cells are applied to the top of the test system in this approach and migration of these is predominantly gravity-driven along the z-axis, with the help of the 3D dynamic tumour model, it was investigated whether the T cells are able to actively

adhere to and migrate into tumour tissues with a higher grade of invasiveness to execute their effector functions. Despite the free floating of T cells throughout the tubing system, migration of these into the tumour tissue as well as increased T cell proliferation and increased tumour cell apoptosis for treatment with ROR1-CAR T compared to control T cells could be observed, indicating their potential for the treatment of epithelial solid tumours. So far, for the testing of T cell therapies in a tissue context only few alternatives like microfluidic-based models exist that challenge T cells in a similar way. These rely on single tumour cells or aggregates incorporated in collagen-based hydrogels as a matrix. T cells are added into adjacent channels and T cell migration and tumour cell lysis are monitored (Parlato *et al.*, 2017; Pavesi *et al.*, 2017). However, these hydrogels do not provide the possibility to simulate different grades of tumour cell invasion like in the biological decellularised scaffold SISmuc with its preserved basement membrane structure.

Even though the here presented model systems do not fully represent the complexity of *in vivo* tumours, it is superior to conventional 2D culture systems in this respect. With the help of this *in vitro* test system both the therapy effect on tumour tissue as well as the functions of the T cells like proliferation, specific activation and cytokine secretion can be assessed. A further advantage of this *in vitro* test system lies in its modularity: The complexity can easily be adapted to the scientific question and focus of the study as individual parameters can be controlled, which is a major advantage over mouse models.

The mid-throughput 3D static tissue model offers the possibility to monitor dose effects, thereby predicting the lowest effective dose for *in vivo* studies in the future. The more sophisticated low-throughput dynamic 3D tissue model allowed the investigation of tumour and infiltrating capabilities of CAR T cells.

Therefore, the *in vitro* 3D tumour model presented here is an innovative, cost-efficient and reproducible alternative for the assessment of efficacy and optimization of CAR T cell therapy and other immunotherapy approaches and might help to reduce animal experiments especially with respect to proof-of-concept studies for efficacy testing that are usually performed in xenograft mouse models (Siegler & Wang, 2018). According to the here presented data, the ROR1-CAR T cell therapy approach is a promising therapeutic option in the future for solid tumours and especially for TNBC expressing the target ROR1.

5.5 Establishment of coculture models

5.5.1 Coculture with dermal fibroblasts

While historically most studies of tumour biology have focused on the epithelial cancer cells, interest in the understanding of the interaction between cancer cells and their surroundings, the tumour microenvironment, has been increasing in the last years. The tumour and its microenvironment are interacting dynamically and in a reciprocal way, thereby affecting a plethora of processes like survival, growth and proliferation, invasion and metastasis as well as chemoresistance (Kalluri & Zeisberg, 2006; Franco *et al.*, 2010). A crucial component of the

stromal compartment of tumours are fibroblasts as they have been described to promote tumourigenesis, enhance angiogenesis, proliferation and invasion and influence the drug response of carcinomas (Pietras & Ostman, 2010; McMillin *et al.*, 2013). Therefore, coculture models with primary dermal fibroblasts were established in order to provide a more accurate and complex simulation of *in vivo* carcinomas. With the synthesis and secretion of ECM components as well as ECM-degrading proteases, fibroblasts actively shape the tumour surrounding ECM (Kalluri & Zeisberg, 2006). This ability to remodel the ECM was also observed on the SISmuc in models with dermal fibroblasts in monoculture as well as in coculture with tumour cells. The coculture with fibroblasts resulted in an altered tissue morphology in the tumour models like the induction of multi-layered tumour cell growth in MCF-7 static 3D models, the formation of larger, nodule-like tumour aggregates surrounded by fibroblasts inside the lamina propria mucosae and high pillars of tumour cells on top of the scaffold in MCF-7 dynamic 3D models and the complete disintegration of former crypt structures accompanied by enhanced tumour cell invasion even into the submucosal compartment of the scaffold in 3D dynamic MDA-MB-231 models. Fibroblasts found in tumour tissue often have an activated phenotype. Such fibroblasts are referred to as CAFs. These can have various origins: They are possibly derived from normal fibroblasts via genetic and transcriptomic changes induced by adjacent carcinoma cells, from epithelial cells via EMT, from bone-marrow derived mesenchymal stem cells or from endothelial cells via endothelial-mesenchymal transition (Xing *et al.*, 2010). During cancer progression, cancer cells can alter the characteristics of the adjacent stroma to create a supportive microenvironment. In breast cancer, over 80 % of the fibroblasts demonstrate an activated phenotype as indicated by the expression of alpha smooth muscle actin (Sappino *et al.*, 1988). Another marker of CAFs is FAP. This type II integral membrane serine protease is not expressed in normal tissue but by fibroblasts in wound healing and in the stroma of more than 90 % of carcinomas including breast cancers and is associated with poor prognosis (Garin-Chesa *et al.*, 1990; Polgar, 2002; Kelly *et al.*, 2012). Here, it was shown, that primary dermal fibroblasts in monoculture are not in an activated state and do therefore not express FAP in monoculture on SISmuc. In static coculture with MCF-7 and MDA-MB-231 cells this phenotype did not change. In dynamic 3D conditions, however, the coculture with tumour cells led to an activation of the fibroblasts indicated by expression of FAP, that was stronger and more abundant in MCF-7 compared to MDA-MB-231 coculture models. This fibroblast activation was accompanied by increased tumour tissue formation and, in the case of the MDA-MB-231 model, with enhanced invasive behaviour and goes in line with reports that FAP enhances tumour cell proliferation and migration (Lai *et al.*, 2012; L. Yang *et al.*, 2013) and promotes tumour cell invasion via its gelatinase activity (P. O'Brien & O'Connor, 2008). Overall, the dynamic 3D coculture models correlated well with the xenograft material of the corresponding cell lines, where similar expression of FAP was observed in the murine stroma. Interestingly, FAP expression has also been described to be associated with platinum resistance and shorter recurrence in ovarian cancer patients (Mhaweche-Fauceglia *et al.*, 2015) indicating the potential of the here presented dynamic test system for drug screening.

5.5.2 Coculture with adipogenically differentiated hASCs

While the role of fibroblasts as part of the tumour stroma and as a key player in tumour progression has long been established, only little attention has been paid to adipocytes as an interaction partner of tumour cells despite their juxtaposition to epithelial cells especially in breast tissue (Wiseman & Werb, 2002). Only in recent years there is an increasing interest in the role of this cell type in human cancers and growing evidence that there is a heterotypic crosstalk between breast cancer cells and adipocytes (Tan *et al.*, 2011; Hoy *et al.*, 2017). Adipocytes enhance tumour cell migration, invasion and proliferation via the secretion of growth factors, adipokines and proinflammatory cytokines (Dirat *et al.*, 2011; Lapeire *et al.*, 2014). On the other hand, it is becoming evident that tumour cells also affect adipocytes: At the invasive front, adipocytes are smaller compared to those in greater distance to the tumour and almost no adipocytes can be found in the tumour centre. This indicates that tumour cells induce delipidation and dedifferentiation of the adipocytes, thereby inducing a fibroblast like-phenotype in the adipocytes. Only recently it has been shown, that this catabolic metabolism in the adipocytes is linked to an anabolic metabolism in the tumour cells. The free fatty acids from lipolysis in adipocytes are transferred to the tumour cells that increasingly store and oxidize those substrates (Balaban *et al.*, 2017; Y. Y. Wang *et al.*, 2017).

Unravelling this complex reciprocal interaction between adipocytes and tumour cells is of major interest as it might lead to the identification of new targets for the improvement of diagnosis and prognosis as well as for the development of innovative therapeutic strategies.

In this work, the 3D cocultures of breast cancer cell lines with adipocytes were sought to be established by differentiation of stromal vascular fraction-derived hASCs from human lipoaspirates or fat flaps. The reason for this approach is, that white mature adipocytes contain single, large lipid droplets that account for the majority of cell volume, thereby causing buoyancy that does not allow cell attachment to a culture plate or scaffold as they float on the medium (Poulos *et al.*, 2010). Classical preadipocyte cell lines like 3T3-L1 or 3T3-F442A are derived from rodents and their usage might therefore not fully recapitulate human adipose tissue. The here used hASCs could be efficiently differentiated along the adipogenic lineage in 3D cultures on the scaffold SISmuc under static and dynamic conditions as indicated by the accumulation of lipid droplets in the cells and static and dynamic 3D coculture models with the breast cancer cell line MDA-MB-231 were successfully established. These models represent a first step towards complex coculture models comprising the *in vivo* relevant stromal compartment of adipose tissue but will need further characterization and optimization. Moreover, one has to keep in mind that the adipogenically differentiated hASCs found in those models still differ from mature adipocytes containing a single lipid vacuole. Due to the complex differentiation protocol these models might be inappropriate for drug screening experiments but could rather be utilized for the investigation of the reciprocal interactions between tumour cells and adipocytes and the consequences for tumour progression in a more mechanistic way in the future.

5.6 Conclusion and outlook

In conclusion, during this work a standardized and reproducible 3D *in vitro* mamma carcinoma model was established that can serve as a basic tool for drug testing as well as for basic research questions in oncology. These 3D models help to bridge the gap between simplistic 2D cultures of cell lines that poorly represent the clinical situation and complex *in vivo* tumours. The better reflection of *in vivo* processes leads to an increase in predictivity, thereby helping to make drug development more efficient. As a good correlation with xenografts in marker expression and morphology was observed, such models could serve as an alternative for time- and cost-intensive animal models.

The here presented test system allows the investigation of compound efficacy via several established read-out parameters like proliferation, tumour cell viability, induction of apoptosis and marker expression. It was successfully used for targeted therapy simulation of trastuzumab that is routinely used in the clinical setting and for testing novel compounds and alternative treatment strategies like therapy with CAR T cells. The optional incorporation of an immunological component provides the possibility to evaluate immunotherapies that depend on the presence of immune cells in the future. Moreover, the models were used to study the process of invasion and can therefore be applied to determine compound efficacy on tumour cells of different progression stages and to test novel anti-metastatic therapy strategies, which target the process of cancer cell invasion. Fibroblasts and adipocytes, the major cell types of the tumour stroma in the breast, that are known to play crucial roles in cancer development and progression and are thought to influence therapy efficacy, were successfully incorporated into the models.

A great advantage of the model lies in its modularity: Complexity can be varied according to the specific need by adding other cell types or applying medium flow. This flexibility to control individual parameters facilitates the investigation of the contribution of single components and processes to the tumour and is a major advantage over *in vivo* tumours in mouse models. In the future, next to fibroblasts, adipocytes or immune cells, endothelial cells could also be added. Instead of generating the models based on the avascular SISmuc, the complex scaffold BioVaSc® could be used to generate a vascularised tumour tissue by reseeding the preserved vessel structures with human endothelial cells as described before (Mertsching *et al.*, 2009). This would be especially interesting for the evaluation of CAR T cell therapies as a vasculature would provide an additional physiological barrier for T cell migration. Additionally, other cell types, such as regulatory T cells, myeloid derived suppressor cells or fibroblasts could be added for further simulation of the immunosuppressive tumour microenvironment. Furthermore, the integration of healthy cells into the test system for the evaluation of possible toxic effects or the usage of primary tumour cells for the establishment of personalised tumour models are future objectives of great interest.

References

- Agrawal, S., Anderson, P., Durbeej, M., van Rooijen, N., Ivars, F., Opdenakker, G. & Sorokin, L. M. (2006). Dystroglycan is selectively cleaved at the parenchymal basement membrane at sites of leukocyte extravasation in experimental autoimmune encephalomyelitis. *J Exp Med*, **203**, 1007-1019.
- Algarra, I., Collado, A. & Garrido, F. (1997). Altered MHC class I antigens in tumors. *Int J Clin Lab Res*, **27**, 95-102.
- Ali, S. & Kolter, K. (2012). Challenges and Opportunities in Oral Formulation Development. *American Pharmaceutical Review*.
- Anand, P., Kunnumakkara, A. B., Newman, R. A. & Aggarwal, B. B. (2007). Bioavailability of curcumin: problems and promises. *Mol Pharm*, **4**, 807-818.
- Anders, C. K. & Carey, L. A. (2009). Biology, metastatic patterns, and treatment of patients with triple-negative breast cancer. *Clin Breast Cancer*, **9 Suppl 2**, S73-81.
- Arrowsmith, J. & Miller, P. (2013). Trial watch: phase II and phase III attrition rates 2011-2012. *Nat Rev Drug Discov*, **12**, 569.
- Bae, S. N., Arand, G., Azzam, H., Pavasant, P., Torri, J., Frandsen, T. L. & Thompson, E. W. (1993). Molecular and cellular analysis of basement membrane invasion by human breast cancer cells in Matrigel-based in vitro assays. *Breast Cancer Res Treat*, **24**, 241-255.
- Balaban, S., Shearer, R. F., Lee, L. S., van Geldermalsen, M., Schreuder, M., Shtein, H. C., Cairns, R., Thomas, K. C., Fazakerley, D. J., Grewal, T., Holst, J., Saunders, D. N. & Hoy, A. J. (2017). Adipocyte lipolysis links obesity to breast cancer growth: adipocyte-derived fatty acids drive breast cancer cell proliferation and migration. *Cancer Metab*, **5**, 1.
- Bamford, S., Dawson, E., Forbes, S., Clements, J., Pettett, R., Dogan, A., Flanagan, A., Teague, J., Futreal, P. A., Stratton, M. R. & Wooster, R. (2004). The COSMIC (Catalogue of Somatic Mutations in Cancer) database and website. *Br J Cancer*, **91**, 355-358.
- Baselga, J., Tripathy, D., Mendelsohn, J., Baughman, S., Benz, C. C., Dantis, L., Sklarin, N. T., Seidman, A. D., Hudis, C. A., Moore, J., Rosen, P. P., Twaddell, T., Henderson, I. C. & Norton, L. (1996). Phase II study of weekly intravenous recombinant humanized anti-p185HER2 monoclonal antibody in patients with HER2/neu-overexpressing metastatic breast cancer. *J Clin Oncol*, **14**, 737-744.
- Beatty, G. L. & O'Hara, M. (2016). Chimeric antigen receptor-modified T cells for the treatment of solid tumors: Defining the challenges and next steps. *Pharmacol Ther*.
- Beck, H., Nahse-Kumpf, V., Larsen, M. S., O'Hanlon, K. A., Patzke, S., Holmberg, C., Mejlvang, J., Groth, A., Nielsen, O., Syljuasen, R. G. & Sorensen, C. S. (2012). Cyclin-dependent kinase suppression by WEE1 kinase protects the genome through control of replication initiation and nucleotide consumption. *Mol Cell Biol*, **32**, 4226-4236.

- Beck, H., Nahse, V., Larsen, M. S., Groth, P., Clancy, T., Lees, M., Jorgensen, M., Helleday, T., Syljuasen, R. G. & Sorensen, C. S. (2010). Regulators of cyclin-dependent kinases are crucial for maintaining genome integrity in S phase. *J Cell Biol*, **188**, 629-638.
- Bhattacharjee, Y. (2012). Biomedicine. Pharma firms push for sharing of cancer trial data. *Science*, **338**, 29.
- Bloom, H. J. & Richardson, W. W. (1957). Histological grading and prognosis in breast cancer; a study of 1409 cases of which 359 have been followed for 15 years. *Br J Cancer*, **11**, 359-377.
- Brentjens, R. J., Davila, M. L., Riviere, I., Park, J., Wang, X., Cowell, L. G., Bartido, S., Stefanski, J., Taylor, C., Olszewska, M., Borquez-Ojeda, O., Qu, J., Wasielewska, T., He, Q., Bernal, Y., Rijo, I. V., Hedvat, C., Kobos, R., Curran, K., Steinherz, P., Jurcic, J., Rosenblat, T., Maslak, P., Frattini, M. & Sadelain, M. (2013). CD19-targeted T cells rapidly induce molecular remissions in adults with chemotherapy-refractory acute lymphoblastic leukemia. *Sci Transl Med*, **5**, 177ra138.
- Brenton, J. D., Carey, L. A., Ahmed, A. A. & Caldas, C. (2005). Molecular classification and molecular forecasting of breast cancer: ready for clinical application? *J Clin Oncol*, **23**, 7350-7360.
- Breslin, S. & O'Driscoll, L. (2013). Three-dimensional cell culture: the missing link in drug discovery. *Drug Discov Today*, **18**, 240-249.
- Bucher, N. & Britten, C. D. (2008). G2 checkpoint abrogation and checkpoint kinase-1 targeting in the treatment of cancer. *Br J Cancer*, **98**, 523-528.
- Burdett, E., Kasper, F. K., Mikos, A. G. & Ludwig, J. A. (2010). Engineering tumors: a tissue engineering perspective in cancer biology. *Tissue Eng Part B Rev*, **16**, 351-359.
- Caponigro, G. & Sellers, W. R. (2011). Advances in the preclinical testing of cancer therapeutic hypotheses. *Nat Rev Drug Discov*, **10**, 179-187.
- Carter, P., Presta, L., Gorman, C. M., Ridgway, J. B., Henner, D., Wong, W. L., Rowland, A. M., Kotts, C., Carver, M. E. & Shepard, H. M. (1992). Humanization of an anti-p185HER2 antibody for human cancer therapy. *Proc Natl Acad Sci U S A*, **89**, 4285-4289.
- Cathcart, J., Pulkoski-Gross, A. & Cao, J. (2015). Targeting Matrix Metalloproteinases in Cancer: Bringing New Life to Old Ideas. *Genes Dis*, **2**, 26-34.
- Cerami, E., Gao, J., Dogrusoz, U., Gross, B. E., Sumer, S. O., Aksoy, B. A., Jacobsen, A., Byrne, C. J., Heuer, M. L., Larsson, E., Antipin, Y., Reva, B., Goldberg, A. P., Sander, C. & Schultz, N. (2012). The cBio cancer genomics portal: an open platform for exploring multidimensional cancer genomics data. *Cancer Discov*, **2**, 401-404.
- Chen, J. Q. & Russo, J. (2009). ERalpha-negative and triple negative breast cancer: molecular features and potential therapeutic approaches. *Biochim Biophys Acta*, **1796**, 162-175.
- Cobleigh, M. A., Vogel, C. L., Tripathy, D., Robert, N. J., Scholl, S., Fehrenbacher, L., Wolter, J. M., Paton, V., Shak, S., Lieberman, G. & Slamon, D. J. (1999). Multinational study of the efficacy and safety of humanized anti-HER2

- monoclonal antibody in women who have HER2-overexpressing metastatic breast cancer that has progressed after chemotherapy for metastatic disease. *J Clin Oncol*, **17**, 2639-2648.
- Cree, I. A., Glaysher, S. & Harvey, A. L. (2010). Efficacy of anti-cancer agents in cell lines versus human primary tumour tissue. *Curr Opin Pharmacol*, **10**, 375-379.
- Cuello, M., Ettenberg, S. A., Clark, A. S., Keane, M. M., Posner, R. H., Nau, M. M., Dennis, P. A. & Lipkowitz, S. (2001). Down-regulation of the erbB-2 receptor by trastuzumab (herceptin) enhances tumor necrosis factor-related apoptosis-inducing ligand-mediated apoptosis in breast and ovarian cancer cell lines that overexpress erbB-2. *Cancer Res*, **61**, 4892-4900.
- Degenhardt, T., Harbeck, N. & Würstlein, R. (2015). Individuelle Tumorthherapie beim Mammakarzinom – Möglichkeiten der Vermeidung von Über- und Untertherapie unter besonderer Berücksichtigung zielgerichteter Therapien. *Deutsche Zeitschrift für Onkologie*, **47**, 57-65.
- Denais, C. M., Gilbert, R. M., Isermann, P., McGregor, A. L., te Lindert, M., Weigelin, B., Davidson, P. M., Friedl, P., Wolf, K. & Lammerding, J. (2016). Nuclear envelope rupture and repair during cancer cell migration. *Science*, **352**, 353-358.
- Dent, R., Trudeau, M., Pritchard, K. I., Hanna, W. M., Kahn, H. K., Sawka, C. A., Lickley, L. A., Rawlinson, E., Sun, P. & Narod, S. A. (2007). Triple-negative breast cancer: clinical features and patterns of recurrence. *Clin Cancer Res*, **13**, 4429-4434.
- Dirat, B., Bochet, L., Dabek, M., Daviaud, D., Dauvillier, S., Majed, B., Wang, Y. Y., Meulle, A., Salles, B., Le Gonidec, S., Garrido, I., Escourrou, G., Valet, P. & Muller, C. (2011). Cancer-associated adipocytes exhibit an activated phenotype and contribute to breast cancer invasion. *Cancer Res*, **71**, 2455-2465.
- Do, K., Doroshov, J. H. & Kummar, S. (2013). Wee1 kinase as a target for cancer therapy. *Cell Cycle*, **12**, 3159-3164.
- Dominguez-Kelly, R., Martin, Y., Koundrioukoff, S., Tanenbaum, M. E., Smits, V. A., Medema, R. H., Debatisse, M. & Freire, R. (2011). Wee1 controls genomic stability during replication by regulating the Mus81-Eme1 endonuclease. *J Cell Biol*, **194**, 567-579.
- Duran-Vilaregut, J., del Valle, J., Manich, G., Camins, A., Pallas, M., Vilaplana, J. & Pelegri, C. (2011). Role of matrix metalloproteinase-9 (MMP-9) in striatal blood-brain barrier disruption in a 3-nitropropionic acid model of Huntington's disease. *Neuropathol Appl Neurobiol*, **37**, 525-537.
- Egeblad, M. & Werb, Z. (2002). New functions for the matrix metalloproteinases in cancer progression. *Nat Rev Cancer*, **2**, 161-174.
- Elston, C. W. & Ellis, I. O. (1991). Pathological prognostic factors in breast cancer. I. The value of histological grade in breast cancer: experience from a large study with long-term follow-up. *Histopathology*, **19**, 403-410.
- Even-Ram, S. & Yamada, K. M. (2005). Cell migration in 3D matrix. *Curr Opin Cell Biol*, **17**, 524-532.

- Fallica, B., Maffei, J. S., Villa, S., Makin, G. & Zaman, M. (2012). Alteration of cellular behavior and response to PI3K pathway inhibition by culture in 3D collagen gels. *PLoS One*, **7**, e48024.
- Fata, J. E., Ho, A. T., Leco, K. J., Moorehead, R. A. & Khokha, R. (2000). Cellular turnover and extracellular matrix remodeling in female reproductive tissues: functions of metalloproteinases and their inhibitors. *Cell Mol Life Sci*, **57**, 77-95.
- Fehrenbacher L., Cecchini R. S., Geyer CE, Rastogi P., Costantino J. P., Atkins J. N., Polikoff J., Boileau J-F., Provencher L., Stokoe C., Moore T. D., Robidoux A., Borges V., Albain K. S., Swain S. M., Paik S., Mamounas E. P. & B., W. N. (2017, 12/2017). NSABP B-47 (NRG oncology): Phase III randomized trial comparing adjuvant chemotherapy with adriamycin (A) and cyclophosphamide (C) → weekly paclitaxel (WP), or docetaxel (T) and C with or without a year of trastuzumab (H) in women with node-positive or high-risk node-negative invasive breast cancer (IBC) expressing HER2 staining intensity of IHC 1+ or 2+ with negative FISH (HER2-Low IBC). Retrieved from https://www.abstracts2view.com/sabcs/view.php?nu=SABCS17L_989&terms=
- Ferlay, J., Soerjomataram, I., Dikshit, R., Eser, S., Mathers, C., Rebelo, M., Parkin, D. M., Forman, D. & Bray, F. (2015). Cancer incidence and mortality worldwide: sources, methods and major patterns in GLOBOCAN 2012. *Int J Cancer*, **136**, E359-386.
- Fischer, K. R., Durrans, A., Lee, S., Sheng, J., Li, F., Wong, S. T., Choi, H., El Rayes, T., Ryu, S., Troeger, J., Schwabe, R. F., Vahdat, L. T., Altorki, N. K., Mittal, V. & Gao, D. (2015). Epithelial-to-mesenchymal transition is not required for lung metastasis but contributes to chemoresistance. *Nature*, **527**, 472-476.
- Franco, O. E., Shaw, A. K., Strand, D. W. & Hayward, S. W. (2010). Cancer associated fibroblasts in cancer pathogenesis. *Semin Cell Dev Biol*, **21**, 33-39.
- Gao, J., Aksoy, B. A., Dogrusoz, U., Dresdner, G., Gross, B., Sumer, S. O., Sun, Y., Jacobsen, A., Sinha, R., Larsson, E., Cerami, E., Sander, C. & Schultz, N. (2013). Integrative analysis of complex cancer genomics and clinical profiles using the cBioPortal. *Sci Signal*, **6**, p11.
- Garin-Chesa, P., Old, L. J. & Rettig, W. J. (1990). Cell surface glycoprotein of reactive stromal fibroblasts as a potential antibody target in human epithelial cancers. *Proc Natl Acad Sci U S A*, **87**, 7235-7239.
- Gennari, R., Menard, S., Fagnoni, F., Ponchio, L., Scelsi, M., Tagliabue, E., Castiglioni, F., Villani, L., Magalotti, C., Gibelli, N., Oliviero, B., Ballardini, B., Da Prada, G., Zambelli, A. & Costa, A. (2004). Pilot study of the mechanism of action of preoperative trastuzumab in patients with primary operable breast tumors overexpressing HER2. *Clin Cancer Res*, **10**, 5650-5655.
- Gerdes, J., Lemke, H., Baisch, H., Wacker, H. H., Schwab, U. & Stein, H. (1984). Cell cycle analysis of a cell proliferation-associated human nuclear antigen defined by the monoclonal antibody Ki-67. *J Immunol*, **133**, 1710-1715.
- Giliyar, C., Fikstad, D. T. & Tyavanagimatt, S. (2006). Challenges and opportunities in oral delivery of poorly water-soluble drugs (**Vol. 6**).
- Goldhirsch, A., Wood, W. C., Coates, A. S., Gelber, R. D., Thurlimann, B., Senn, H. J. & Panel, m. (2011). Strategies for subtypes--dealing with the diversity of breast

- cancer: highlights of the St. Gallen International Expert Consensus on the Primary Therapy of Early Breast Cancer 2011. *Ann Oncol*, **22**, 1736-1747.
- Göttlich, C., Müller, L. C., Kunz, M., Schmitt, F., Walles, H., Walles, T., Dandekar, T., Dandekar, G. & Nietzer, S. L. (2016). A Combined 3D Tissue Engineered In Vitro/In Silico Lung Tumor Model for Predicting Drug Effectiveness in Specific Mutational Backgrounds. *J Vis Exp*.
- Griffith, L. G. & Swartz, M. A. (2006). Capturing complex 3D tissue physiology in vitro. *Nat Rev Mol Cell Biol*, **7**, 211-224.
- Guertin, A. D., Li, J., Liu, Y., Hurd, M. S., Schuller, A. G., Long, B., Hirsch, H. A., Feldman, I., Benita, Y., Toniatti, C., Zawel, L., Fawell, S. E., Gilliland, D. G. & Shumway, S. D. (2013). Preclinical evaluation of the WEE1 inhibitor MK-1775 as single-agent anticancer therapy. *Mol Cancer Ther*, **12**, 1442-1452.
- Hanahan, D. & Weinberg, R. A. (2011). Hallmarks of cancer: the next generation. *Cell*, **144**, 646-674.
- Hansmann, J., Groeber, F., Kahlig, A., Kleinhans, C. & Walles, H. (2013). Bioreactors in tissue engineering - principles, applications and commercial constraints. *Biotechnol J*, **8**, 298-307.
- Hirai, H., Arai, T., Okada, M., Nishibata, T., Kobayashi, M., Sakai, N., Imagaki, K., Ohtani, J., Sakai, T., Yoshizumi, T., Mizuarai, S., Iwasawa, Y. & Kotani, H. (2010). MK-1775, a small molecule Wee1 inhibitor, enhances anti-tumor efficacy of various DNA-damaging agents, including 5-fluorouracil. *Cancer Biol Ther*, **9**, 514-522.
- Hirai, H., Iwasawa, Y., Okada, M., Arai, T., Nishibata, T., Kobayashi, M., Kimura, T., Kaneko, N., Ohtani, J., Yamanaka, K., Itadani, H., Takahashi-Suzuki, I., Fukasawa, K., Oki, H., Nambu, T., Jiang, J., Sakai, T., Arakawa, H., Sakamoto, T., Sagara, T., Yoshizumi, T., Mizuarai, S. & Kotani, H. (2009). Small-molecule inhibition of Wee1 kinase by MK-1775 selectively sensitizes p53-deficient tumor cells to DNA-damaging agents. *Mol Cancer Ther*, **8**, 2992-3000.
- Hirt, C., Papadimitropoulos, A., Muraro, M. G., Mele, V., Panopoulos, E., Cremonesi, E., Ivanek, R., Schultz-Thater, E., Droeser, R. A., Mengus, C., Heberer, M., Oertli, D., Iezzi, G., Zajac, P., Eppenberger-Castori, S., Tornillo, L., Terracciano, L., Martin, I. & Spagnoli, G. C. (2015). Bioreactor-engineered cancer tissue-like structures mimic phenotypes, gene expression profiles and drug resistance patterns observed "in vivo". *Biomaterials*, **62**, 138-146.
- Holliday, D. L. & Speirs, V. (2011). Choosing the right cell line for breast cancer research. *Breast Cancer Res*, **13**, 215.
- Hoy, A. J., Balaban, S. & Saunders, D. N. (2017). Adipocyte-Tumor Cell Metabolic Crosstalk in Breast Cancer. *Trends Mol Med*, **23**, 381-392.
- Hudecek, M., Lupo-Stanghellini, M. T., Kosasih, P. L., Sommermeyer, D., Jensen, M. C., Rader, C. & Riddell, S. R. (2013). Receptor Affinity and Extracellular Domain Modifications Affect Tumor Recognition by ROR1-Specific Chimeric Antigen Receptor T Cells. *Clinical Cancer Research*, **19**, 3153-3164.
- Hudecek, M., Schmitt, T. M., Baskar, S., Lupo-Stanghellini, M. T., Nishida, T., Yamamoto, T. N., Bleakley, M., Turtle, C. J., Chang, W. C., Greisman, H. A.,

- Wood, B., Maloney, D. G., Jensen, M. C., Rader, C. & Riddell, S. R. (2010). The B-cell tumor-associated antigen ROR1 can be targeted with T cells modified to express a ROR1-specific chimeric antigen receptor. *Blood*, **116**, 4532-4541.
- Hutchinson, L. & Kirk, R. (2011). High drug attrition rates--where are we going wrong? *Nat Rev Clin Oncol*, **8**, 189-190.
- Inwald, E. C., Klinkhammer-Schalke, M., Hofstadter, F., Zeman, F., Koller, M., Gerstenhauer, M. & Ortmann, O. (2013). Ki-67 is a prognostic parameter in breast cancer patients: results of a large population-based cohort of a cancer registry. *Breast Cancer Res Treat*, **139**, 539-552.
- Johannessen, L. E., Haugen, K. E., ostvold, A. C., Stang, E. & Madshus, I. H. (2001). Heterodimerization of the epidermal-growth-factor (EGF) receptor and ErbB2 and the affinity of EGF binding are regulated by different mechanisms. *Biochem J*, **356**, 87-96.
- Jurenka, J. S. (2009). Anti-inflammatory properties of curcumin, a major constituent of *Curcuma longa*: a review of preclinical and clinical research. *Altern Med Rev*, **14**, 141-153.
- Kalaitsidou, M., Kueberuwa, G., Schutt, A. & Gilham, D. E. (2015). CAR T-cell therapy: toxicity and the relevance of preclinical models. *Immunotherapy*, **7**, 487-497.
- Kalluri, R. & Zeisberg, M. (2006). Fibroblasts in cancer. *Nat Rev Cancer*, **6**, 392-401.
- Kamb, A. (2005). What's wrong with our cancer models? *Nat Rev Drug Discov*, **4**, 161-165.
- Kelly, T., Huang, Y., Simms, A. E. & Mazur, A. (2012). Fibroblast activation protein-alpha: a key modulator of the microenvironment in multiple pathologies. *Int Rev Cell Mol Biol*, **297**, 83-116.
- Kessenbrock, K., Plaks, V. & Werb, Z. (2010). Matrix metalloproteinases: regulators of the tumor microenvironment. *Cell*, **141**, 52-67.
- Kleinman, H. K., McGarvey, M. L., Hassell, J. R., Star, V. L., Cannon, F. B., Laurie, G. W. & Martin, G. R. (1986). Basement membrane complexes with biological activity. *Biochemistry*, **25**, 312-318.
- Kochenderfer, J. N., Dudley, M. E., Feldman, S. A., Wilson, W. H., Spaner, D. E., Maric, I., Stetler-Stevenson, M., Phan, G. Q., Hughes, M. S., Sherry, R. M., Yang, J. C., Kammula, U. S., Devillier, L., Carpenter, R., Nathan, D. A., Morgan, R. A., Laurencot, C. & Rosenberg, S. A. (2012). B-cell depletion and remissions of malignancy along with cytokine-associated toxicity in a clinical trial of anti-CD19 chimeric-antigen-receptor-transduced T cells. *Blood*, **119**, 2709-2720.
- Kohrmann, A., Kammerer, U., Kapp, M., Dietl, J. & Anacker, J. (2009). Expression of matrix metalloproteinases (MMPs) in primary human breast cancer and breast cancer cell lines: New findings and review of the literature. *BMC Cancer*, **9**, 188.
- Komuro, T. (1985). Fenestrations of the basal lamina of intestinal villi of the rat. Scanning and transmission electron microscopy. *Cell Tissue Res*, **239**, 183-188.
- Kreahling, J. M., Gemmer, J. Y., Reed, D., Letson, D., Bui, M. & Altiook, S. (2012). MK1775, a selective Wee1 inhibitor, shows single-agent antitumor activity against sarcoma cells. *Mol Cancer Ther*, **11**, 174-182.

- Krummel, M. F. & Allison, J. P. (1995). CD28 and CTLA-4 have opposing effects on the response of T cells to stimulation. *J Exp Med*, **182**, 459-465.
- Lai, D., Ma, L. & Wang, F. (2012). Fibroblast activation protein regulates tumor-associated fibroblasts and epithelial ovarian cancer cells. *Int J Oncol*, **41**, 541-550.
- Lakhani, S. R., Ellis, I. O., Schnitt, S. J., Tan, P. H. & Van de Vijver, M. J. (2012). WHO Classification of Tumours of the Breast. Fourth Edition (**Vol. 4**).
- Lamouille, S., Xu, J. & Derynck, R. (2014). Molecular mechanisms of epithelial-mesenchymal transition. *Nat Rev Mol Cell Biol*, **15**, 178-196.
- Lapeire, L., Hendrix, A., Lambein, K., Van Bockstal, M., Braems, G., Van Den Broecke, R., Limame, R., Mestdagh, P., Vandesompele, J., Vanhove, C., Maynard, D., Lehuède, C., Muller, C., Valet, P., Gespach, C. P., Bracke, M., Cocquyt, V., Denys, H. & De Wever, O. (2014). Cancer-associated adipose tissue promotes breast cancer progression by paracrine oncostatin M and Jak/STAT3 signaling. *Cancer Res*, **74**, 6806-6819.
- Lebeau, A., Nerlich, A. G., Sauer, U., Lichtinghagen, R. & Lohrs, U. (1999). Tissue distribution of major matrix metalloproteinases and their transcripts in human breast carcinomas. *Anticancer Res*, **19**, 4257-4264.
- Leijen, S., Beijnen, J. H. & Schellens, J. H. (2010). Abrogation of the G2 checkpoint by inhibition of Wee-1 kinase results in sensitization of p53-deficient tumor cells to DNA-damaging agents. *Curr Clin Pharmacol*, **5**, 186-191.
- Leijen, S., van Geel, R. M., Pavlick, A. C., Tibes, R., Rosen, L., Razak, A. R., Lam, R., Demuth, T., Rose, S., Lee, M. A., Freshwater, T., Shumway, S., Liang, L. W., Oza, A. M., Schellens, J. H. & Shapiro, G. I. (2016). Phase I Study Evaluating WEE1 Inhibitor AZD1775 As Monotherapy and in Combination With Gemcitabine, Cisplatin, or Carboplatin in Patients With Advanced Solid Tumors. *J Clin Oncol*, **34**, 4371-4380.
- Leijen, S., van Geel, R. M., Sonke, G. S., de Jong, D., Rosenberg, E. H., Marchetti, S., Pluim, D., van Werkhoven, E., Rose, S., Lee, M. A., Freshwater, T., Beijnen, J. H. & Schellens, J. H. (2016). Phase II Study of WEE1 Inhibitor AZD1775 Plus Carboplatin in Patients With TP53-Mutated Ovarian Cancer Refractory or Resistant to First-Line Therapy Within 3 Months. *J Clin Oncol*, **34**, 4354-4361.
- Levin, M., Udi, Y., Solomonov, I. & Sagi, I. (2017). Next generation matrix metalloproteinase inhibitors - Novel strategies bring new prospects. *Biochim Biophys Acta*, **1864**, 1927-1939.
- Linke, K., Schanz, J., Hansmann, J., Walles, T., Brunner, H. & Mertsching, H. (2007). Engineered liver-like tissue on a capillarized matrix for applied research. *Tissue Eng*, **13**, 2699-2707.
- Lipson, E. J. & Drake, C. G. (2011). Ipilimumab: an anti-CTLA-4 antibody for metastatic melanoma. *Clin Cancer Res*, **17**, 6958-6962.
- Lovitt, C. J., Shelper, T. B. & Avery, V. M. (2014). Advanced cell culture techniques for cancer drug discovery. *Biology (Basel)*, **3**, 345-367.
- Lowden, S. & Heath, T. (1994). Ileal Peyer's patches in pigs: intercellular and lymphatic pathways. *Anat Rec*, **239**, 297-305.

- Lübtow, M. M., Hahn, L., Haider, M. S. & Luxenhofer, R. (2017). Drug Specificity, Synergy and Antagonism in Ultrahigh Capacity Poly(2-oxazoline)/Poly(2-oxazine) based Formulations. *J Am Chem Soc*, **139**, 10980-10983.
- Lübtow, M. M., Nelke, L. C., Brown, A., Sahay, G., Dandekar, G. & Luxenhofer, R. (2017). Drug induced micellization into ultra-high capacity and stable curcumin nanoformulations: Comparing in vitro 2D and 3D-tumor model of triple-negative breast cancer. *ChemRxiv. Preprint*. doi: 10.26434/chemrxiv.5661736.v1
- Luca, A. C., Mersch, S., Deenen, R., Schmidt, S., Messner, I., Schafer, K. L., Baldus, S. E., Huckenbeck, W., Piekorz, R. P., Knoefel, W. T., Krieg, A. & Stoecklein, N. H. (2013). Impact of the 3D microenvironment on phenotype, gene expression, and EGFR inhibition of colorectal cancer cell lines. *PLoS One*, **8**, e59689.
- Luporsi, E., Andre, F., Spyrtos, F., Martin, P. M., Jacquemier, J., Penault-Llorca, F., Tubiana-Mathieu, N., Sigal-Zafrani, B., Arnould, L., Gompel, A., Egele, C., Poulet, B., Clough, K. B., Crouet, H., Fourquet, A., Lefranc, J. P., Mathelin, C., Rouyer, N., Serin, D., Spielmann, M., Haugh, M., Chenard, M. P., Brain, E., de Cremoux, P. & Bellocq, J. P. (2012). Ki-67: level of evidence and methodological considerations for its role in the clinical management of breast cancer: analytical and critical review. *Breast Cancer Res Treat*, **132**, 895-915.
- Maheswaran, S. & Haber, D. A. (2015). Cell fate: Transition loses its invasive edge. *Nature*, **527**, 452-453.
- Matheson, C. J., Backos, D. S. & Reigan, P. (2016). Targeting WEE1 Kinase in Cancer. *Trends Pharmacol Sci*, **37**, 872-881.
- Maude, S. L., Teachey, D. T., Porter, D. L. & Grupp, S. A. (2015). CD19-targeted chimeric antigen receptor T-cell therapy for acute lymphoblastic leukemia. *Blood*, **125**, 4017-4023.
- McCluggage, S. G. & Low, F. N. (1984). Microdissection by ultrasonication: porosity of the intestinal epithelial basal lamina. *Am J Anat*, **171**, 207-216.
- McGowan, P. M. & Duffy, M. J. (2008). Matrix metalloproteinase expression and outcome in patients with breast cancer: analysis of a published database. *Ann Oncol*, **19**, 1566-1572.
- McMillin, D. W., Negri, J. M. & Mitsiades, C. S. (2013). The role of tumour-stromal interactions in modifying drug response: challenges and opportunities. *Nat Rev Drug Discov*, **12**, 217-228.
- Mehner, C., Hockla, A., Miller, E., Ran, S., Radisky, D. C. & Radisky, E. S. (2014). Tumor cell-produced matrix metalloproteinase 9 (MMP-9) drives malignant progression and metastasis of basal-like triple negative breast cancer. *Oncotarget*, **5**, 2736-2749.
- Mellor, J. D., Brown, M. P., Irving, H. R., Zalcborg, J. R. & Dobrovic, A. (2013). A critical review of the role of Fc gamma receptor polymorphisms in the response to monoclonal antibodies in cancer. *J Hematol Oncol*, **6**, 1.
- Merisko-Liversidge, E. M. & Liversidge, G. G. (2008). Drug nanoparticles: formulating poorly water-soluble compounds. *Toxicol Pathol*, **36**, 43-48.

- Mertsching, H., Schanz, J., Steger, V., Schandar, M., Schenk, M., Hansmann, J., Dally, I., Friedel, G. & Walles, T. (2009). Generation and transplantation of an autologous vascularized bioartificial human tissue. *Transplantation*, **88**, 203-210.
- Mertsching, H., Walles, T., Hofmann, M., Schanz, J. & Knapp, W. H. (2005). Engineering of a vascularized scaffold for artificial tissue and organ generation. *Biomaterials*, **26**, 6610-6617.
- Mhawech-Fauceglia, P., Yan, L., Sharifian, M., Ren, X., Liu, S., Kim, G., Gayther, S. A., Pejovic, T. & Lawrenson, K. (2015). Stromal Expression of Fibroblast Activation Protein Alpha (FAP) Predicts Platinum Resistance and Shorter Recurrence in patients with Epithelial Ovarian Cancer. *Cancer Microenviron*, **8**, 23-31.
- Miriyala, S., Panchatcharam, M. & Rengarajulu, P. (2007). Cardioprotective effects of curcumin. *Adv Exp Med Biol*, **595**, 359-377.
- Mishra, D. K., Thrall, M. J., Baird, B. N., Ott, H. C., Blackmon, S. H., Kurie, J. M. & Kim, M. P. (2012). Human lung cancer cells grown on acellular rat lung matrix create perfusable tumor nodules. *Ann Thorac Surg*, **93**, 1075-1081.
- Mohsin, S. K., Weiss, H. L., Gutierrez, M. C., Chamness, G. C., Schiff, R., Digiovanna, M. P., Wang, C. X., Hilsenbeck, S. G., Osborne, C. K., Allred, D. C., Elledge, R. & Chang, J. C. (2005). Neoadjuvant trastuzumab induces apoptosis in primary breast cancers. *J Clin Oncol*, **23**, 2460-2468.
- Moreno, L. & Pearson, A. D. (2013). How can attrition rates be reduced in cancer drug discovery? *Expert Opin Drug Discov*, **8**, 363-368.
- Morris, S. R. & Carey, L. A. (2006). Trastuzumab and beyond: New possibilities for the treatment of HER2-positive breast cancer. *Oncology (Williston Park)*, **20**, 1763-1771; discussion 1771-1762, 1774-1766.
- Mougiakakos, D., Choudhury, A., Lladser, A., Kiessling, R. & Johansson, C. C. (2010). Regulatory T cells in cancer. *Adv Cancer Res*, **107**, 57-117.
- Moustakas, A. & Heldin, C. H. (2007). Signaling networks guiding epithelial-mesenchymal transitions during embryogenesis and cancer progression. *Cancer Sci*, **98**, 1512-1520.
- Mudvari, P., Ohshiro, K., Nair, V., Horvath, A. & Kumar, R. (2013). Genomic insights into triple-negative and HER2-positive breast cancers using isogenic model systems. *PLoS One*, **8**, e74993.
- Nahta, R., Yu, D., Hung, M. C., Hortobagyi, G. N. & Esteva, F. J. (2006). Mechanisms of disease: understanding resistance to HER2-targeted therapy in human breast cancer. *Nat Clin Pract Oncol*, **3**, 269-280.
- Nakajima, H., Mizuta, N., Sakaguchi, K., Fujiwara, I., Yoshimori, A., Takahashi, S., Takasawa, R. & Tanuma, S. (2008). Development of HER2-antagonistic peptides as novel anti-breast cancer drugs by in silico methods. *Breast Cancer*, **15**, 65-72.
- Nelson, K. M., Dahlin, J. L., Bisson, J., Graham, J., Pauli, G. F. & Walters, M. A. (2017). The Essential Medicinal Chemistry of Curcumin. *J Med Chem*, **60**, 1620-1637.
- Newick, K., Moon, E. & Albelda, S. M. (2016). Chimeric antigen receptor T-cell therapy for solid tumors. *Mol Ther Oncolytics*, **3**, 16006.

- Nietzer, S., Baur, F., Sieber, S., Hansmann, J., Schwarz, T., Stoffer, C., Hafner, H., Gasser, M., Waaga-Gasser, A. M., Walles, H. & Dandekar, G. (2016). Mimicking Metastases Including Tumor Stroma: A New Technique to Generate a Three-Dimensional Colorectal Cancer Model Based on a Biological Decellularized Intestinal Scaffold. *Tissue Eng Part C Methods*, **22**, 621-635.
- O'Brien, F. J. (2011). Biomaterials & scaffolds for tissue engineering. *Materials Today*, **14**, 88-95.
- O'Brien, P. & O'Connor, B. F. (2008). Seprase: an overview of an important matrix serine protease. *Biochim Biophys Acta*, **1784**, 1130-1145.
- Okazaki, T. & Honjo, T. (2007). PD-1 and PD-1 ligands: from discovery to clinical application. *Int Immunol*, **19**, 813-824.
- Ostrand-Rosenberg, S. & Sinha, P. (2009). Myeloid-derived suppressor cells: linking inflammation and cancer. *J Immunol*, **182**, 4499-4506.
- Overall, C. M. & Lopez-Otin, C. (2002). Strategies for MMP inhibition in cancer: innovations for the post-trial era. *Nat Rev Cancer*, **2**, 657-672.
- Page-McCaw, A., Ewald, A. J. & Werb, Z. (2007). Matrix metalloproteinases and the regulation of tissue remodelling. *Nat Rev Mol Cell Biol*, **8**, 221-233.
- Pardoll, D. M. (2012). The blockade of immune checkpoints in cancer immunotherapy. *Nat Rev Cancer*, **12**, 252-264.
- Parlato, S., De Ninno, A., Molfetta, R., Toschi, E., Salerno, D., Mencattini, A., Romagnoli, G., Fragale, A., Roccuzzello, L., Buoncervello, M., Canini, I., Bentivegna, E., Falchi, M., Bertani, F. R., Gerardino, A., Martinelli, E., Natale, C., Paolini, R., Businaro, L. & Gabriele, L. (2017). 3D Microfluidic model for evaluating immunotherapy efficacy by tracking dendritic cell behaviour toward tumor cells. *Sci Rep*, **7**, 1093.
- Pavesi, A., Tan, A. T., Koh, S., Chia, A., Colombo, M., Antonecchia, E., Miccolis, C., Ceccarello, E., Adriani, G., Raimondi, M. T., Kamm, R. D. & Bertoletti, A. (2017). A 3D microfluidic model for preclinical evaluation of TCR-engineered T cells against solid tumors. *JCI Insight*, **2**.
- Pavlaki, M. & Zucker, S. (2003). Matrix metalloproteinase inhibitors (MMPIs): the beginning of phase I or the termination of phase III clinical trials. *Cancer Metastasis Rev*, **22**, 177-203.
- Pietras, K. & Ostman, A. (2010). Hallmarks of cancer: interactions with the tumor stroma. *Exp Cell Res*, **316**, 1324-1331.
- Polgar, L. (2002). The prolyl oligopeptidase family. *Cell Mol Life Sci*, **59**, 349-362.
- Poulos, S. P., Dodson, M. V. & Hausman, G. J. (2010). Cell line models for differentiation: preadipocytes and adipocytes. *Exp Biol Med (Maywood)*, **235**, 1185-1193.
- Pusch, J. (2009). Etablierung einer 3D-Darmgewebestruktur zur in vitro Untersuchung der Resorption potentieller Wirkstoffe auf Basis einer natürlichen Kollagenmatrix. *Dissertation*.
- Rakha, E. A., Reis-Filho, J. S. & Ellis, I. O. (2010). Combinatorial biomarker expression in breast cancer. *Breast Cancer Res Treat*, **120**, 293-308.

- Riddell, S. R. & Greenberg, P. D. (1990). The use of anti-CD3 and anti-CD28 monoclonal antibodies to clone and expand human antigen-specific T cells. *J Immunol Methods*, **128**, 189-201.
- Rueckert, S., Ruehl, I., Kahlert, S., Konecny, G. & Untch, M. (2005). A monoclonal antibody as an effective therapeutic agent in breast cancer: trastuzumab. *Expert Opin Biol Ther*, **5**, 853-866.
- Santo, V. E., Rebelo, S. P., Estrada, M. F., Alves, P. M., Boghaert, E. & Brito, C. (2017). Drug screening in 3D in vitro tumor models: overcoming current pitfalls of efficacy read-outs. *Biotechnol J*, **12**.
- Sappino, A. P., Skalli, O., Jackson, B., Schurch, W. & Gabbiani, G. (1988). Smooth-muscle differentiation in stromal cells of malignant and non-malignant breast tissues. *Int J Cancer*, **41**, 707-712.
- Schanz, J. (2007). Etablierung einer biologischen vaskularisierten Matrix als Grundlage für ein in vitro Lebertestsystem. *Dissertation*.
- Schmitt, T. (2017). Establishment and Characterization of a Breast Cancer Model Integrating Endothelial Cells. (Master's Thesis), *Universität Würzburg, Lehrstuhl für Tissue Engineering und Regenerative Medizin*.
- Scholzen, T. & Gerdes, J. (2000). The Ki-67 protein: from the known and the unknown. *J Cell Physiol*, **182**, 311-322.
- Schreiber, R. D., Old, L. J. & Smyth, M. J. (2011). Cancer immunoediting: integrating immunity's roles in cancer suppression and promotion. *Science*, **331**, 1565-1570.
- Schuhmacher, A., Gassmann, O. & Hinder, M. (2016). Changing R&D models in research-based pharmaceutical companies. *J Transl Med*, **14**, 105.
- Schultheiss, D., Gabouev, A. I., Cebotari, S., Tudorache, I., Walles, T., Schlote, N., Wefer, J., Kaufmann, P. M., Haverich, A., Jonas, U., Stief, C. G. & Mertsching, H. (2005). Biological vascularized matrix for bladder tissue engineering: matrix preparation, reseeding technique and short-term implantation in a porcine model. *J Urol*, **173**, 276-280.
- Seidel, U. J., Schlegel, P. & Lang, P. (2013). Natural killer cell mediated antibody-dependent cellular cytotoxicity in tumor immunotherapy with therapeutic antibodies. *Front Immunol*, **4**, 76.
- Sharpless, N. E. & Depinho, R. A. (2006). The mighty mouse: genetically engineered mouse models in cancer drug development. *Nat Rev Drug Discov*, **5**, 741-754.
- Siegler, E. L. & Wang, P. (2018). Preclinical models in chimeric antigen receptor-engineered T cell therapy. *Hum Gene Ther*.
- Sikora, M. J., Johnson, M. D., Lee, A. V. & Oesterreich, S. (2016). Endocrine Response Phenotypes Are Altered by Charcoal-Stripped Serum Variability. *Endocrinology*, **157**, 3760-3766.
- Slamon, D. J., Leyland-Jones, B., Shak, S., Fuchs, H., Paton, V., Bajamonde, A., Fleming, T., Eiermann, W., Wolter, J., Pegram, M., Baselga, J. & Norton, L. (2001). Use of chemotherapy plus a monoclonal antibody against HER2 for metastatic breast cancer that overexpresses HER2. *N Engl J Med*, **344**, 783-792.

- Snoek-van Beurden, P. A. & Von den Hoff, J. W. (2005). Zymographic techniques for the analysis of matrix metalloproteinases and their inhibitors. *Biotechniques*, **38**, 73-83.
- Sommers, C. L., Byers, S. W., Thompson, E. W., Torri, J. A. & Gelmann, E. P. (1994). Differentiation state and invasiveness of human breast cancer cell lines. *Breast Cancer Res Treat*, **31**, 325-335.
- Sommers, C. L., Thompson, E. W., Torri, J. A., Kemler, R., Gelmann, E. P. & Byers, S. W. (1991). Cell adhesion molecule uvomorulin expression in human breast cancer cell lines: relationship to morphology and invasive capacities. *Cell Growth Differ*, **2**, 365-372.
- Stockmeyer, B., Beyer, T., Neuhuber, W., Repp, R., Kalden, J. R., Valerius, T. & Herrmann, M. (2003). Polymorphonuclear granulocytes induce antibody-dependent apoptosis in human breast cancer cells. *J Immunol*, **171**, 5124-5129.
- Stratmann, A. T., Dandekar, G. & Nietzer, S. L. (2013). Three-dimensional in vitro Tumor Models as an Alternative for Animal Models in Preclinical Studies. *pharm. Ind.*
- Stratmann, A. T., Fecher, D., Wangorsch, G., Göttlich, C., Walles, T., Walles, H., Dandekar, T., Dandekar, G. & Nietzer, S. L. (2014). Establishment of a human 3D lung cancer model based on a biological tissue matrix combined with a Boolean in silico model. *Mol Oncol*, **8**, 351-365.
- Tan, J., Buache, E., Chenard, M. P., Dali-Youcef, N. & Rio, M. C. (2011). Adipocyte is a non-trivial, dynamic partner of breast cancer cells. *Int J Dev Biol*, **55**, 851-859.
- Thompson, E. W., Paik, S., Brunner, N., Sommers, C. L., Zugmaier, G., Clarke, R., Shima, T. B., Torri, J., Donahue, S., Lippman, M. E. & et al. (1992). Association of increased basement membrane invasiveness with absence of estrogen receptor and expression of vimentin in human breast cancer cell lines. *J Cell Physiol*, **150**, 534-544.
- Tsai, J. H. & Yang, J. (2013). Epithelial-mesenchymal plasticity in carcinoma metastasis. *Genes Dev*, **27**, 2192-2206.
- Vandooren, J., Geurts, N., Martens, E., Van den Steen, P. E. & Opdenakker, G. (2013). Zymography methods for visualizing hydrolytic enzymes. *Nat Methods*, **10**, 211-220.
- Vidi, P. A., Bissell, M. J. & Lelievre, S. A. (2013). Three-dimensional culture of human breast epithelial cells: the how and the why. *Methods Mol Biol*, **945**, 193-219.
- Virtanen, I., Gullberg, D., Rissanen, J., Kivilaakso, E., Kiviluoto, T., Laitinen, L. A., Lehto, V. P. & Ekblom, P. (2000). Laminin alpha1-chain shows a restricted distribution in epithelial basement membranes of fetal and adult human tissues. *Exp Cell Res*, **257**, 298-309.
- Vogel, C. L., Cobleigh, M. A., Tripathy, D., Gutheil, J. C., Harris, L. N., Fehrenbacher, L., Slamon, D. J., Murphy, M., Novotny, W. F., Burchmore, M., Shak, S., Stewart, S. J. & Press, M. (2002). Efficacy and safety of trastuzumab as a single agent in first-line treatment of HER2-overexpressing metastatic breast cancer. *J Clin Oncol*, **20**, 719-726.

- Vu, T. & Claret, F. X. (2012). Trastuzumab: updated mechanisms of action and resistance in breast cancer. *Front Oncol*, **2**, 62.
- Vuong, D., Simpson, P. T., Green, B., Cummings, M. C. & Lakhani, S. R. (2014). Molecular classification of breast cancer. *Virchows Arch*, **465**, 1-14.
- Wang, H., Huang, S., Shou, J., Su, E. W., Onyia, J. E., Liao, B. & Li, S. (2006). Comparative analysis and integrative classification of NCI60 cell lines and primary tumors using gene expression profiling data. *BMC Genomics*, **7**, 166.
- Wang, W., Erbe, A. K., Hank, J. A., Morris, Z. S. & Sondel, P. M. (2015). NK Cell-Mediated Antibody-Dependent Cellular Cytotoxicity in Cancer Immunotherapy. *Front Immunol*, **6**, 368.
- Wang, Y. Y., Attane, C., Milhas, D., Dirat, B., Dauvillier, S., Guerard, A., Gilhodes, J., Lazar, I., Alet, N., Laurent, V., Le Gonidec, S., Biard, D., Herve, C., Bost, F., Ren, G. S., Bono, F., Escourrou, G., Prentki, M., Nieto, L., Valet, P. & Muller, C. (2017). Mammary adipocytes stimulate breast cancer invasion through metabolic remodeling of tumor cells. *JCI Insight*, **2**, e87489.
- Weigelt, B., Ghajar, C. M. & Bissell, M. J. (2014). The need for complex 3D culture models to unravel novel pathways and identify accurate biomarkers in breast cancer. *Adv Drug Deliv Rev*, **69-70**, 42-51.
- Weigelt, B., Horlings, H. M., Kreike, B., Hayes, M. M., Hauptmann, M., Wessels, L. F., de Jong, D., Van de Vijver, M. J., Van't Veer, L. J. & Peterse, J. L. (2008). Refinement of breast cancer classification by molecular characterization of histological special types. *J Pathol*, **216**, 141-150.
- Wendt, M. K., Tian, M. & Schiemann, W. P. (2012). Deconstructing the mechanisms and consequences of TGF-beta-induced EMT during cancer progression. *Cell Tissue Res*, **347**, 85-101.
- Wetzels, R. H., Holland, R., van Haelst, U. J., Lane, E. B., Leigh, I. M. & Ramaekers, F. C. (1989). Detection of basement membrane components and basal cell keratin 14 in noninvasive and invasive carcinomas of the breast. *Am J Pathol*, **134**, 571-579.
- Wiseman, B. S. & Werb, Z. (2002). Stromal effects on mammary gland development and breast cancer. *Science*, **296**, 1046-1049.
- Wistuba, II, Behrens, C., Milchgrub, S., Syed, S., Ahmadian, M., Virmani, A. K., Kurvari, V., Cunningham, T. H., Ashfaq, R., Minna, J. D. & Gazdar, A. F. (1998). Comparison of features of human breast cancer cell lines and their corresponding tumors. *Clin Cancer Res*, **4**, 2931-2938.
- Xing, F., Saidou, J. & Watabe, K. (2010). Cancer associated fibroblasts (CAFs) in tumor microenvironment. *Front Biosci (Landmark Ed)*, **15**, 166-179.
- Xu, X., Farach-Carson, M. C. & Jia, X. (2014). Three-dimensional in vitro tumor models for cancer research and drug evaluation. *Biotechnol Adv*, **32**, 1256-1268.
- Yakes, F. M., Chinratanalab, W., Ritter, C. A., King, W., Seelig, S. & Arteaga, C. L. (2002). Herceptin-induced inhibition of phosphatidylinositol-3 kinase and Akt is required for antibody-mediated effects on p27, cyclin D1, and antitumor action. *Cancer Res*, **62**, 4132-4141.

- Yamada, K. M. & Cukierman, E. (2007). Modeling tissue morphogenesis and cancer in 3D. *Cell*, **130**, 601-610.
- Yan, S. J. & Blomme, E. A. (2003). In situ zymography: a molecular pathology technique to localize endogenous protease activity in tissue sections. *Vet Pathol*, **40**, 227-236.
- Yang, L., Ma, L. & Lai, D. (2013). Over-expression of fibroblast activation protein alpha increases tumor growth in xenografts of ovarian cancer cells. *Acta Biochim Biophys Sin (Shanghai)*, **45**, 928-937.
- Yang, L., Pang, Y. & Moses, H. L. (2010). TGF-beta and immune cells: an important regulatory axis in the tumor microenvironment and progression. *Trends Immunol*, **31**, 220-227.
- Yang, X., Li, Z., Wang, N., Li, L., Song, L., He, T., Sun, L., Wang, Z., Wu, Q., Luo, N., Yi, C. & Gong, C. (2015). Curcumin-encapsulated polymeric micelles suppress the development of colon cancer in vitro and in vivo. *Sci Rep*, **5**, 10322.
- Yarden, Y. & Sliwkowski, M. X. (2001). Untangling the ErbB signalling network. *Nat Rev Mol Cell Biol*, **2**, 127-137.
- Yerushalmi, R., Woods, R., Ravdin, P. M., Hayes, M. M. & Gelmon, K. A. (2010). Ki67 in breast cancer: prognostic and predictive potential. *Lancet Oncol*, **11**, 174-183.
- Zhang, B. L., Qin, D. Y., Mo, Z. M., Li, Y., Wei, W., Wang, Y. S., Wang, W. & Wei, Y. Q. (2016). Hurdles of CAR-T cell-based cancer immunotherapy directed against solid tumors. *Sci China Life Sci*, **59**, 340-348.
- Zhang, H., Ye, Z. L., Yuan, Z. G., Luo, Z. Q., Jin, H. J. & Qian, Q. J. (2016). New Strategies for the Treatment of Solid Tumors with CAR-T Cells. *Int J Biol Sci*, **12**, 718-729.
- Zhang, S., Chen, L., Cui, B., Chuang, H. Y., Yu, J., Wang-Rodriguez, J., Tang, L., Chen, G., Basak, G. W. & Kipps, T. J. (2012). ROR1 is expressed in human breast cancer and associated with enhanced tumor-cell growth. *PLoS One*, **7**, e31127.
- Zhang, S., Chen, L., Wang-Rodriguez, J., Zhang, L., Cui, B., Frankel, W., Wu, R. & Kipps, T. J. (2012). The onco-embryonic antigen ROR1 is expressed by a variety of human cancers. *Am J Pathol*, **181**, 1903-1910.
- Zhao, F., Grayson, W. L., Ma, T. & Irsigler, A. (2009). Perfusion affects the tissue developmental patterns of human mesenchymal stem cells in 3D scaffolds. *J Cell Physiol*, **219**, 421-429.
- Zheng, P. P., Kros, J. M. & Li, J. (2018). Approved CAR T cell therapies: ice bucket challenges on glaring safety risks and long-term impacts. *Drug Discov Today*.
- Zheng, X., Carstens, J. L., Kim, J., Scheible, M., Kaye, J., Sugimoto, H., Wu, C. C., LeBleu, V. S. & Kalluri, R. (2015). Epithelial-to-mesenchymal transition is dispensable for metastasis but induces chemoresistance in pancreatic cancer. *Nature*, **527**, 525-530.

Supplementary data

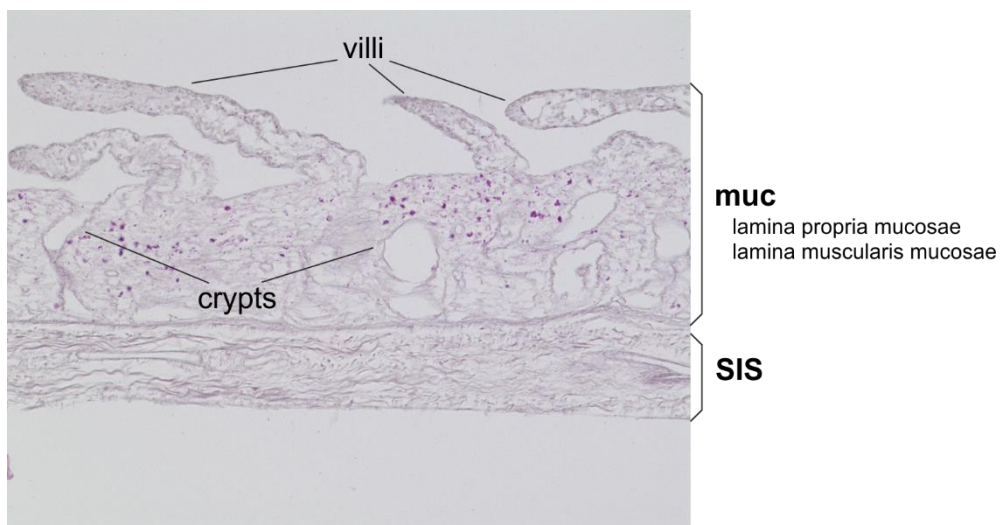


Figure S 1: Structure of the scaffold SISmuc

H&E staining of the scaffold SISmuc which is composed of the small intestinal submucosa (SIS) and the mucosa (muc). The mucosa consists of the lamina propria mucosae and the lamina muscularis mucosae which forms the barrier to SIS. In the mucosa former villi and crypt structures are preserved.

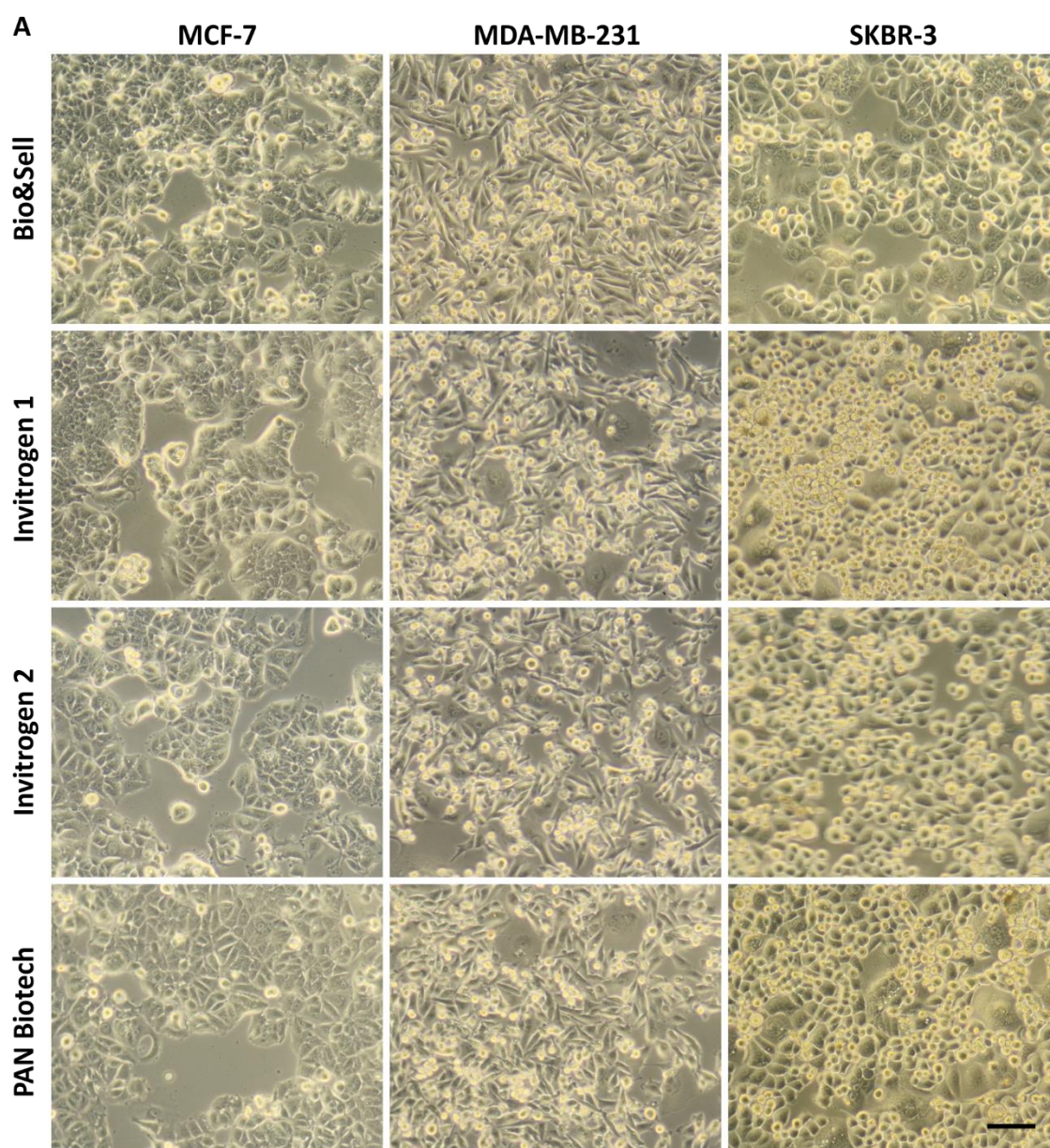


Figure S 2: FBS batch testing - cell morphology in 2D

Bright field images of MCF-7 (left column), MDA-MB-231 (middle column) or SKBR-3 cells (right column) cultured in their specific growth media supplemented with different batches of FBS (Bio&Sell, Invitrogen 1, Invitrogen 2, PAN Biotech) for 4 days. Scale bar: 100 μ m.

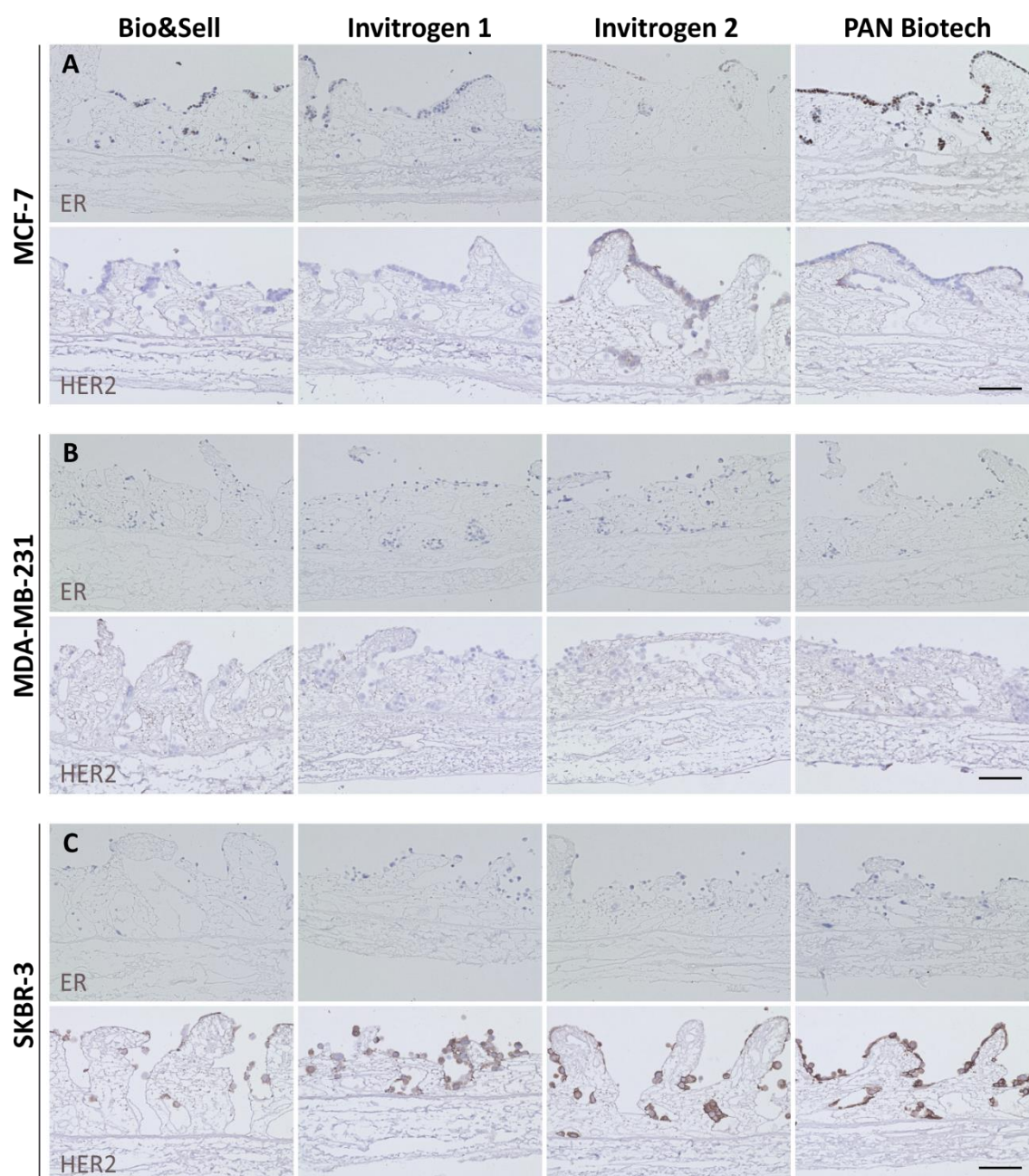


Figure S 3: Expression of mamma carcinoma-relevant markers in different FBS batches

Immunohistochemical staining against ER and HER2 of mamma carcinoma models of MCF-7 (A), MDA-MB-231 (B) or SKBR-3 cells (C) cultured for 14 days on SIS mucin in their specific growth media supplemented with different batches of FBS (Bio&Sell, Invitrogen 1, Invitrogen 2, PAN Biotech). Scale bar: 100 μm.

Affidavit/Eidesstattliche Erklärung

Affidavit

I hereby confirm that my thesis entitled „Establishment and optimization of 3-dimensional mamma carcinoma models for therapy simulation and drug testing” is the result of my own work. I did not receive any help or support from commercial consultants. All sources and / or materials applied are listed and specified in the thesis.

Furthermore, I confirm that this thesis has not yet been submitted as part of another examination process neither in identical nor in similar form.

Place, Date

Signature

Eidesstattliche Erklärung

Hiermit erkläre ich an Eides statt, die Dissertation „Etablierung und Optimierung 3-dimensionaler Mammakarzinommodelle für die Therapiesimulation und die Wirkstofftestung“ eigenständig, d.h. insbesondere selbständig und ohne Hilfe eines kommerziellen Promotionsberaters, angefertigt und keine anderen als die von mir angegebenen Quellen und Hilfsmittel verwendet zu haben.

Ich erkläre außerdem, dass die Dissertation weder in gleicher noch in ähnlicher Form bereits in einem anderen Prüfungsverfahren vorgelegen hat.

Ort, Datum

Unterschrift

Acknowledgement

An dieser Stelle möchte ich mich ganz herzlich bei allen Personen bedanken, die mich in den letzten Jahren im Rahmen dieser Arbeit begleitet und unterstützt haben und damit zu deren Gelingen beigetragen haben.

Mein ganz besonderer Dank gilt Prof. Dr. Heike Walles für die Möglichkeit, meine Dissertation unter Ihrer Betreuung am Lehrstuhl für Tissue Engineering und Regenerative Medizin in Würzburg anfertigen zu dürfen. Ihre motivierende und offene Art sowie ihre Anregungen haben maßgeblich zum Gelingen dieser Arbeit beigetragen. Vielen Dank auch für die Möglichkeit der Teilnahme an zahlreichen Kongressen und Symposien, durch die ich wertvolle Erfahrungen sammeln konnte.

Bei Prof. Dr. Torsten Blunk und Dr. Julia Schüler bedanke ich mich herzlich dafür, dass sie mich stets engagiert als weitere Gutachter dieser Arbeit betreut haben und mich mit Anregungen und Ratschlägen sowie nicht zuletzt durch die Bereitstellung von Zell- bzw. Xenograft-Material unterstützt haben.

Mein besonderer Dank gilt außerdem Dr. Gudrun Dandekar für die Betreuung meiner Arbeit als weiteres Mitglied meines Promotionskomitees. Gemeinsam mit Dr. Sarah Nietzer begleitete sie mich sowohl in der experimentellen als auch in der Schreibphase der Arbeit. Vielen Dank für eure enthusiastische Art, das Teilen eures Wissens, eure Anleitung und Ratschläge, aber auch für die Möglichkeit, meine eigenen Ideen einzubringen.

Darüber hinaus danke ich Prof. Dr. Thomas Dandekar für die Übernahme des Prüfungsvorsitzes.

Viele Kooperationspartner haben zum Gelingen dieser Arbeit beigetragen, auch bei Ihnen möchte ich mich herzlich bedanken. Besonderer Dank gilt hier Prof. Dr. Krohne sowie Daniela Bunsen und Claudia Gehrig für die kompetente Hilfe bei der TEM- und SEM-Analyse und die Zeit, die sie sich dafür genommen haben. Bei Prof. Dr. Luxenhofer und Michael Lübtow für die Gelegenheit, die von ihnen hergestellte Nanoformulierung für meine Arbeit zu nutzen sowie den stets sehr engagierten Austausch über die Ergebnisse. Dr. Michael Hudecek und Lars Wallstabe gilt mein Dank für die großartige Möglichkeit die ROR1-CAR T-Zellen in unseren Modellen zu testen und bei Christiane Höfner aus der Arbeitsgruppe von Prof. Dr. Torsten Blunk bedanke ich mich ganz herzlich für die große Unterstützung und kompetente Einarbeitung im Bereich der humanen ASCs.

Außerdem möchte ich dem gesamten Team des Lehrstuhls für Tissue Engineering und Regenerative Medizin für die großartige und fröhliche Arbeitsatmosphäre danken. Es gab immer ein offenes Ohr und ein aufmunterndes Wort oder eine helfende Hand.

Besonders danke ich Heide Häfner für ihre Aushilfe während Krankheit, Dienstreisen oder Urlaub und Sabine Gätzner, die immer einen Bioreaktor und Inkubatorplatz für mich frei hatte.

Claudia Göttlich danke ich dafür, dass sie mir in ihre strukturierte und gut organisierte Arbeitsweise Einblick gegeben hat und für die vielen lustigen und unterhaltsamen Stunden gemeinsamer Laborarbeit. Florentin Baur danke ich dafür, dass er sein eindrucksvolles Wissen über alles, was es dort draußen in der Welt gibt, mit mir geteilt hat und für die vielen Gespräche,

egal ob wissenschaftlicher oder privater Natur. Ihr beide seid in den letzten Jahren von Kollegen zu engen Freunden geworden, die mich durch diese spezielle Zeit meines Lebens begleitet haben, und diese wertvolle Freundschaft möchte ich auch in Zukunft nicht missen!

Vielen Dank auch an die Leute aus meinem Büro (Doktoranden-WG/International Office): Lisa, Miguel, Ji and Ives. The chats with you provided the perfect distraction on long working days and always helped to get back to work with a fresh mind.

Zudem möchte ich mich bei Tina Schmitt bedanken, die ich während meiner Zeit als Doktorandin betreuen durfte. Es hat viel Spaß gemacht, mein Wissen mit dir zu teilen, mit dir zusammenzuarbeiten und dich in die Welt der 3D Tumormodelle einführen zu dürfen.

Zuletzt möchte ich von ganzem Herzen meiner Familie und meinen Freunden danken für ihre endlose und uneingeschränkte Unterstützung und den Glauben in mich, selbst wenn einige keine Ahnung davon haben, woran ich in den letzten Jahren gearbeitet habe.

Danke Johannes, dafür, dass du alle Höhen und Tiefen mit mir durchlebt hast, mir immer grenzenlose Unterstützung, Stärke und Selbstbewusstsein schenkst und du mir jeden Tag zeigst, dass es mehr im Leben gibt, als Arbeit und eine Doktorarbeit. Danke dafür, dass du bist wie du bist. Mit dir an meiner Seite kann ich allen Hürden auf meinem weiteren Weg mit Gelassenheit entgegensehen.

Und zum Schluss ein warmes Dankeschön an das kleine Wesen in meinem Bauch, das mich mit sanften Tritten kleiner Füße stets motiviert hat, an dieser Arbeit weiterzuschreiben und mich daran erinnert hat: Wenn ein Projekt endet, beginnt ein neues ☺

List of publications and conference contributions

Articles

Manuscript completed: Göttlich C.*, Wallstabe L.*, **Nelke L. C.***, Nietzer S. L., Schwarz T., Nerreter T., Walles H., Einsele H., Dandekar G., Hudecek M. “Novel three dimensional tissue models of solid tumors to study efficacy of ROR1-specific chimeric antigen receptor T-cell therapy”

Manuscript completed and available as a preprint: Lübtow, M. M.*, **Nelke, L. C.**, Brown, A., Sahay, G., Dandekar, G., & Luxenhofer, R. (2017). “Drug induced micellization into ultra-high capacity and stable curcumin nanoformulations: Comparing *in vitro* 2D and 3D-tumor model of triple-negative breast cancer” ChemRxiv. Preprint

Göttlich, C.*; **Müller, L. C.***; Kunz, M.*; Schmitt, F.; Walles, H.; Walles, T.; Dandekar, T.; Dandekar, G. und Nietzer, S. L. (2016). „A Combined 3D Tissue Engineered *In vitro/In Silico* Lung Tumor Model for Predicting Drug Effectiveness in Specific Mutational Backgrounds”, J Vis Exp.

* First author

Oral Presentations

Müller L. C. et al., “Establishment and characterization of a 3D mamma carcinoma test system on a biological scaffold”, 32. Deutscher Krebskongress (DKK). 2016, Berlin, Germany

Poster Presentations

Nelke L. C. et al., “Novel 3D models of lung and breast cancer to evaluate the efficacy of immunotherapy with gene-engineered T cells expressing a ROR1-specific CAR”, 2nd World Preclinical Congress Europe. 2017, Lisbon, Portugal

Nelke L. C. et al., “Establishment and characterization of a 3D mamma carcinoma test system on a biological scaffold”, Goodbye Flat Biology: Models, Mechanisms and Microenvironment. 2016, Berlin, Germany

Müller L. C. et al., “A 3D mamma carcinoma test system on a decellularized scaffold for drug screening”, Functional Analysis and Screening Technologies (FAST). 2015, Boston (MA), USA

Müller L. C. et al., “Establishment of a 3D mamma carcinoma test system on a decellularized scaffold”, World Conference on Regenerative Medicine. 2015, Leipzig, Germany

Müller L. C. et al., “Establishment of a 3D mamma carcinoma test system on a decellularized scaffold”, 4th International Conferences: Strategies in Tissue Engineering. 2015, Würzburg, Germany

Müller L. C. et al., “Establishment of a 3D mamma carcinoma test system on a decellularized scaffold”, 18th International AEK Cancer Congress. 2015, Heidelberg, Germany

Curriculum vitae

Lena Christine Nelke (née Müller)

Education

Professional Experience

Place, Date

Signature